Research Instruments at the Budapest Neutron Centre

Handbook
of the Central European Training School
on Neutron Techniques

BNC
Budapest Neutron Centre

mtaEK   Wigner

Research Instruments at the

Budapest Neutron Centre

Handbook

of the Central European Training School

on Neutron Techniques

2019

Research Instruments at the Budapest Neutron Centre

Handbook of the Central European Training School on Neutron Techniques

www.bnc.hu/cets

Extended second edition

Edited by

János Füzi, Adél Len, Katalin Bajnok

Preface

This volume as a handbook on a number of neutron beam instruments aims to provide a study-aid for the training courses at the Budapest Neutron Centre (BNC). In general, training of young scientists or new-comers at European neutron centres have been organized since nearly 40 years (Berlin 1980, Oxford 1987). Nowadays basic or advanced/specialised schools are becoming more and more popular. Approximately 400 early career European researchers receive training via one or more of the various schools each year. There is a healthy oversubscription for the schools, suggesting that they are in high demand, and that there is a large number of European researchers seeking training in neutron techniques.

The Budapest neutron school was one of the first to offer – besides theoretical lectures – also hands-on-training on real working neutron spectrometers. The first such event was held in 1998 as an Austro-Hungarian training course. A widely opened international school was first organised on the occasion of the 2nd European Conference on Neutron Scattering in 1999. 120 participants (!) attended the school and a booklet of *Lecture Notes* was also edited[1]. This volume containing lecture materials on neutron scattering from 12 renowned scientists became quite popular – after several reprinting nearly 3000 copies were distributed. In 2001 we decided to extend the school into a training course, and offer the hands-on-training possibilities of the cold and thermal neutron beam instruments at BNC for the international user community. This training – like most of the other schools at neutron facilities – receives financial support within the Framework Programmes of the European Union (mostly to cover mobility expenses of the trainees). In this way our school has become a regular event, now organised every year, and it has got its name CETS – Central-European Training School, that responds, indeed, to the situation that most of the students come from our neighbour countries. In the past 20 years over 500 young scientists from nearly 40 countries have been trained at CETS.

In 2017 we decided to introduce a new structure of the usual one-week programme: instead of mixing lectures and instrumental training, now the lectures are condensed for the first two days, which is followed by the experimental part with extended exercises on the selected instruments. In this way, CETS provides, now in a didactic way, insight into the basics of neutron physics and the experimental procedures. The lectures cover the commonly used beam techniques: diffraction, radiography, reflectometry, three-axis spectroscopy, small-angle scattering, prompt gamma activation analysis, time-of-flight techniques and neutron polarisation.

This booklet focuses on practical problems related to the experimental work to be carried out during the training course. The short introduction gives a basic guidance on neutron properties and application of neutron beams for studies on structure and dynamics in condensed matter research. A very practical chapter outlines the basics of radioprotection indispensable for performing experiments in a nuclear reactor environment. The remaining chapters describe those instruments at BNC, which are included in the hands-on training programme. An insight into data interpretation is also given.

László Rosta

---

[1] http://www.iaea.org/inis/collection/NCLCollectionStore/_Public/30/054/30054765.pdf

Contents

List of authors

László Bottyán
Wigner Research Centre for Physics, Functional Nanostructures Laboratory
bottyan@bnc.hu

Margit Fábián
Wigner Research Centre for Physics, Neutron Spectroscopy Department
Centre for Energy Research, Environmental Physics Department
fabian@bnc.hu

Katalin Gméling
Centre for Energy Research, Nuclear Analysis and Radiography Department
gmeling@bnc.hu

Zsolt Kasztovszky
Centre for Energy Research, Nuclear Analysis and Radiography Department
kzsolt@bnc.hu

Zoltán Kis
Centre for Energy Research, Nuclear Analysis and Radiography Department
kis@bnc.hu

Adél Len
Centre for Energy Research, Nuclear Analysis and Radiography Department
len@bnc.hu

Dániel Géza Merkel
Wigner Research Centre for Physics, Functional Nanostructures Laboratory
merkel@bnc.hu

Gérard Pépy
Retired from Laboratoire Léon Brillouin, Saclay
gpepy@laposte.net

László Rosta
Wigner Research Centre for Physics, Neutron Spectroscopy Department
rosta@bnc.hu

Alex Szakál
Wigner Research Centre for Physics, Neutron Spectroscopy Department
szakal@bnc.hu

László Szentmiklósi
Centre for Energy Research, Nuclear Analysis and Radiography Department
szentm@bnc.hu

László Temleitner
Wigner Research Centre for Physics, Complex Fluid Research Department
temleitner@bnc.hu

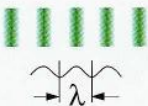# Introduction to neutron beam experiments

László Rosta

1. Basics of neutron physics

In order to design novel materials, devices and drugs, scientists are increasingly exploiting information about the properties and behaviour of matter at the atomic and molecular level. This information is acquired using advanced techniques, and neutron methods constitute an essential and unique part of the science toolkit. Neutrons can probe structure and dynamics of matter from mesoscale to nanoscale and from seconds to nanoseconds.

Neutrons have distinct particle properties, which influence the experimental scattering results. They have nearly no electrical properties: "no" electrical charge, "no" electrical dipole momentum. Neutrons mainly obey nuclear interaction. However, their magnetic moment couples to the local magnetic field, including that atoms and ions. Neutrons also exhibit weak interaction which is responsible for neutron decay. The most important properties of neutrons are summarised in **Table 1**.

Table 1. *Neutron Properties*
GS Bauer, http://indico.ictp.it/event/a04211/session/6/contribution/3/material/0/1.pdf

An important characterisation of neutrons is made by their classification into energy ranges, that shown in **Figure 1**. Neutrons with the mass *m* and a velocity *v* (for thermal neutrons $v \sim 2000$ m/s) have a de Broglie wavelength λ and a wave vector *k* (or often denoted as *q*).

$$mv = \hbar k = \frac{h}{\lambda} \qquad (1)$$

The wavelength is in the order of tenths of nanometres, and it is comparable to atomic distances, similarly to X-rays.
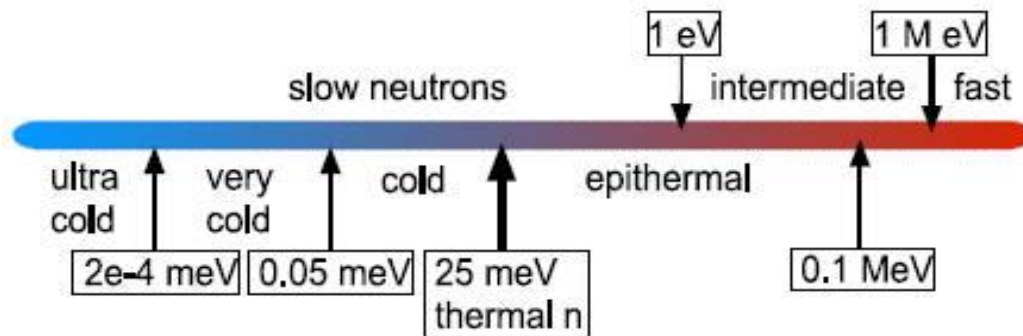

Figure 1. Energy scale of neutrons

By choosing the proper energy/wavelength of the probing neutrons structures, or in general, correlations can be investigated. If the correlations (atomic, molecular or nano-scale structural arrangements) are static, the corresponding scattering is elastic. If the correlations depend on time, i.e. the structure is seen in dynamics, the resulting scattering is inelastic, at least partly. Fortunately, thermal neutrons have kinetic energies E (~ 25 meV) comparable to excitations (fluctuations in time) in condensed matter.

$$E = k_B T = \frac{mv^2}{2} = \frac{\hbar^2 k^2}{2m} \qquad (2)$$

Therefore, in an inelastic scattering process, neutrons loose or gain energy in the same order as their kinetic energy. This can be readily observed. On the contrary, hard X-rays have energies 6 orders of magnitude higher (~ 10 keV) and the observation of inelastic scattering in the meV region became only recently possible, with limited resolution.

Besides the possibility of inelastic scattering, neutrons have other advantages. These unique properties of neutrons that make them indispensable in modern research are listed below:

a) neutrons have wavelengths and energies allowing us to obtain information on structural patterns from 10^{-10} m to 10^{-2} m and dynamic events from 10^{-12} s to 1 s;

b) neutrons are deeply penetrating, providing information from the hidden interior of a sample as well as from the surface without the effects of beam-damage as found with electron or X-ray probes;

c) neutrons interact with the atomic nucleus, the scattering length *b* varies strongly from element to element and also from isotope to isotope, so they are the only scattering probe to provide isotopic contrast. They can easily distinguish between atoms of comparable atomic number providing a unique tool in deciphering the organisation of biomedical and soft-matter systems; this particular technique is called "contrast variation" where Hydrogen (H) is replaced by its heavier isotope Deuterium (D).

d) neutrons possess a magnetic moment, making them an irreplaceable probe for the study of magnetism;

e)   the scattering of neutrons can be calculated exactly, making neutrons a precise, quantitative probe of matter. This last property underlines the value of neutron experiment coupled to methods of computer simulation and modelling.

2. Scattering of neutrons in condensed media

The interaction of the neutron with matter is described by its particle and wave nature. A simple scheme of a scattering experiment is shown in **Figure 2**. Neutrons emitted from a source are directed to the sample via a monochromator which defines the direction and the energy (velocity, wavelength) of the particles. Neutrons scattered from the sample can be detected at a given position and energy in the detector.
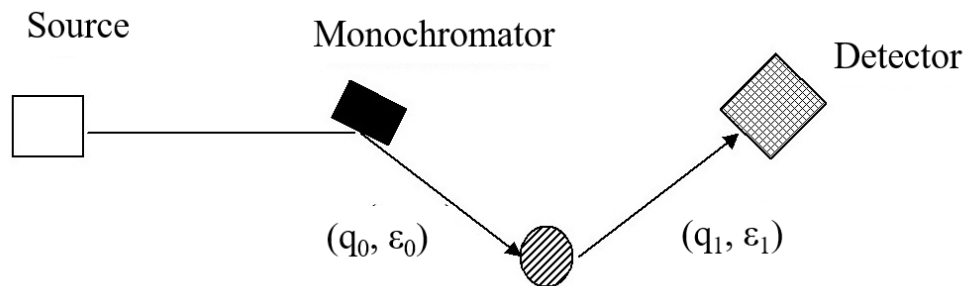
Figure 2. Scheme of a scattering experiment

The wave vectors of the incoming and scattered neutrons are denoted with $\vec{q_0}$ and $\vec{q_1}$, $\vec{Q}$ is the difference between them, and it is called scattering vector. Its absolute value is given by **Equation 3**, where θ is the half of the scattering angle, λ is the wavelength of the neutrons. The neutron vectors can be illustrated in the so called scattering triangle (**Figure 3**). The scattering law derived from the scattering triangle can be written by the momentum conservation and the energy conversation **Equations 5, 6**.
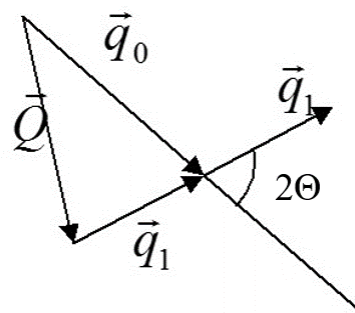
Figure 3. The scattering vector triangle

$$|\vec{Q}| = |\vec{q_0} - \vec{q_1}| = \frac{4\pi}{\lambda} sin\theta \qquad (3)$$

$$|\vec{q_0}| = \frac{2\pi}{\lambda} \qquad (4)$$

$$\vec{Q} = \vec{q}_0 - \vec{q}_1 \qquad (5)$$

$$\Delta\varepsilon = \varepsilon_0 - \varepsilon_1 = \frac{\hbar q_0^1}{2m} - \frac{\hbar q_1^2}{2m} = \hbar\omega \qquad (6)$$

The scattering law characteristic for the sample is given by

$$S(\vec{Q},\omega) = \frac{mq_0}{\hbar} W(\vec{q_0},\vec{q_1}) \qquad (7)$$

where $W(\vec{q_0},\vec{q}_1)$ is the scattering probability. The number of neutrons scattered into a unit angular space volume is proportional to the neutron intensity measured in the detector and can be described by the double (momentum and energy dependent) differential cross section (8)

$$\frac{d^2\sigma}{d\Omega dE} = \frac{q_1}{\hbar q_0} A S(\vec{Q},\omega) \qquad (8)$$

Here *A* denotes the atomic scattering cross section. **Equation 3–8** are valid in general for all kind of particles/waves scattered in condensed media consisting of atomic - molecular or larger scale structural components. The scattering cross section characteristic for a given material depends on one hand on the scattering law *S,* which itself is featured by the structure, i.e. the spatial distribution and motion of the scattering kernels. On the other hand, it depends on the nature of the interaction on the scattering kernels (atomic – molecular assemblies) with the given sort of irradiation which is applied in the experiment. In order to characterize structural and dynamic features of materials the adequate type of irradiation should be used. In a "good measurement" the scattering should be sensitive enough to be able to detect reasonably large changes in the scattering process, i.e. a significant difference in the incoming and outgoing particle parameters should be detected. The most commonly used irradiations are compared and a schematic representation of the atomic scattering lengths for certain elements are shown for X-rays and neutrons in **Figure 4**.
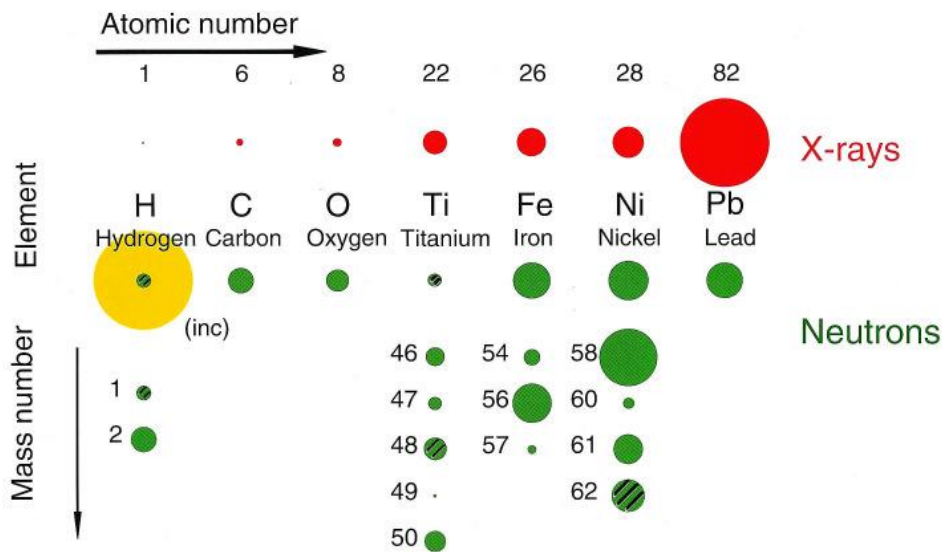

Figure 4. Illustration of the difference in atomic scattering lengths for X-rays and neutrons

Bauer GS, http://indico.ictp.it/event/a04211/session/6/contribution/3/material/0/1.pdf

In the case of *light scattering* (e.g. laser spectroscopy) photons of typical energy of 10 eV (500 nm wavelength) interact with the matter through an electromagnetic interaction described as the polarizability of the scattering kernels. Relatively large assemblies of atomic structures and a wide range of energies (but in a very limited reciprocal space) can be studied.

X-rays with typical energy of 10 000 eV ($0.1 < \lambda < 0.5$ nm) interact with the electron shell of the atoms and in this way the atomic scattering length scales with the atomic (isotopic) number, i.e. the heavier of an atom in a material the larger is the scattering cross section characteristic for this substance. Due to the very suitable wavelength scale of X-ray photons comparable to atomic distances, X-ray techniques are essential for a wide range of investigation of materials structures. Because of the weak interaction of X-rays with light elements (e.g. hydrogen), X-ray scattering has, however, strong limitations in the study of organic materials.

Neutrons have typical energies in the range from neV to hundreds of meV ($0.01 < \lambda < 5$ nm). The interaction is of nuclear nature and varies from isotope to isotope. The atomic scattering length can be positive or negative. For example, light water (H_2O) or heavy water (D_2O) has neutron scattering length of -0.165 and +1.92 barn, respectively. This enables neutron experiments to use the contrast variation technique, i.e. distinguish for example between organic atomic-molecular fragments in mixture solutions of light and heavy water.

3. Coherent and Incoherent Scattering

The differentiation between coherent and incoherent scattering represents a particular feature of neutron scattering. There are different ways to explain coherent and incoherent scattering.

1) In coherent scattering the scattered amplitudes are summed up and then squared; in incoherent scattering the intensities (amplitudes squared) from individual particles are summed up. Therefore, coherent scattering contains interference between different particles. This interference is absent in incoherent scattering. But interference may occur if one incoherently scattering particle is distributed over several positions with a certain probability. This is related to tunnelling or jump diffusion of hydrogen or hydrogen containing molecules.

2) Incoherent scattering yields information on the self-correlation function, which means the probability to find a particle at position *r* at time *t*, if the same particle has been at *r* = 0 at time *t* = 0. Coherent scattering is given by the Fourier-transform of the sum of the self and the pair correlation functions. The pair correlation function gives the probability to find a particle at *r* at *t*, if another particle has been at *r* = 0 at *t* = 0.

3) It would be wrong to say that coherent scattering comes from waves from different atoms, which are suited for interference and incoherent scattering comes from another kind of wave, where different atoms do not interfere. Correct is, that all scattered waves – at least as far as this text is concerned – do interfere. If we consider only elastic scattering, then in the simultaneous presence of coherent and incoherent scattering the intensity from a single crystal does not go to zero between Bragg peaks. It is just an artificial – but very useful – trick to separate the elastically scattered intensity from a single crystal into a system of Bragg-peaks (coherent) and a Q independent (neglecting the Debye-Waller factor) part (incoherent). The incoherent scattering has its origin in some disorder in the scattering lengths *b* for chemically identical particles.

$$\sigma_{inc} = 4\pi(<b^2> - <b>^2) \qquad (9)$$

Different isotopes of an element have different values of **b**. If one grows a crystal from one isotope (which has no nuclear spin) one can observe exclusively coherent scattering. If the scattering nucleus has a spin such as hydrogen (S = 1/2) then the scattering lengths are different for the two configurations, neutron spin parallel (b_{trip} = 1.085*10^{-12} cm) or antiparallel (b_{sing} = -4.750*10^{-12} cm) to the nuclear spin. It follows

$$<b> = {}^3\!/_4\, b_{trip} + {}^1\!/_4\, b_{sing} = -0{,}374 \cdot 10^{-12}\ cm \qquad (10)$$

$$<b^2> = {}^3\!/_4\, b^2_{trip} + {}^1\!/_4\, b^2_{sing} = 6{,}52 \cdot 10^{-24}\ cm^2 \qquad (11)$$

This type of phenomenon is called spin-incoherence. In the hydrogen case the incoherent scattering disappears only if the neutrons and all H-atoms would be polarised parallel to each other.

The simultaneous existence of coherent and incoherent scattering is a nuisance, unfortunately in many cases impossible to be avoided. Generally, one wants to study either coherent or incoherent scattering phenomena. Fortunately, in the case of hydrogen the incoherent cross section (80 barns) is very large, therefore it dominates very often.

4. Neutron sources

Neutrons can be produced by fission in nuclear reactors, by spallation using high power proton accelerators and nuclear reactions with low energy proton accelerators. The first two techniques are used worldwide with great success and offer versatile highest flux neutron production. The third technique to produce neutrons based on low energy proton accelerators has been less considered so far for neutron scattering purposes due to the relative low neutron flux available. This technique, however, has a great potential in building compact high brilliance sources thanks to novel developments, such as low-dimensional moderators, focusing optics.

In the past *fission* of the uranium isotope ^{235}U by slow neutron capture has been the most frequently used reaction in neutron sources. The reaction can be made self-sustaining because it is exothermal and releases more neutrons per fission process than are needed to initiate the process. If a slow neutron is captured by a fissionable nucleus, the resulting deformation can cause the nucleus to break up into two fragments (**Figure 5**). Very often a neutron is released directly during this process but mostly the neutrons "evaporate" off the surface of the fragments. This is a very important feature because a small fraction of these evaporation neutrons are released with a time delay of the order of seconds and thus enable a critical arrangement to be run in a controlled fashion.

Spallation. The term "spallation" is applied to a sequence of events that take place, if target nuclei are bombarded with particles of a de-Broglie wavelength, which is shorter than the linear dimensions of the nucleus. In this case collisions can take place with individual nuclides inside the nucleus and large amounts of energy are transferred to the nuclides which, in turn, can hit other nuclides in the same nucleus. The net effect of this intra-nuclear cascade is twofold:

i) Energetic particles may leave the nucleus and carry the cascade on to other nuclei (inter-nuclear cascade) or escape from the target.

ii) Energy is more or less evenly distributed over the nucleus leaving it in a highly excited state.
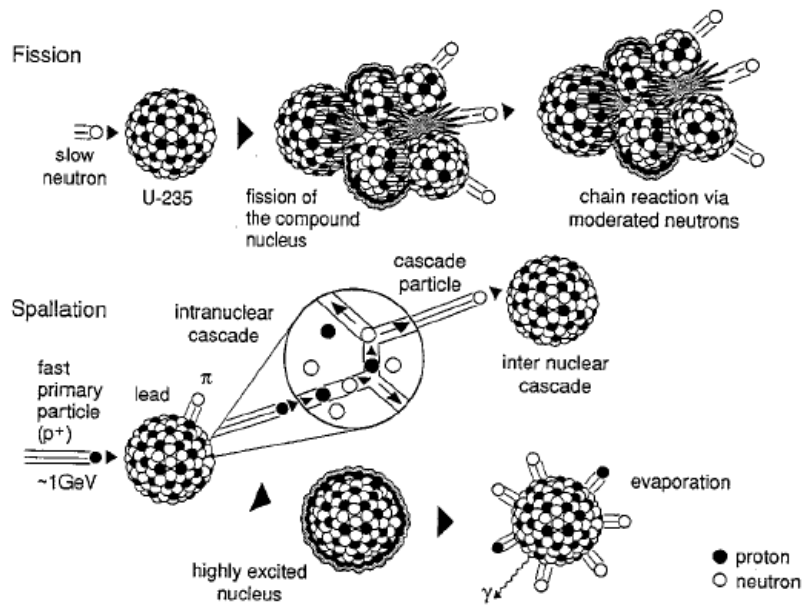
Figure 5. Illustration of the fission and spallation processes (Bauer GS, 1999)

The excited nucleus left behind will start evaporating neutrons - and to a lesser extent protons and other light nuclei - from, its surface. The spectrum of these evaporation neutrons is quite similar to the one resulting from fission, but as a consequence of the neutron escape during the intra-nuclear cascade, the overall spectrum extends to energies up to that of the incident particles (see curve in **Figure 6**). The release of spallation neutrons takes place within less than 10^{-15} sec after the nucleus was hit. This means, that the time distribution of spallation neutrons is exclusively determined by the time distribution of the driving particle pulse.
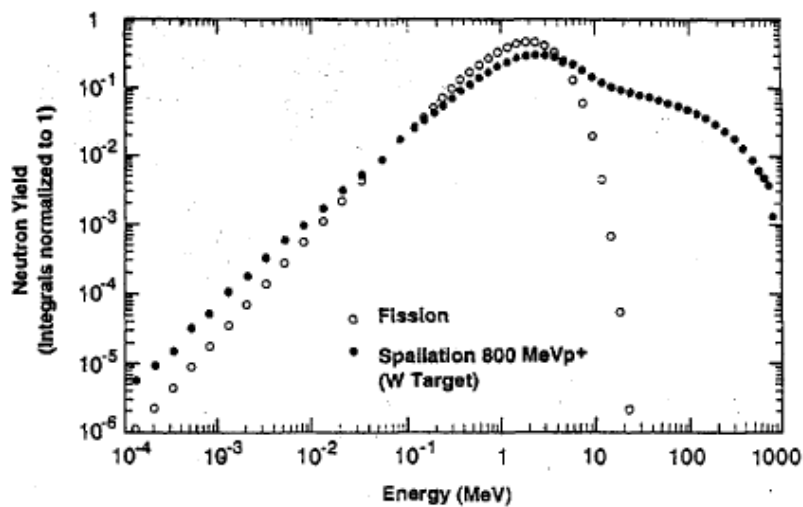
Figure 6. Logarithmic representation of neutron spectra from fission and spallation

There are only a few thermally fissionable isotopes, spallation can occur in every nucleus, although the neutron yield increases with the nuclear mass. Finally, whereas about 200 MeV of energy are deposited in a reactor core per useful neutron generated, this value is down to somewhere near 25 MeV in a spallation target (lead).

Nowadays spallation neutron sources are taking over the role from reactors to serve for neutron beam research for the following main reasons: no fission products (highly radioactive waste) are produced, thus the public acceptance is much less problematic; higher peak neutron flux (neutrons/cm²/sec) can be achieved; the pulsed structure of the neutron beams enables sophisticated beam manipulations to enhance spectral range, intensity and resolution performance of experiments.

Moderators. The energy spectrum of neutrons released in the primary neutron sources (reactor fuel or spallation target) is in the MeV range whereas meV or at most eV neutrons are required for scattering experiments. Therefore, a shift of several orders of magnitude is necessary, which is accomplished by collisions with the atoms of a "moderator" substance. The goal in the layout of a moderator is to create the highest possible flux of moderated neutrons either in the shortest possible time (pulsed neutron sources) or in the largest possible volume (steady state neutron sources). It is therefore important to consider the number of collisions that occur per unit time and the energy transferred in each collision. The important quantities to characterize the performance of a moderator for steady state neutron sources are called its "slowing-down power" and its "moderating ratio". Values for the moderator substances of practical importance are given in **Table 2**.

Table 2. Slowing-down power and moderating ratio of common moderator substances

Moderator	Density (g/cm³)	Slowing-Down Power $\xi \cdot \Sigma_s$ (cm^{-1})	Moderating Ratio $(\xi \cdot \Sigma_s / \Sigma_a)$
H_2O	1.00	1.35	71
D_2O (pure)	1.10	0.176	5670
D_2O (99.8 mole %)	1.10	0.178	2540
Graphite	1.60	0.060	192
Beryllium	1.85	0.158	143

In *research reactors* it is attempted to obtain most of the neutron moderation outside the core in order to maximize the neutron flux in regions where it is accessible for beam extraction. Since the neutron flux is essentially the product of neutron density and their velocity, achieving a high density is the design goal. To this end fast slowing down and long life time are required. The quantity characterizing the combination of these properties is the moderating ratio listed in Table 2. It is obvious that D_2O is the favoured candidate although H_2O moderated reactors are widely used with combination of a beryllium moderator as it is shown in **Figure 7**.

In addition to the ambient temperature reflector supplying beams of thermal neutrons, all modern research reactors are equipped with low temperature moderators, mostly liquid hydrogen or deuterium, to enhance the supply of long wavelength ("cold") neutrons. Some also have so called "hot" sources which consist in small masses of thermally insulated and radiation heated graphite to re-thermalize neutrons at a higher mean energy. **Figure 7**

shows the liquid hydrogen cold moderator chamber placement in the Budapest Research Reactor. This is a highly efficient way to enhance the cold neutron yield in the range of 0.4 – 2 nm and extract intense neutron beams from the reactor by a neutron guide system. **Figure 8** shows the schematic view of a similar installation, from the left: reactor core, moderator vessel with horizontal pipelines to feed it with liquid hydrogen and a set of neutron guides inside the reactor shielding vessel.
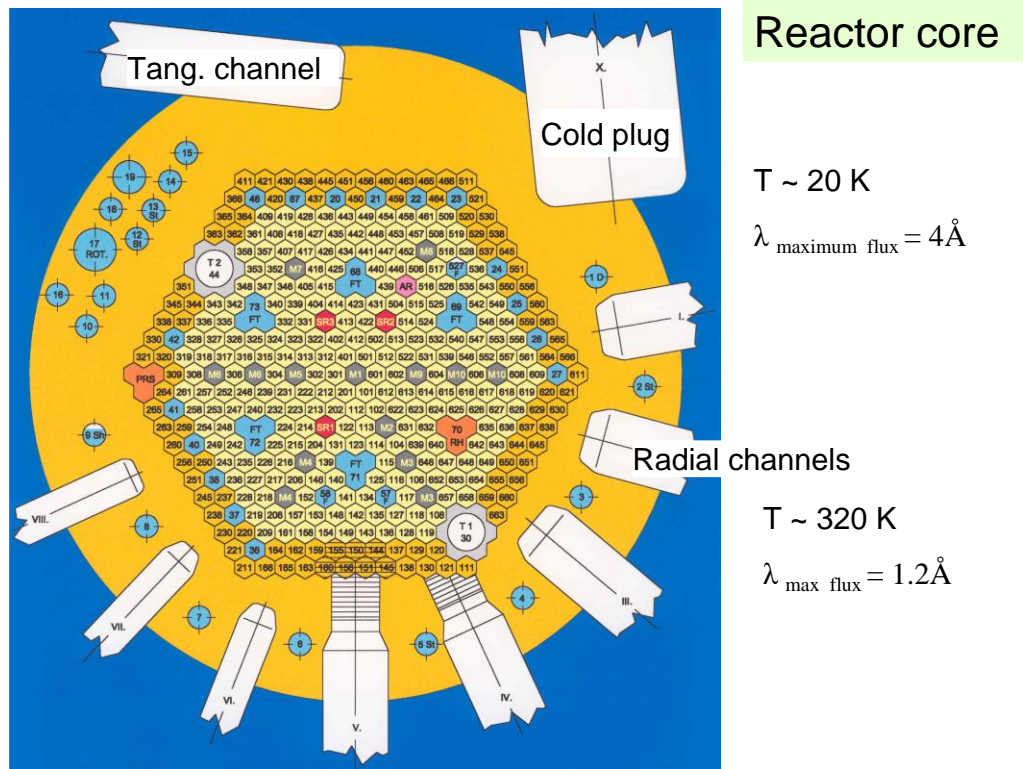

Figure 7. Schematic view of the core of the 10MW Budapest Research Reactor

Neutron experimental stations might be located close to the neutron source (reactor, spallation target) or at a considerable distance away from the source. In this latter case the beam is transported to the instruments by ***neutron guide tubes***. The principle of total reflection is the basis of neutron guides that are used to transmit neutron beams to instruments situated up to 100 m away from the source. A standard neutron guide is constructed from glass plates assembled into a rectangular cross section, the dimensions of which may be up to 200 mm high by 50 mm wide. The inner, reflecting surface of the guide is coated with approximately 120 nm of nickel, or a "supermirror". The guide is usually evacuated to reduce losses from absorption and scattering of neutrons in air. The great advantage of neutron guides, in addition to the transport of neutrons to areas of low background, is that they can be multiplexed, that is, one guide can serve many instruments. This is achieved either by deflecting only a part of the total cross section to a given instrument or by selecting a small wavelength range from the guide spectrum. In the latter case, the selection device (usually a crystal monochromator) must have a high transmission for other wavelengths. If the neutron guide is curved, the transmission becomes wavelength dependent. Nowadays supermirrors (a large number of alternating bi-layers of Ni/Ti) can be produced, which extend the critical angle of nickel by a factor

m, between 3 and 7 with reflectivity 92 – 70 %. Such high reflectivities enable sophisticated focusing supermirror neutron guides to be constructed with important flux gains.
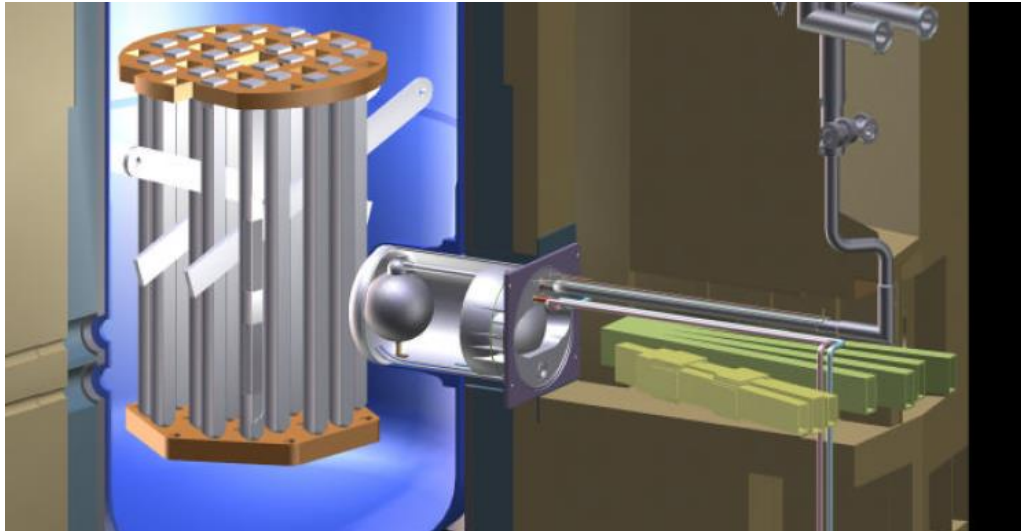

Figure 8. Neutron beam extraction form a cold moderator of a reactor (NIST)

5. Neutron beam experiments

Intense neutron beams extracted from a source, for example from a research reactor like the one at Budapest are used to perform neutron scattering or nuclear reaction type of experiments using various kinds of equipment (spectrometers) usually dedicated to solve a given sort or range of physical, chemical, biological, materials science, engineering or even archaeological problems. Experimental stations at neutron beam facilities should fulfil a few basic requirements:

- A good spectrometer should deliver a *high flux* of neutrons with a *good collimation* at the sample position.

- As much as possible scattered neutrons should be detected, with adequate angular and energy resolution.

- Low background, wide accessible momentum and *energy* range and a versatile sample environment are advantageous.

A major part of neutron beam experiments is performed as scattering ones to probe the structural and dynamic properties of materials, as illustrated in **Figure 9**. Another class of measurements is using nuclear reactions, when by neutron capture an atom is getting into an excited state and this is followed by an energy cascade with emitting gamma rays characteristic for the given atom (isotope). Thus, this technique – as called prompt and/or delayed gamma activation analysis – is very practical for the determination of elemental composition of materials. A widely applied neutron beam method is the combination of both the scattering and absorption phenomena, when beam transmission through bulk composite materials or objects consisting of various chemical and/or structural elements provides images according to the contrast due to the variation of the transmitted beam intensity. This neutron radiography technique or its 3D imaging version (tomography) gets more and more applications in industry and Cultural Heritage research.
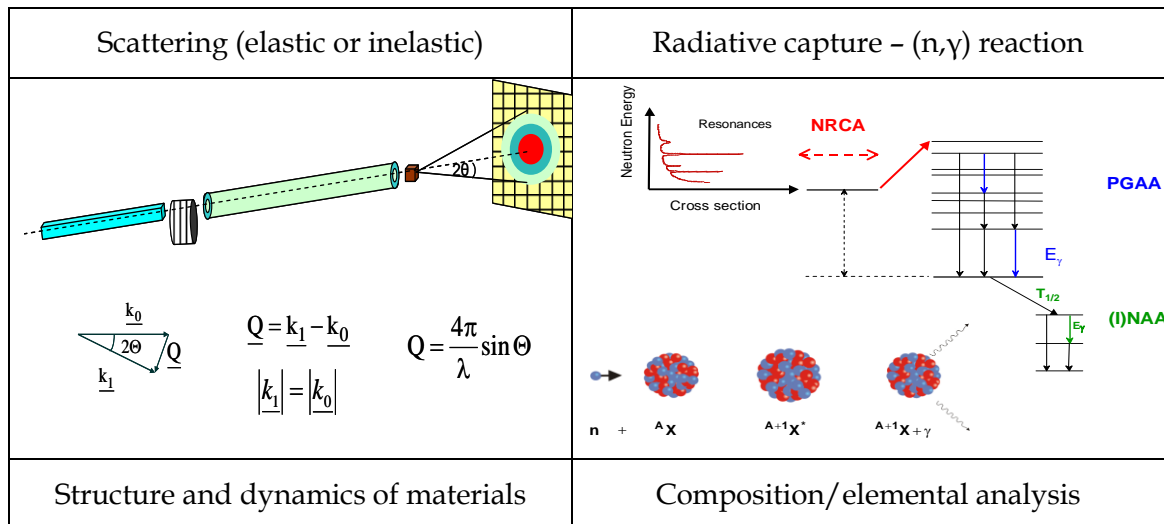
Scattering (elastic or inelastic)	Radiative capture – (n,γ) reaction
Structure and dynamics of materials	Composition/elemental analysis

Figure 9. Type of neutron beam experiments

The major neutron research centres in Europe or worldwide based on reactor or spallation sources are equipped with a versatile suite of instruments. Nowadays there are about 25 neutron beam facilities, which offer experimental services on their state of the art instruments. They are called user facilities, since academic or industrial users might access the various kinds of instruments. These centres operate some 10 to 30 scattering or capture type of instruments, which are usually located on cold, thermal or hot neutron beam-lines. The Budapest Research Reactor is one of these principal neutron research centres.

6. Neutron beam facilities at the Budapest Research Reactor

History. The Budapest Research Reactor (BRR) has been utilized as a neutron source for basic and applied research or direct applications in various fields of industry, healthcare as well as in exploration and conservation for objects of cultural heritage. The reactor was first started in 1959. BRR is one of the leading research infrastructures in Hungary and in Central-Europe. The basic scientific activity at BRR is the use of neutron beam lines for neutron scattering investigations. Originally, the reactor power was 2 MW, but it was upgraded to 5 MW in 1967. A second full-scale reactor refurbishment was started in 1986, fully designed and performed by Hungarian companies. The project was supported by the International Atomic Energy Agency (IAEA) and the European Union. The reconstruction was completed and the license for reactor start-up was issued in 1992. The reactor reached its 10 MW nominal power in May 1993. Thanks to a continuous development the number of experimental stations is now 15 (**Figure 10** shows the lay-out of the horizontal beam-lines). The research staff has grown by now to nearly 60 scientists. In 2010 a core conversion programme was completed, namely the change of the fuel from high enriched uranium to low (20 %) enriched uranium.

Facilities. For neutron beam measurements various types of horizontal channels are available: six radial thermal, two fast neutron channels and two tangential beam tubes. A 15x27 m^2 guide hall extending from the reactor hall, housing three neutron guides, was constructed in 1990. In 2000 a liquid hydrogen cold neutron source (CNS) was built and installed. The construction of the CNS has been followed by the replacement of the

obsolete neutron guides by a new supermirror guide system both for the in-pile and out-of-pile part.

THERMAL NEUTRON INSTRUMENTS:
RAD: DYNAMIC N/GAMMA & STATIC RADIOGRAPHY
BIO: PORT USED FOR BIOLOGICAL IRRADIATION
MTEST: MATERIAL TESTING DIFFRACTOMETER
TAST/HOLO: TRIPLE AXIS SPECTROMETER ON THERMAL BEAM
PSD: POWDER DIFFRACTOMETER

COLD NEUTRON INSTRUMENTS:
GINA: POLARIZED NEUTRON REFLECTOMETER
IMBS: IN-BEAM MÖSSBAUER SPECTROMETER
FSANS: TIME OF FLIGHT SMALL ANGLE NEUTRON SCATTERING
SANS-YS: SMALL ANGLE SCATTERING SPECTROMETER
PGAA: PROMPT GAMMA ACTIVATION ANALYSIS
NIPS: NEUTRON INDUCED PROMPT GAMMA SPECTROMETER
NORMA: NEUTRON OPTICS AND RADIGRAPHY FOR MATERIAL ANALYSIS
REF: REFLECTOMETER
ATHOS: TRIPLE AXIS SPECTROMETER

Figure 10. Layout of the horizontal neutron beam facilities at the Budapest Research Reactor

BRR is a recognized component of the European network of neutron centres. The neutron based laboratories around BRR are associated into a consortium called Budapest Neutron Centre (BNC). The number of experiments at BNC (including PhD and contract-based works) is 120-150 per year, the number of publications (typically quoted in annual reports) is ~100. Industrial and medical applications (e.g. production of radioisotopes, scientific instruments) provide important economic benefit.

Pioneering works. The Hungarian neutron community has made significant contribution to neutron research for many decades. A few highlights from BRR of the past decades are given here. Outstanding achievements are related to inventions of our leading scientists like Ferenc Mezei, who invented neutron spin-echo spectroscopy (1972), neutron supermirrors (1976) and the long pulse spallation source concept (1995). László Cser was the first to propose and realize neutron techniques for atomic scale holography (2002). BNC teams have played a pioneering role in developing combined dynamic neutron-gamma radiography that has found a widespread application in various industrial fields. In the middle of the nineties, researchers of BNC installed a Prompt Gamma Activation Analysis (PGAA) instrument on a cold guide end position. With a second instrument installed recently, this PGAA station became a world-leading facility. The work with largest impact from this team is the foundation of a coherent PGAA library. They were also among the first to perform non-invasive neutron beam investigations of archaeological objects.

Future. BRR in the present form can be operated until 2023 and even beyond. Europe has started to construct powerful new infrastructures intended to serve the needs of the entire continent in various fields of R&D by dedicated facilities; a most important of them is the European Spallation Source in Lund, Sweden. In neutron science ESS will take over and extend partly the traditional roles of the present multipurpose research reactors or spallation sources. On one hand, the activity of existing reactors, including BRR, however, is important in the transition period, i.e. at least up to the middle of the next decade in order to provide continued services for the user communities. On the other hand, planned compact accelerator driven neutron sources of national/regional scale to be constructed by the middle of 20s will provide new opportunities for research and training purposes of a broader community and they will complement existing (ISIS, ILL) or future (ESS) leading-edge European facilities.

References

Bauer GS, Neutron sources, in Lecture Notes on Neutron Scattering, Introductory Course to ECNS'99. Kádár Gy, Rosta L (Eds): Report KFKI-1999-04/E, 12-26 (1999)

Dorner B, Basic concepts, in Lecture Notes on Neutron Scattering, Introductory Course to ECNS'99. Kádár Gy, Rosta L (Eds): Report KFKI-1999-04/E, 1-11 (1999)

Cser L. Investigation of condensed matter by neutron scattering (in Hungarian), Typotex, ISBN: 978 963-2790-77-0, 1-188 (2010)

Mezei F, The basic physics of neutron scattering experiments, in Lecture Notes on Neutron Scattering, Introductory Course to ECNS'99. Kádár Gy, Rosta L (Eds): Report KFKI-1999-04/E, 27-39 (1999)

Rosta L, Baranyai R: Budapest Research Reactor – 20 years of international operation, Neutron News **22**, (2011) 31-36

Rosta L, Cold Neutron Research Facility at BNC, Applied Physics A 74, S52 (2002)

Radiation safety for users of neutron facilities

Alex Szakál

1. Introduction, basic concepts

Numerous kinds of radiations surround us in the everyday life, but because we don't have the sense to detect these radiations, usually people do not notice it. The sources of these radiations are diverse. They can originate from natural sources like the space, the Earth or even from our body. In 1985 Wilhelm Röntgen discovered the X-rays, since then man-made radiation sources exist. When the first effects of ionizing radiations started to appear, it became clear that even if ionizing radiations can be useful for various purposes, radiation safety is a real issue which has to be treated in an appropriate way. This chapter aims to summarize the basics of radiation safety and give some special notes for users of neutron facilities.

The three most common types of ionizing radiations are the alpha-, beta- and electromagnetic (X-ray, gamma) radiations. Neutron radiation is much rarer in nature, but because the experiments are done with neutrons, the properties of the neutron radiation is discussed as well.

X-ray radiation is the most widely known type of ionizing radiation, used in many areas of science and medicine. This radiation belongs to the family of electromagnetic waves. X-rays are produced in X-ray tubes when accelerated electrons hit a metal target. The target is made of high-Z metals, e.g. W, Mo, Cu. The spectrum of the produced radiation is divided into two parts. X-ray photons produced by the slow-down of electrons (Bremsstrahlung) have a continuous spectrum. The electrons bombarding the sample can knock out an inner electron of the target atoms. The hole generated by the missing electron is filled from an outer shell which involves characteristic (fluorescent) radiation. The energy of X-ray photons is in the range of 1-100keV.

Gamma-radiation is an electromagnetic wave emitted from an excited nucleus when it decays to the ground state or a lower energy level. Gamma-radiation is the same type of radiation as visible light or X-rays, the difference is that the origin of the radiation is the nucleus. Usually gamma-photons have energies above 100keV which distinguish them also. Gamma radiation can penetrate deeply into condensed matter. Shielding of them is usually done using dense materials containing high-Z elements e.g. Pb.

The alpha- and beta-radiation consist of particles with mass. **Beta-radiation** is emitted when a neutron in a nucleus is converted to a proton. This conversion is followed by the emission of an electron which is called beta-radiation. An anti-neutrino is also ejected but the effect of neutrinos on living organs is negligible because they interact very weakly with matter. The general form of beta-decay is:

$$_{Z}^{A}X \rightarrow \, _{Z+1}^{A}Y + e^- \, + \, \bar{\nu}_e \quad .$$
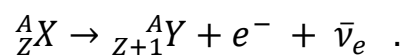
The atomic number of the radioactive isotope decreased by 1 in the process. The electron interacts with matter through the Coulomb interaction, thus it penetrates weakly in

condensed matter. Penetration depth of electrons in tissue and water is a few mm. A sheet of aluminium foil, thick clothing or cardboard can provide protection from beta-radiation. The use of elements with high atomic numbers (e.g. Pb) is not recommended because Bremsstrahlung X-ray is produced when the electrons slow down in the material.

Alpha-radiation is produced when a nucleus emits a helium nucleus, also known as an alpha-particle. The general form is

$$\,_Z^A X \rightarrow \,_{Z-2}^{A-4} Y + He^{2-} \quad .$$
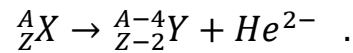
The atomic number of the radioactive isotope is decreased by 2 and the atomic mass is decreased by 4. Because the ejected alpha-particle is larger compared to the electrons and carry a double positive charge, the penetration depth is much shorter and a sheet of paper is enough to stop the particle. This short penetration makes this type of radiation harmful, because the energy of the particle is deposited in a short path producing great damage.

Neutron radiation can be emitted when a radioactive isotope decays, but those neutrons that are used in experiments are emitted in fission or spallation reactions. Fission is the reaction when a big nucleus decays into two smaller nuclei and the excess neutrons are emitted as free particles. Spallation reaction can be induced by bombarding heavy elements with protons. Collision with the energetic protons induce that the heavy nuclei are decomposed to smaller nuclei and free neutrons are ejected. Neutrons are electrically neutral and interact mainly with the nucleus, therefore the penetration depth is usually deeper than the penetration of gamma-photons. Effective shielding of neutrons is possible by using materials possessing high neutron capture cross-sections (e.g. B, Cd, Gd, ^{6}Li). These capture reactions are usually followed by the emission of a gamma-photon requiring additional gamma protection.

The strength of a radioactive source is called **activity**. The definition of activity is

$$A = \frac{dN}{dt} \, ,$$

where A is the activity, N is the number of radioactive nuclei and t is the time. The unit of activity is called becquerel [bq]. 1 bq= 1 decay per second. The number of radioactive isotopes and the activity of the sample decrease following the universal law of radioactive decay

$$A = A_0 e^{-\lambda t},$$

where A_0 is the activity when t=0 and λ is the decay constant. The half-life of a radioactive isotope is the time required for the activity to decrease to the half of the initial value. The connection of half-life and the decay constant is

$$T_{1/2} = \frac{\ln 2}{\lambda} \, .$$

Activity only describes the number of radioactive decays per unit time in a radiation source, but it cannot be connected to the biological effects of the emitted radiations. The biological effects are connected to the energy deposited in the tissue. The absorbed dose is this deposited energy by ionizing radiation per unit mass

$$D = \frac{dE}{dm} \ ,$$

where D is the absorbed dose, dE is the deposited energy in a dV volume with dm mass.

Different types of radiations have different biological effects even if the absorbed dose is the same because the amount of ions generated is different. To take this into account the equivalent dose quantity is used. The equivalent dose is the weighted average of absorbed doses

$$H_T = \sum_R w_R D_{T,R} \ ,$$

where H_T is the equivalent dose in the tissue T, $D_{T,R}$ is the absorbed dose of radiation R in tissue T and w_R is the weighting factor of radiation R. The weighting factors are summarized in **Table 1**.

Table 1. *Weight factors for equivalent dose calculation for different radiations and energies (ICRP 103, (2007))*

Radiation type and energy	Weight factor w_R
Gamma photons, X-rays, electrons, muons	1
Neutrons: <1 MeV	$2.5+18.2*\exp(-[\ln(E)]^2/6)$
1-50 MeV	$5+17*\exp(-[\ln(2E)]^2/6)$
> 50 MeV	$2.55+3.25*\exp(-[\ln(0.04E)]^2/6)$
Protons	2
Alpha particles, fission products, heavy nuclei	20

Alpha particles and other heavy nuclei cause high damage because they deposit all of their energy in a small volume, even inside one single cell. Neutrons have a weight factor depending on energy. For thermal neutrons this weight is ~2.5 but the peak value of the function is 20 at 1 MeV neutron energy.

Equivalent dose can be used only if the body is uniformly irradiated because the sensitivity for radiation is different for the organs. The **effective dose** has to be used if only a part of the body is irradiated and the effects must be described by one numerical value. The effective dose takes into account the sensitivity of different tissues by weighting the equivalent doses received by the different tissues

$$E = \sum_T w_T H_T \ ,$$

where E is the effective dose, w_T is the weight of tissue T and H_T is the equivalent dose received by tissue T. The weighting factors of different tissues are shown in **Table 2**.

Organ	W_T	Organ	W_T
Gonads	0.08	Oesophagus	0.04
Red Bone Marrow	0.12	Thyroid	0.04
Colon	0.12	Skin	0.01
Lung	0.12	Bone surface	0.01
Stomach	0.12	Salivary glands	0.01
Breasts	0.12	Brain	0.01
Bladder	0.04	Remainder of body	0.12
Liver	0.04	**TOTAL**	**1.00**

2. Risks of radiations

Radiations are present in nature since the universe was born and surround us in every moment. Thus, the living organisms are used to this environment and are prepared to repair the damages caused by radiations. These repair mechanisms usually work well, but if the radiation level is higher, the possibility of these mechanisms to fail is increased. If the radiation level reach a threshold, these mechanisms can no longer repair the damages. The effects of irradiations are divided into two categories based on the probability of consequences: the deterministic and stochastic effects.

Ionizing radiations transfer energy to the body like radiating heat. The transferred energy is small compared to the typical values in heat radiation, but the energy concentration is very high. This high energy concentration means that ionizing radiations are capable to induce chemical changes in the matter. They can create ions or break chemical bonds. The produced ions are called free radicals which are harmful because they are highly reactive.

The **deterministic effects** occur if high amount of cells are killed by the radiation. Contrary to the stochastic effects, the deterministic effects have a threshold dose and the effects are more severe if the dose was higher. To describe the deterministic effects of doses, absorbed dose (D) quantity is used. The threshold dose varies person to person but it is in the range of 0.5Gy-2Gy. The half lethal dose which cause death to 50 percent of an exposed population in 30 days is 3-5 Gy for the whole body. In radiotherapy, the deterministic effect is used to kill the tumour cells and doses of 10-20 Gy are normal but these doses are received by the tumour and not the whole body.

The **stochastic effects** occur if the DNS molecule of a cell is modified in such a way which results in a tumour cell, and the repair mechanisms of the body fail to eliminate it. The probability of biological damage in function of received dose is shown in **Figure 1**. Statistical information about the stochastic effects of radiation is available for example from the survivors of radiation accidents, atomic bombs, uranium miners. These exposures are higher than the normal levels but does not reach the threshold for deterministic effects. Reliable data for the determination of effects of small doses is not

available because the effects occur years after irradiation and they cannot be connected directly to radiation exposure, because other factors (e.g. smoking) can lead to the same diseases. The consensus of the experts is that the probability of stochastic effects can be extrapolated from the higher doses supposing a linear connection at the smallest dose values. In this model – called linear no threshold model – there is no connection between the dose and the severity of the effects and there is no threshold dose. To compare the stochastic effects of doses the weight factor of radiation has to be taken into account, therefore the equivalent dose (H_T) is used. According to ICRP 103 (2007) the risk of cancer is 5.5 %/Sv and the risk of heritable effects is 0.2 %/Sv.

The average background exposure from natural sources is 2.4 mSv/year. The largest source of this exposure is the inhaled radioactive radon and daughter elements. Other significant sources are the radiation from the naturally existing and radioactive [40]K and [14]C , the radiation from space, and the radiation from uranium and thorium in the ground and in construction materials. The average exposure from artificial sources is 0.6 mSv/year. The majority of this exposure is due to medical imaging and radiotherapy. In countries with advanced health services the exposure due to artificial sources can be as high as 3 mSv while in other developing countries this value can be close to zero. Other sources like radionuclides from atmospheric nuclear testing, nuclear accidents is below 1% of the artificial background.
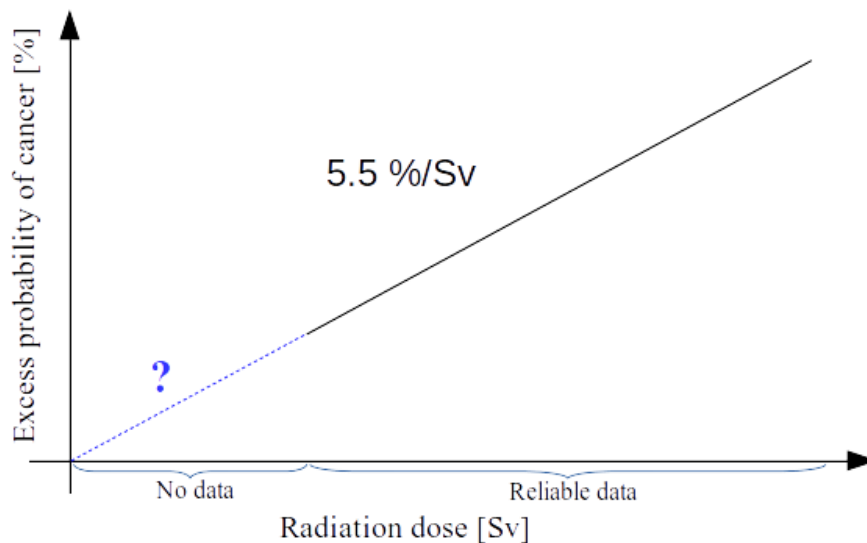

Figure 1. *Linear no threshold model of stochastic risks of radiation exposure*

3. Principles of radiation protection

Radiation protection is based on three principles: justification, optimization and dose limitation.

The **principle of justification** states that application of ionizing radiation is allowed only if the application has more benefit for the exposed individual or the society than the detriment of the exposition and all costs taking into account the costs of application and radiation protection. Activities with radiation danger can be applied only in those cases where other methods with similar costs and results are not available.

Once the use of radiations is justified, the process involving radiation danger has to be optimized. **Optimization** means the use of available resources in order to reduce the risks connected to radiations. Radiation doses has to be reduced "As Low As Reasonably Achievable" which usually cited as the ALARA principle. The excess dose due to the application and the release of radioactive materials has to be reduced by applying all reasonable methods.

According to the **limitation** principle, the effective dose for individuals must remain below the recommended dose limits. The occupational dose limit is 20 mSv averaged over 5 years but exceeding 50 mSv in any 1 year period. For the public, this limit is 1 mSv/year. The only exception where the dose limitations does not apply is radiotherapy. According to the ALARA principle, these dose limits should not be reached if there is a reasonable way to reduce the exposition.

4. Radiation protection regulations of the Budapest Research Reactor

The three factors used in order to reduce the dose from a given radiation source are time, distance and shielding. In practice, these three strategies are used simultaneously to suppress the doses.

The dose is proportional to the **time** of exposition, thus, reduction of time spent in a radiation environment is a straightforward way to reduce dose. Reduction of time means also that only those activities are allowed in environments where ionizing radiation is present that are not possible to do at other places. Exposition time can be reduced by careful planning of operations and, if necessary, by rehearsing the processes using inactive materials. This is a cheap and easy way to reduce dose, but usually the achievable dose reduction is not very significant.

The dose rate follows the inverse square law in function of distance to source, i.e. $D \sim 1/d^2$, where D is the dose and d is the distance from source. This dependence of the dose on the distance can be used to suppress the dose rate by increasing the **distance** from source. In practice this protection strategy is used when radioactive materials are moved by using pincers or other types of manipulators. It is forbidden to hold radioactive sample in hand, because even weak sources can cause considerable dose on the hand.

The dose rate can be suppressed by using **shielding** materials between the radiation source and the environment. The shielding must be designed for a given type and intensity

of radiation. Alpha particles can be effectively stopped by a thin material – even a sheet of paper – or some cm of air. Shielding of beta particles is possible by using plastic, glass, water of low-Z metals like aluminium. For X-rays and gamma radiation the usage of high-Z metals is the widespread solution. Shielding of neutron radiation usually requires a sandwich-type shielding. If the neutrons have energy above the thermal energy range, a thermalizing layer with high hydrogen concentration is used. Then the thermalized neutrons can be captured by materials like B, Cd, Gd. The neutron capture is followed by the emission of gamma radiation, thus, a third layer is needed to shield the gamma photons.

4.1. General rules

The Instrument Responsible (IR) manages the work of visitors and other workers on the instrument. The IR is responsible for the radiation protection and general safety training and the observance of the Work and Radiation Protection Rules of the Reactor.

Visitors are obliged to follow the instructions of the supervising person.

Proper clothing (white coat, overshoes) has to be worn in every case when work with radiation risk is performed. Additionally, wearing the dose-rate monitor is needed. The Environmental Protection Office can issue a certificate about the received dose.

4.2. Entry and exit procedures of the Reactor Building

Entrance to the reactor is only possible after application and receipt of entry permission and inspection at the gate. The ID card has to be given to the guard who gives a visitor entry card marked with a letter „V". Upon exit the ID card is interchanged with the visitor card. Entrance to the reactor building is allowed only in the presence of the host person. Before leaving the building contamination has to be measured using the contamination monitor installed at the gate. If contamination was detected, the person on duty of radiation protection has to be informed and waited to arrive. Henceforward his/her instructions have to be followed.

4.3. Entry to the Reactor Hall

Entrance to the Reactor Hall is possible only through the interlock gate on the 1st floor, in front of the control room. Entry is controlled, the operator on duty or the deputy operator allows the entrance. Laboratory coat and overshoes must be worn by visitors and must be accompanied by a supervising person to be allowed to enter into the reactor hall. Before leaving the reactor hall, the coat must be hanged on the coat stand and the shoe cover thrown into the bin in front of the interlock gate. Before leaving the reactor hall it is obligatory to check the radioactive contamination with the contamination monitoring instrument with special emphasis on the hands and feet. Contamination has to be reported immediately to the operators in the control room.

It is forbidden to stay in the reactor hall when the reactor starts, stops or changes operating power.

4.4. Rules for using the vertical beam ports

 The safety of experiments at the vertical beam ports and shielding around the beam port are the responsibility of the leader of the experiment. Opening the beam is enabled by the

member of the radiation safety group on duty after the appropriate shielding, and, if needed, a fence is installed. The responsible of each horizontal channel must ensure that workers and visitors at the belonging channels know and respect these rules.

Three indicator lamps are installed above the vertical channels indicating the closure of the channels. If the green lamp is on, the channel is closed. If the green and white lamps are simultaneously on, it means that the opening of the beam port is allowed by the radiation safety group and the channel can be opened any time, thus, it has to be considered as open. If only the white lamp is on, it means that the opening is started but not finished yet. If the red light is on, the channel is open. It is forbidden to enter behind the shielding while the beam port is open.

References

A Magyar Tudományos Akadémia Energiatudományi Kutatóközpont Sugárvédelmi Szabályzata, Sz-1.3/V4, 2015 (összeállította: Elter Dénes) [Radiation protection regulation of the Centre for Energy Research of the Hungarian Academy of Sciences]

ICRP, 2007. The 2007 Recommendations of the International Commission on Radiological Protection. ICRP Publication 103. Ann. ICRP 37 (2-4)

Neutron imaging

Laboratory exercise

Zoltán Kis, László Szentmiklósi

1. Introduction to neutron imaging

1.1. Using neutrons for imaging

Radiography is a material testing technique that provides the 2-D projected visual representation of an object by detecting the interaction between a radiation and the sample in a transmission geometry. The history of neutron imaging dates back to the mid 1930's, when H. Kallman and E. Kuhn established the first setup to record images by means of neutron radiation in Germany [1]. Starting from the 1950's research reactors were commissioned, providing intense neutron beamlines also for imaging purposes. This made possible to enhance the image quality and to develop a multitude of scientific and industrial applications. In parallel, important steps are being made to detect neutrons more efficiently and with better spatial and temporal resolution. Film-based detection had a dominating role for decades, but with the advent of digital technology and specialized detectors it was supplanted in the 2000's. Nowadays, in addition to the traditional (absorption) radiography, specialized imaging techniques (e.g. computed tomography, energy-selective imaging, imaging with polarized neutrons, dark-field imaging) also became available.

Applications of radiography or tomography at large-scale neutron centers can be divided into scientific and industrial utilization [2-3]. These two fields are of course not strictly separated. Here, without being exhaustive, some examples are listed:

Traditional radiography (static imaging):

- Non-destructive characterization of valuable cultural heritage objects
- Material science studies (foams, structured materials)
- Industrial quality assurance, product development, reverse engineering
- Nuclear technology (integrity check of reactor fuel cladding)

Dynamic radiography:

- Real-time visualization of combustion engines, two-phase flow
- Water and ion uptake in plants, transport processes in soils or minerals

Tomography:

- Extension of traditional radiography towards 3-D imaging by numerical algorithms and rotation of the object
- Hidden materials inside bulky objects
- Virtual cuts and opaque regions to enhance visual impression

During the **laboratory practice** we will visualize in real time the water uptake of a pH paper and/or a building material soaked in water by means of dynamic radiography.

1.2. The theory of neutron imaging [1-2]

The neutrons are particles without charge, so they penetrate deep into the sample. Without any interactions, they are transmitted along a straight path. The interactions between the neutron and the matter, however, result in the attenuation of the transmitted neutron beam. In case of slow neutrons there are two main interactions, the absorption and the scattering. The overall attenuation of the neutron beam when traveling through the objects is the superposition of these two effects. The depth of penetration and the probability of an interaction depend strongly on the energy-distribution of the incident neutron beam and the material-properties along its path. This makes us able to observe a contrast between different materials and ultimately to record their visual representation as a radiogram (NR, 2-D image) or tomogram (NT, 3-D image). Neutrons are able to pierce through several cm thick materials, so the inner structure of even a bulky object can be characterized, in a non-destructive way.
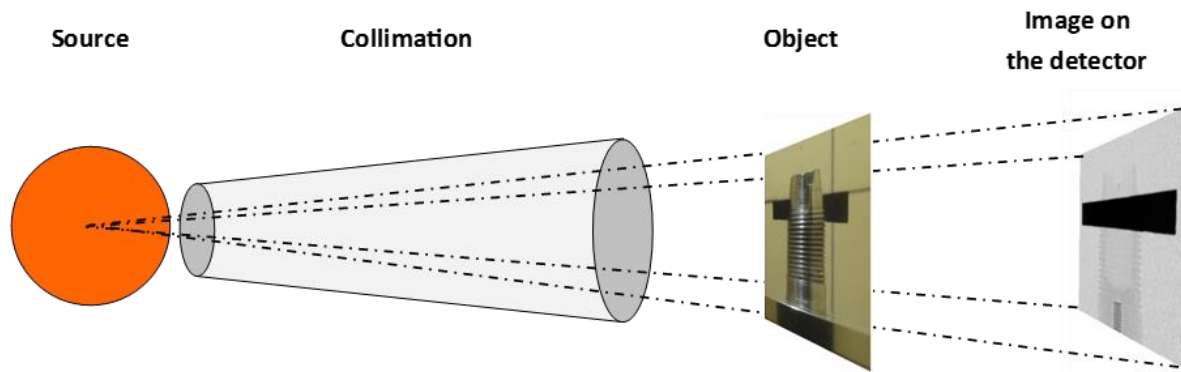

Figure 1. The basic idea of the radiographic imaging

According to the basic arrangement of imaging (**Figure 1**) the object, placed in the path of the neutron beam, creates a shadow in a downstream-placed position sensitive detector, as neutrons interacting with the object's material will not strike the given pixel of the detector. The image (i.e. a contrast pattern) is developed by the different number of neutrons traversing through the sample without interaction and reaching each pixel. The Beer-Lambert law determines the intensity of the transmitted beam (I_{tr}), normalized to the incident beam (I_0) intensity, through a material with thickness d as follows:

$$\frac{I_{tr}}{I_0} = exp(-\Sigma d)$$

where Σ is the linear attenuation coefficient (cm^{-1}). The coefficient is a macroscopic quantity, which can be obtained from basic microscopic quantities:

$$\Sigma = \rho_a(\sigma_{abs} + \sigma_{scat})$$

where ρ_a is the atomic density (cm^{-3}), σ_{abs} is the absorption and σ_{scat} is the scattering cross section (cm^2 = 10^{24} barn). The law above strictly speaking is valid only if the detector is point like, there is a well collimated pencil beam, and there is no so-called build-up effect. When there are different materials in the path of the neutron beam, the attenuation effect

of each material is added along the path and it can theoretically be represented by the following integral quantity:

$$\frac{I_{tr}}{I_0} = exp - \int_{beam\ path} \Sigma(x,y)ds$$

The mass attenuation coefficient (Σ_m, cm² g⁻¹) and the surface density (d_m, g cm⁻²) are frequently used quantities for some elements; they are used in the following form:

$$\frac{I_{tr}}{I_0} = exp\left(-\frac{\Sigma}{\rho_m} \cdot \rho_m d\right) = exp(-\Sigma_m \cdot d_m)$$

where ρ_m is the mass density (g cm⁻³), and $\Sigma_m = \Sigma/\rho_m$ has the same value in solid, liquid and gas phases of an element.
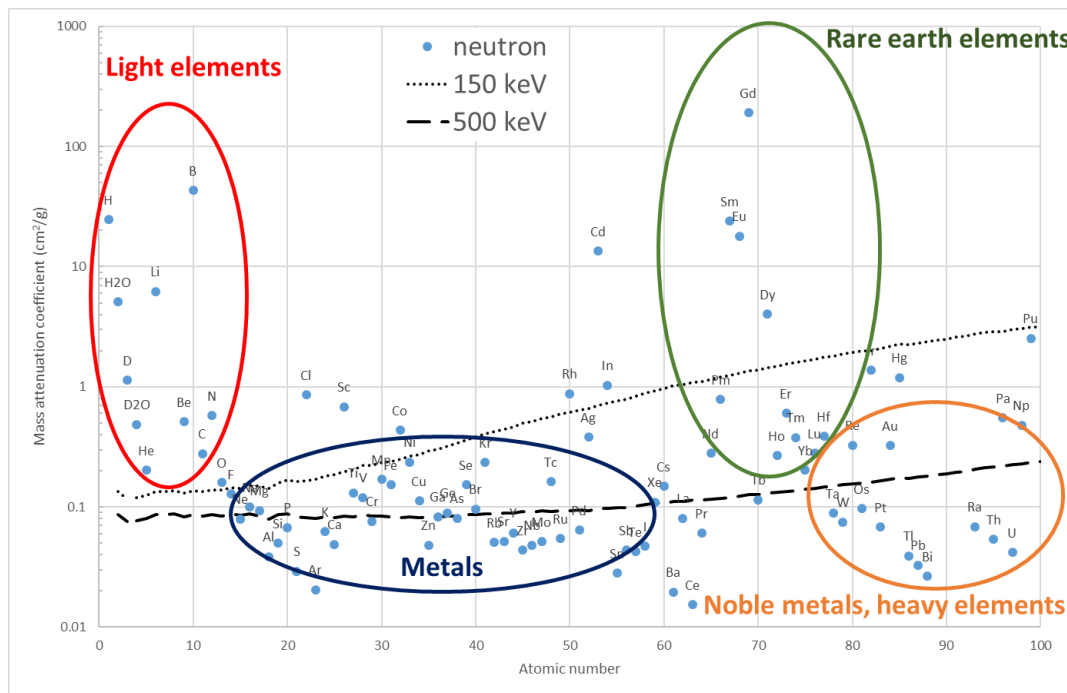

Figure 2. Mass attenuation coefficients of elements on logarithmic scale for thermal neutrons (dots), for 500 keV gamma radiation (dashed line), for 150 kV X-ray (dotted line)

Mass attenuation coefficients of elements are shown in **Figure 2** for thermal neutrons, for 500 keV gamma-radiation and for 150 kV X-ray radiation. Values in the case of neutrons show rather large differences, sometimes even orders of magnitudes, between neighbouring elements, while in case of X-rays they increase monotonically with the atomic number. The reason is that the neutrons interact with atomic nuclei, while photons interact with the electrons of an atom. Neutron imaging can be beneficial in visualizing objects including organic and inorganic materials (the neutron attenuation is significant

due to the hydrogen content), in transillumination of metals (e.g. Fe, Pb) and for discriminating between elements with similar atomic numbers (which do not give appropriate contrast in X-ray radiography).

Due to the different attenuations at different parts of the samples the inner structure can be visualized. To be able to create a reasonable image it is important to keep the transmission of the sample between a minimum and a maximum value, typically 2% to 98%, from which the corresponding thickness can be calculated as follows:

$$d_{max} < \frac{-ln(0.02)}{\Sigma} = \frac{3.91}{\Sigma} \qquad\qquad d_{min} > \frac{-ln(0.98)}{\Sigma} = \frac{0.02}{\Sigma}$$

The thickness range depends on the material and the energy of the neutron beam, some examples are shown in **Table 1**.

Table 1. *Maximal (d_{max}) and minimal (d_{min}) thickness for some materials corresponding to minimal (2 %) and maximal (98 %) transmission of thermal energy (0.0253 eV) neutron beam.*

Element	Σ (cm^{-1})	d_{min} (cm) < d < d_{max} (cm)
Al	0.10	0.193 – 37.45
Bi	0.26	0.078 – 15.15
Ag	4.00	0.005 – 0.977

Figure 3 shows a comparison of the transmission for a thermal neutron beam (0.0253 eV) and 0.5 MeV gamma-radiation in 1 cm sample material. In the case of this exercise the most important is water's very low neutron transmission, which is caused by the high scattering cross section (82 barn) of hydrogen. This makes neutron radiography well suited to analyze hydrogen-containing materials.
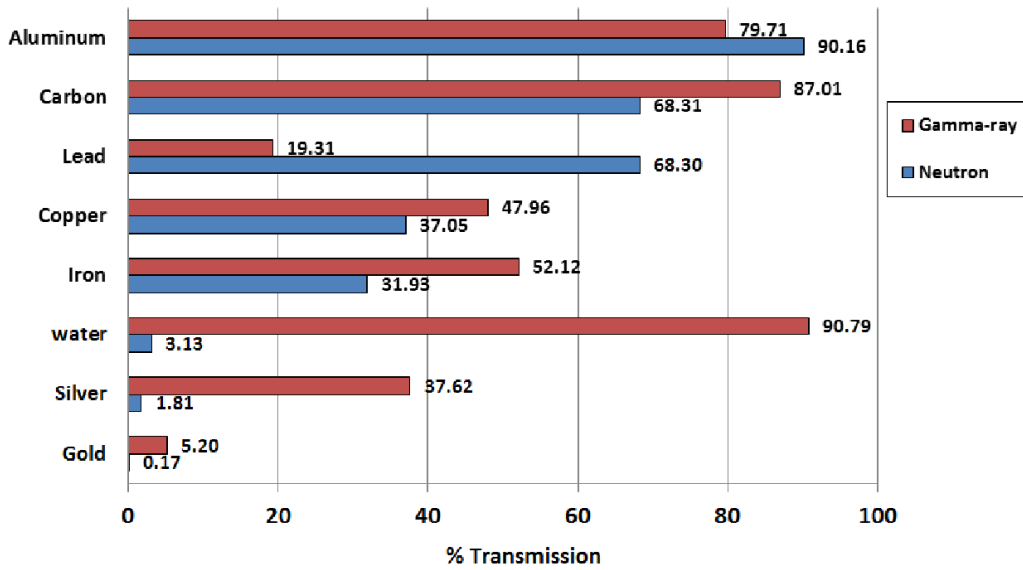
Figure 3. Transmission of thermal neutrons (0.0253 eV) and 0.5 MeV gamma-radiation through 1 cm material [1].

1.3. Basics of practical neutron imaging

The sketch of modern radiography/tomography equipment is shown in **Figure 4**. Image emerges in a form of visible light emitted from certain points of the neutron-sensitive scintillator screen. The light is then directed towards the optical system (objective + digital camera) by a mirror set in 45° angle relative to the beam. The light-sensitive chip's pixels in the camera are collecting the incoming light during the exposition time, and after readout, provide a grayscale value proportional to the intensities of each (*x*,*y*) pixels. The image processing software and hardware do the necessary calculations, and the image emerges as a matrix of data.
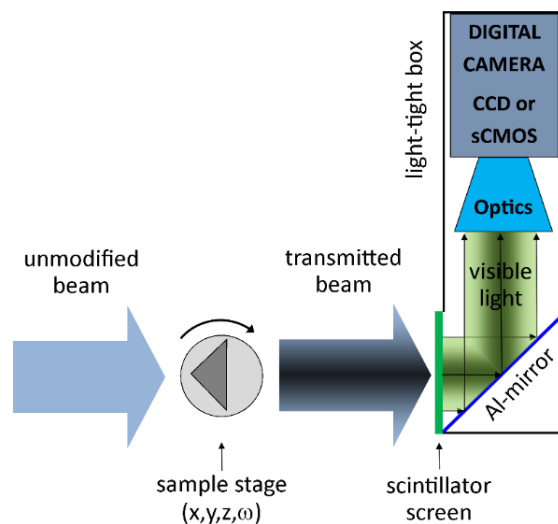

Figure 4. Sketch of a modern radiograph/tomograph setup.

During quantitative imaging it is necessary to correct the projections for the noise related to the dark current of the camera, as well as for the spatial inhomogeneity of the beam. The normalization is calculated for each (x,y) pixel with the following expression:

$$\frac{I_{tr}}{I_0} = \frac{I_{transmitted} - I_{darkcurrent}}{I_{openbeam} - I_{darkcurrent}}$$

where $I_{transmitted}$ is the grayscale value measured by the beam just crossing the sample, $I_{darkbeam}$ the grayscale value level measured in the pixel without the beam (i.e. the dark current of the camera chip), $I_{openbeam}$ is the grayscale value level measured in the pixel with open beam but without sample. The effect of normalization on the picture is show in **Figure 5**.
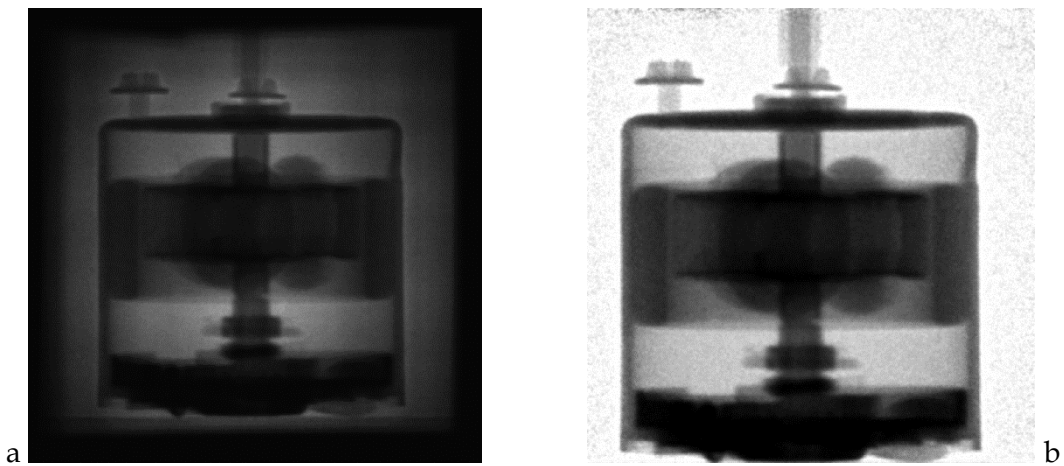

Figure 5. The raw (a) and the normalized (b) neutron radiographic image of a stepper motor

There is a figure of merit describing how close the beam geometry approaches the ideal point-source configuration. It is called collimation ratio, or in short *L/D* value. In **Figure 6** it can be seen that a larger *L/D* ratio provides better image resolution because image blur (*d*) is smaller. One has to make a trade-off between intensity and geometrical sharpness. A larger *L* or a smaller *D* results in a more collimated beam, i.e. sharper images, at the expense of lower intensity and, consequently, higher exposure times. For a beam with a given L/D ratio, a closer sample-to-scintillation screen distance (l_d) means, theoretically, less blurring effect. In this case, in practice, the inherent spatial resolution of the image detector and the effect of the scattering will determine the ultimate spatial resolution. The *L/D* values can be calculated from the geometrical dimensions of the beamline or can be experimentally measured. These two values are not necessarily equal because the geometrical calculations do not take into account the energy- and the angular distribution of neutrons in the actual beam.
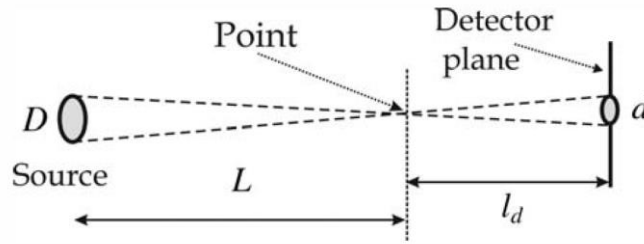
Figure 6. *The role of the collimation ratio in the blurring effects*

2. Description of the neutron imaging facility RAD

Two neutron-imaging facilities (NIPS-NORMA [4] station and RAD station [5], see **Figure 7**) are located at the Budapest Neutron Centre (BNC). The RAD facility is intended to study larger objects with bimodal (neutron and X-ray) imaging, even in real-time. The NIPS-NORMA facility is designed to make neutron imaging of smaller objects with cold neutrons, also in combination of position-sensitive element analysis by prompt-gamma activation imaging (PGAI).
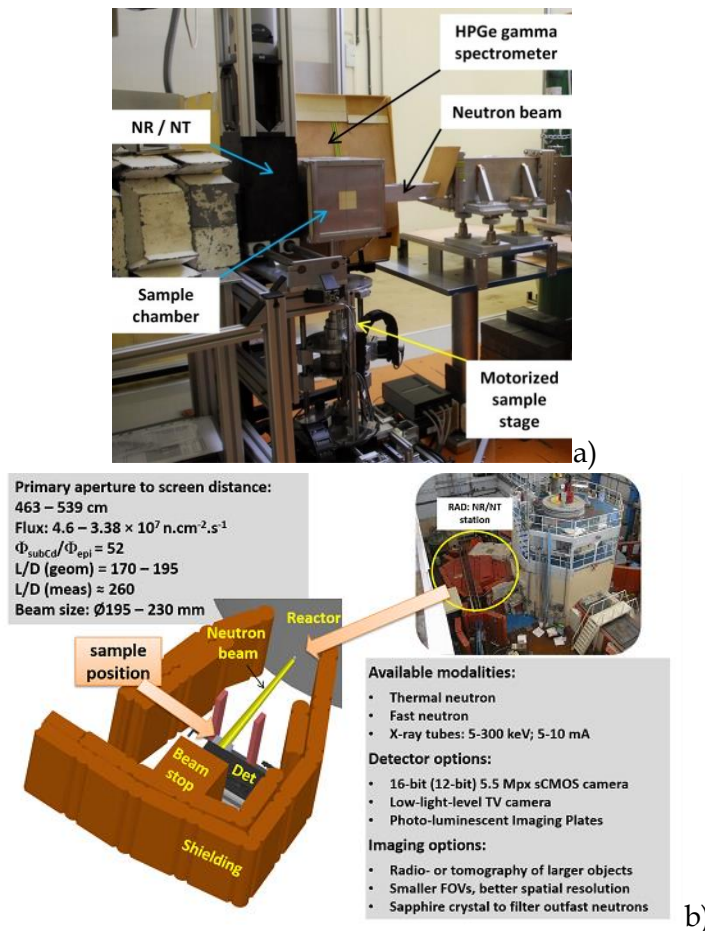

Figure 7. *The two neutron imaging stations at the Budapest Neutron Centre (BNC). (a) NIPS-NORMA station and (b) RAD station.*

In the following section some technical details are given for the RAD station, where the laboratory practice will take place.

The RAD thermal neutron imaging facility is served by a Cd-covered pin-hole-type collimator located at the No 2. radial horizontal channel, inside the biological shielding. The imaging device can be moved parallel to the beam axis on a rail system. Its closest and farthest measurement positions (see **Figure 7b**) are used for dynamic (DNR at 209 cm from beam port, to prefer intensity) and for static (SNR at 282 cm from beam port, to prefer beam quality) imaging, respectively. The measured L/D ratios are around 260, which are reasonably good values for a traditional imaging beamline. The beam diameter is adjustable up to a maximum of 230 mm at the SNR position. The thermal neutron fluxes at the two positions are 4.64×10^7 cm^{-2} s^{-1} and 3.38×10^7 cm^{-2} s^{-1}, respectively. The beam has a neutron-to-gamma ratio of 1.72×10^5 cm^{-2}mR^{-1} and a cadmium ratio of 3.3. The thermal to epithermal flux measured by the cadmium covered and bare gold monitor method is about 51. The gamma-ray intensity is about 8.5 Gy/h. The RAD facility is also equipped with a set of X-ray generator tubes, covering the energy range between 5-200 keV with max. 10 mA current, for dual beam imaging. A massive, motorized sample manipulator with maximum load up to 250 kg, and a smaller one up to 5 kg are available to position the investigated objects.

The RAD station has an up-to-date digital imaging equipment (**Figure 8**). The facility is able to carry out radiographic or tomographic imaging based on scintillation screens; for neutron imaging, scintillation screens with resolutions of 50 - 450 μm; for X-ray imaging, intensifying screens with resolutions of 100 - 200 μm. To make the instrument more flexible it is possible to set larger or smaller fields of view with respective lower or higher spatial resolutions. The static radiography and tomography are accomplished by an Andor Neo 5.5 sCMOS 2560×2160 px camera. In the light-tight optical box, three different optics can be used (computer-controlled interchangeable lenses with 50 mm, 105 mm and 300 mm fixed focal lengths) coupled to the digital camera, as shown in **Figure 9**. Real-time radiography can be done by means of a low-light-level TV camera (640×480 px) with a light sensitivity of 10^{-4} lux. The imaging cycle of this camera is 40 ms (25 Hz), making possible the high-frame rate imaging, resulting in a video file. A zoom optics coupled to this camera provides inherently a variable field of view. The two cameras can be used as alternatives in the light-tight camera box. A mirror placed at 45 degree reflects the light towards the camera.

- static imaging:
  - radiography and tomography using sCMOS camera (Andor Neo 5.5)

- dynamic and real-time imaging:
  - radiography based on low-level-light analog TV camera (Vidicon tube) and digital sCMOS

- scintillator screens:
  - neutron: Li^{6}F/ZnS (100, 200, 250 and 450 μm) and Gadox (10 and 20 μm)
  - X-ray: intensifying screens

- different field of views:
  - 250×250 mm^2 (Sigma 50mm)
  - 100×100 mm^2 (Nikon 105mm)
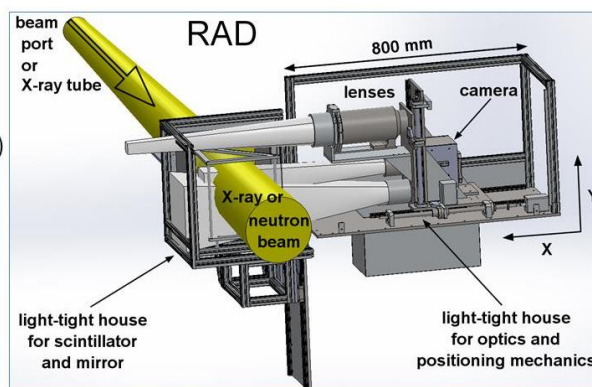 - 40×40 mm^2 (Nikon 300mm)

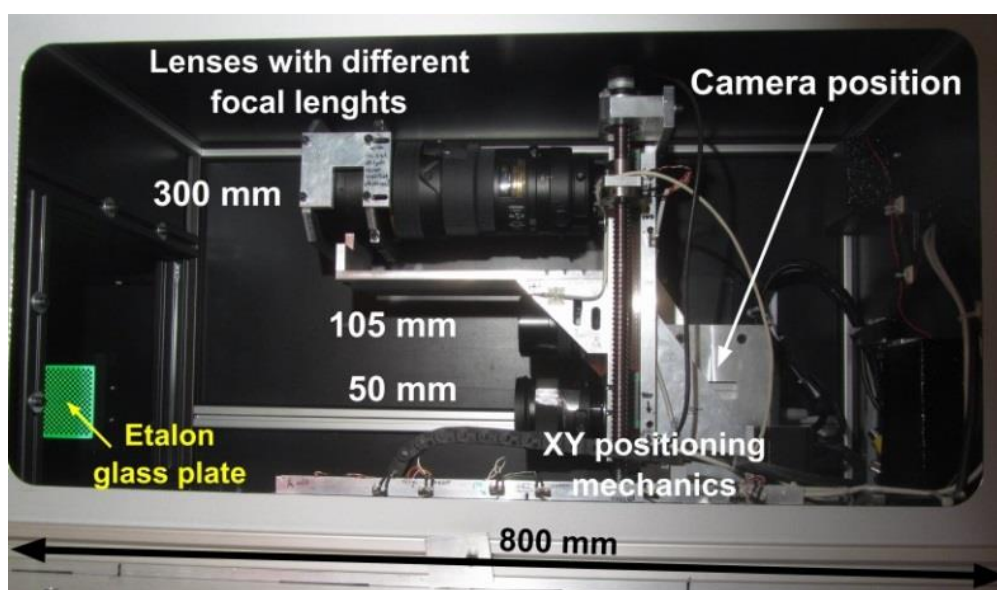*Figure 8. Features available at the RAD system*

Figure 9. The light-tight box and the opto-mechanical system of the RAD facility

A modern system applying digital imaging like the RAD and the NIPS-NORMA station at BNC (**Figure 7**) has several advantages:

- Applying cold or thermal neutrons gives better detectability and good contrast for most materials. Thermal neutrons and guided cold neutrons are used for imaging at the RAD and NIPS-NORMA stations, respectively
- For detection of neutrons, scintillators with ^{6}Li and Gd-oxide are widespread. The neutron detectors used at RAD and NIPS-NORMA station have ^{6}LiF/ZnS(Cu) scintillator material in 100 μm – 450 μm thicknesses, mounted on a pure Al support plate.

- More collimated beam geometry (increasing the so-called L/D ratio) improves the spatial resolution and reduces blurring. Spatial resolution is the highest if a thin sample is positioned as close as possible to the scintillator screen. Spatial resolutions 50 - 450 μm are reached at RAD, depending on the thickness of the scintillator layers and the sample dimensions. At NIPS-NORMA the spatial resolution of the imaging system changes linearly between 230–660 μm (corresponding to the distance of 1.5–100 mm from the scintillator screen, respectively). The measured L/D ratio, characteristic to the neutron beam's divergence, is 233.
- For digital image detection, use 5.5 Mpx sCMOS and 1 Mpx CCD (max. 16-bit, i.e. 65536 shades of gray) cameras at RAD and NIPS-NORMA station, respectively. Gray values of the images are corrected for the dark current of the detector and for the beam's inhomogeneity (**Figure 5**).
- During data collection it is possible to follow dynamic processes in time, e.g. water absorption, by consecutive recording of snapshot images (**Figure 10**). The time resolution is in the seconds range for a 16-bit image.

3. The laboratory exercise

The aim of the laboratory exercise:

- The moving of the water front on litmus paper and/or a building material immersed in water can be followed well with consecutive exposures (**Figure 10**). Based on the velocity of water front propagation, the so-called *sorptivity of the sample* can be calculated during the image processing with simple calculations.
- Demonstration (if there is some leftover time): Tomography: 3D imaging presented with the VG Studio MAX software.
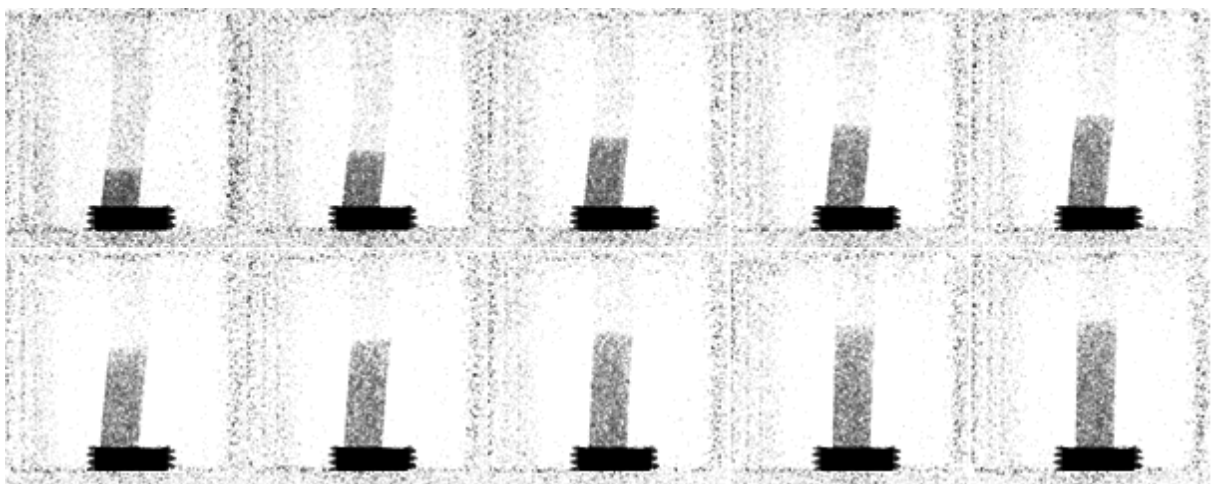

Figure 10. *Incremental snapshots of water uptake by a pH paper*

During the laboratory exercise we will visualize the rate of water uptake in a paper and/or a building material soaked in water by measuring the propagation speed of the water front.

1. In the course of the laboratory training the hardware of the RAD station and software to be used for data evaluation will be presented.

2. In order to increase the contrast, a concentrated water solution of boric acid (H_3BO_3) is used instead of plain water ($\Sigma_m = 3.5$ cm^2 g^{-1}). The boron content of this solution increases the mass attenuation coefficient to $\Sigma_m = 48.8$ cm^2 g^{-1}.

3. We record the 5 *openbeam* and 5 *darkcurrent* images, saved under filenames bi_001–005.tif, and di_001–005.tif for the normalization, using the ANDOR SOLIS program.

4. At 16-bit grayscale resolution and 2 s/image frame rate the imaging system is adequate to follow the rate of transport process. The displacement of the horizontal water front is followed with 100 consecutive images, recorded in each 2 s. The first image is recorded immediately after SOAKING THE SAMPLE IN THE SOLUTION with open beam. We name the 100 files to WaterUptake_001–100.tif.

4. Analysis of the recorded images

1. The recorded images should be normalized (corrected to the dark current of the detector and for the beam's inhomogeneity) by the FIJI plugin called *IMAGE REFERENCING* and saved as results to be analyzed.

2. We import some of the images using the FIJI program's *IMAGE SEQUENCE* module.

3. We mark out the water front's moving area with the rectangle of ROI selection, and record the gray value vertical profile of each picture by the *CTRL+ALT+K* key. We find the profile's pixel coordinates halving the 10 and 90% vertical pixel coordinates distance.

4. In an Excel spreadsheet we plot the above coordinate, after recalculating it to mm units, as a function of the square root of the elapsed time. We fit a straight line to these points; the slope of the regression line gives the *sorptivity of the sample material*.

5. Interpretation of the results

Sorptivity is defined as a measure of the capacity of the medium to absorb or desorb liquid by capillarity. The sorptivity is widely used in characterizing soils and porous construction materials such as brick, stone and concrete.

John R. Philip showed [6] that sorptivity can be determined from horizontal infiltration where water flow is mostly controlled by capillary absorption: $I = S\sqrt{t}$, where S is sorptivity and I is the cumulative infiltration (i.e. distance) at time t. Its associated SI unit is m $\cdot$s$^{-1/2}$.

For vertical infiltration, Philip's solution is adapted using a parameter A_1. This results in the following equation, which is valid only for short times: cumulative $I = S\sqrt{t} + A_1 t$.

Water uptake experiments by neutron imaging can be best applied to the non-destructive characterization of porous materials [7-8].

References

[1] N. Chankow, Neutron Radiography, in: M. Omar (Ed.), Nondestruct. Test. Methods New Appl., InTech, Rijeka, 2012. http://www.intechopen.com/books/nondestructive-testing-methods-and-new-applications/neutron-radiography

[2] I.S. Anderson, R.L. McGreevy, H.Z. Bilheux, eds., Neutron Imaging and Applications, Springer Verlag, New York, 2009.

[3] Neutron Imaging & Activation Group, Neutron Imaging at the spallation source SINQ, (2011). http://www.psi.ch/niag/ImagingBrochureEN/Neutron_Imaging_m3.pdf

[4] Z. Kis, L. Szentmiklósi, T. Belgya (2015) NIPS–NORMA station—A combined facility for neutron-based nondestructive element analysis and imaging at the Budapest Neutron Centre. Nuclear Instruments Methods A 779:116–123.

[5] Z. Kis, L. Szentmiklósi, T. Belgya, et al (2015) Neutron Based Imaging and Element-mapping at the Budapest Neutron Centre. Physics Procedia 69:40–47.

[6] Philip, John R (1957). "The theory of infiltration: 4. Sorptivity and algebraic infiltration equations". Soil Science. 84: 257–264.

[7] Z. Kis, F. Sciarretta, L. Szentmiklósi (2017) Water uptake experiments of historic construction materials from Venice by neutron imaging and PGAI methods. Mater Struct Constr 50:159–173.

[8] V. Crupi, B. Fazio, A. Gessini, et al (2018) TiO2–SiO2–PDMS nanocomposite coating with self-cleaning effect for stone material: Finding the optimal amount of TiO2. Constr Build Mater 166:464–471.

Neutron Activation Analysis

Laboratory exercise

László Szentmiklósi, Katalin Gméling

1. Introduction to neutron activation analysis (NAA)

Instrumental neutron activation analysis (NAA) is a method for quantitative determination of chemical elements based on the conversion of stable nuclei in the sample to radioactive nuclei by nuclear reactions, followed by the quantitation of these reaction products via their gamma radiations. NAA utilizes the delayed gamma rays from the radioactive daughter nucleus (with short or long half-lives), observed after the irradiation. The selective measurement of the radiation gives quantitative and qualitative information about the produced radioactive atoms.

The NAA is especially capable of the determination of trace elements in µg/g concentration-range or below (e.g. impurities in high-purity materials). The typical limits of detection are less than 0.01 µg for 30-50 elements, depending on the nuclear properties of the elements of interest, the actual measurement conditions, the neutron flux, density and, in some cases, the matrix composition.
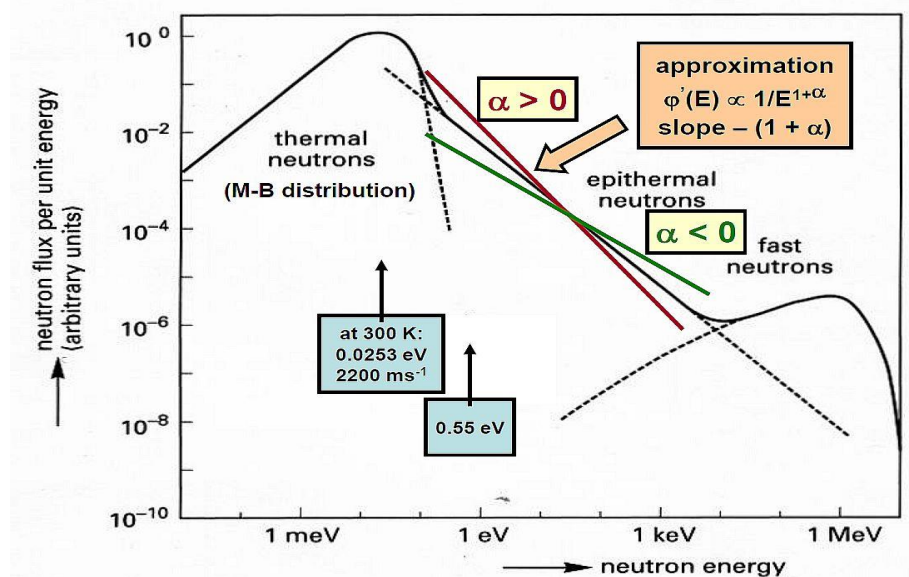

Figure 1. Typical distribution of neutron flux in a thermal nuclear reactor

The fuel elements of the active zone in thermal reactors are surrounded by a moderator. The neutrons generated during nuclear fission within the fuel elements (the so-called fission neutrons) penetrate into the moderator, and undergo elastic scattering on the nuclei of the moderator medium, consequently they gradually slow down. The kinetic energy of these moderated neutrons became into thermal equilibrium with the media, therefore they are called thermal neutrons. Their behavior, in many ways, is similar to the diffusion of noble gases. Neutrons at the irradiation sites of the research reactor have a continuous energy distribution while interacting with the sample. The neutron-energy spectrum of

the thermal reactor spans over a wide energy range and usually divided into three categories (**Figure 1**):

- thermal neutron flux (the energy of thermal neutrons is in equilibrium with the environment) they follow the Maxwell-Boltzmann distribution (E<0.5 eV)
- epithermal neutron flux (0.5 <E<100 eV)
- fission fast neutron flux (100 eV<E<20 MeV)

The epithermal and the thermal neutrons usually induce (n, γ) nuclear reactions; the contribution of fission neutrons is negligible in this reaction channel. The separation of the neutron spectrum to thermal and epithermal ranges has a particular advantage, as in a well-moderated reactor the shape of the energy spectra in these ranges can be well parametrized with model functions: a) The thermal energy neutrons follow a Maxwellian distribution. b) The epithermal neutron energy range distribution can be approximated with a $1/E$ function on a log-log scale. The shape of the thermal/epithermal neutron spectra depends on the design and the power of the reactor, the layout of the active zone and the location of the irradiation site. A further advantage is that thermal neutrons can be filtered with cadmium shielding, so it is possible to activate the samples mainly with epithermal neutrons; the calculation of the epithermal activation contribution is straightforward.

The cross section of the (n, γ) reactions is very low in the fission reactions range, only the thermal and the epithermal ranges are important. However, threshold reactions induced by fast neutrons can also have analytical importance. They can be used for quantitative determination (e.g. ^{58}Ni (n, p) ^{58}Co), and, on the other hand, if the resulting isotope of an interfering (n, x) reaction, where x particle can be p, γ, n, etc. is the same as the product of the (n, γ) reaction, this interference should be taken into account.

All irradiation channels can be characterized by the thermal and epithermal neutron flux (or their ratio instead, i.e. the *f* parameter), the epithermal flux shape factor (*a*), and perhaps with the neutron temperature.

2. Characteristics of NAA

- High sensitivity for minor and trace elements in a wide range of matrices
- Multi-elemental and mostly non-destructive determination
- Small sample amount is enough for analysis
- Significant matrix independence
- Bulk analysis
- External contamination does not disturb or can be eliminated
- Standardization is relatively simple
- It can be considered as a reference method in metrology

The NAA is especially capable of trace element determination (e.g. impurities in high purity materials) in ppm and ppt concentration range. The limit of detection is less than 0.01 μg for 60-70 elements, depending on the nuclear properties of the elements of interest, the measurement conditions, and the neutron flux density and in some cases the matrix composition.

Using one or two activation cycles and subsequent gamma spectrometry measurements 30 to 40 elements can be determined in favorable matrices (multi-elemental or panoramic analysis). By this means, theoretically, it is possible to measure about 2/3 of the chemical

elements. The uncertainties of measurements are between 1-10%, depending on the sample composition and measurement conditions.

For NAA measurements a few milligrams of samples are sufficient. This allows that several samples can be packed together enabling the simultaneous irradiation of these samples under identical irradiation conditions. This feature is extremely important when a standard reference material is co-irradiated during relative standardization (see **Section 3.2.**).

An advantage of the instrumental approach over radiochemical NAA is that only minimal sample preparation or treatment is needed (e.g., homogenization, eliminating surface contamination or pre-concentration). In most cases, non-destructive measurements of the induced radioactivity can be carried out selectively with a high-resolution gamma spectrometer. Element identification based on nuclear characteristics is of high reliability. The mentioned advantages together give the possibility to solve analytical challenges (i.e. rare earth elements analysis in geological samples) which hardly can be carried out by other means. The chemical state of the element does not influence the analytical results at all.

In cases of special needs, the selectivity and precision can be increased using chemical processes (preconcentration, radiochemical separation, pre-irradiation separation).

Planning of the irradiation and measurement conditions is a very important aspect of INAA practice. Unknown samples may contain unexpected, highly activating components. Therefore, before irradiation, the irradiation parameters/conditions must be calculated. The weight of the sample prepared for irradiation should also be estimated, in order to reach suitable activity levels for successful detection, but avoiding instrumental and health physics issues related to highly activated samples. Time parameters are chosen based on calculations and earlier experiences, regarding the temperature and irradiation conditions at the channel. The optimization of irradiation, cooling and measuring times should be done together, considering all important radionuclides formed that have an influence on the selectivity of the measurement and the sensitivity of the analysis via increasing the background or spectral/irradiation interferences.

Like any other analytical method, instrumental NAA has its own methodological and technical limitations. Because of their disadvantageous nuclear properties, some elements cannot or can only be detected with poor sensitivity, e.g. H, B, C, N, O, P (light elements), or Pb, Bi, and Tl. These elements (e.g. O, Pb) can be analyzed well with special measurement set-ups (neutron generator-based NAA) or other activation techniques like PGAA (e.g., H and B). However, matrices composed of the above-listed elements are very advantageous for measuring all other constituents.

3. Standardization methods of NAA

In the case of instrumental neutron activation analysis, the irradiation of the samples is not followed by chemical or physical separation, but the masses of the analyses are determined by mathematical interpretation of the (energy-dispersive) experimental data. There are several methods for quantitative data evaluation – calculating the concentration – in NAA multi-element analysis, depending on the standardization conventions.

3.1. Absolute standardization

One of the experimentally simplest ways to obtain the mass of the element of interest with NAA is based on the following equation:

$$m = \frac{M}{N_A \Theta \varepsilon_{p,\gamma} (\Phi_{th}\sigma_{th} + \Phi_e I_0)} \cdot \frac{\frac{N_p}{t_m}}{SDC},$$ (1)

where m is the mass of the element, M is the atomic weight, N_p is the net peak area, N_A is the Avogadro number, Θ is the isotopic abundance, ε_p is the full-energy peak detection efficiency, γ is the absolute intensity of the gamma-line with energy E_γ. Φ_{th} is the thermal neutron flux, Φ_e is the epithermal neutron flux, σ_{th} is the thermal neutron capture cross-section (at 2200 m/s neutron velocity). I_0 is the resonance integral (integral cross-section for epithermal neutrons), $S= 1\text{-}exp(\text{-}\lambda t_i)$ is the saturation factor, $D=exp(\text{-}\lambda t_d)$ is the decay factor, and $C= [1\text{-}exp(\text{-}\lambda t_m)]/[\lambda t_m]$ is the counting factor, λ is the decay constant: $\lambda=ln2/T_{1/2}$, where $T_{1/2}$ is the half-life, t_i is the irradiation time, t_m measuring time, and t_d is the cooling time.

High-precision experimental determination of ε_p, the absolute detection efficiency is an important prerequisite to the accurate analysis (Szentmiklósi et al. 2018). The M, N_A, Φ, γ and λ constants are usually known with adequate accuracy and precision (uncertainty < 1%) and are tabulated in open nuclear databases. The inaccuracies of the activation cross sections (σ, I_0) and some decay constants can be, problematic. The uncertainty of experimental neutron field parameters' (Φ_{th} and Φ_e) determination can be up to 5-20%. A disadvantage is that it can only be applied for the given measurement set-up.

3.2. Relative standardization

In the relative standardization method, a chemical standard (index s) with a known mass (m_s) of the element to be determined co-irradiated with the sample, and both of them are subsequently measured in the same geometry, on the identical counting system. The weight to be determined m_x is obtained as:

$$m_x = \frac{\left[\frac{N_p/t_m}{D \cdot C}\right] sample}{\left[\frac{N_p/t_m}{D \cdot C}\right] standard} \cdot m_s,$$ (2)

where

$S_x = S_s$, $A_p = N_p/t_m$ is the count rate

$A_{sp} = \frac{N_p/t_m}{S \cdot D \cdot C \cdot m}$ is the specific count rate of the element.

For evaluation the same analytical line of the nuclei is applied. The advantage is that the characterization of the neutron field and use of nuclear constants (Φ_{th}, Φ_{epi}, σ, I_0,... ε_p) are not necessary at all, as the method is based on direct comparison. Although 1% uncertainty can be achieved this way, it is very laborious for routine multi-element determinations.

3.3. Comparator standardisation

Only one carefully chosen comparator standard is co-irradiated with the sample, and all elements are analysed relative to one comparator. The experimental determination of the so-called k_c **factors** is necessary for all investigated elements. Mostly high purity Au-, Ir-, Co-, Zn-, Cu-, Ni- or Fe-foils are used, depending on activation time. The analysed samples

are activated together with the comparators and the quantitative analysis can be done with the known k_c factors. The k_c factor is constant, if the measurement conditions are always the same (e.g. when setting up a new detector, k_c factors must be re-determined) and if the neutron spectrum and the thermal/epithermal neutron flux ratio in the reactor does not change.

3.4. The theory of k0-method

As the neutron channels of the Budapest Research Reactor at BNC are well thermalized and have a high neutron flux ($\Phi_s > 10^{13}$ n/cm²s), we implemented the k_0-**method** that has been developed in a collaboration between the Budapest NAA Laboratory and the University of Gent (Simonits et al. 1976, 1982; De Corte 1987; De Corte Simonits 2003).

Assuming that the sample is point-like (i.e. the neutron attenuation and the gamma absorption are negligible), the epithermal flux distribution (1/E-law) is ideal, and the sample-detector distance is large (d=100-250 mm, so the real coincidence effect is negligible), the k_0-factor can be defined as follows:

$$k_0 = \frac{M* \cdot \theta \cdot \gamma \cdot \sigma_0}{M \cdot \theta* \cdot \gamma* \cdot \sigma_0*} \tag{3}$$

Here the * refers to the comparator element. The k_0-factor is an experimentally determined composite nuclear constant which gives the ratio of the specific activities (A_{sp}) of two elements during irradiation in pure thermal flux ($\Phi_e = 0$).

$$A_{sp} = \frac{N_p / t_m}{S \cdot D \cdot C \cdot w}, \tag{4}$$

where w is the mass of the sample (g).

The k_0 data are nowadays available in the literature, therefore it is enough to determine the thermal/epithermal flux ratio of the irradiation channel $f = \Phi_{th} / \Phi_{epi}$ and the detector's efficiency-energy curve for data evaluation. This way the so-called literature k_0-factors can be converted to our given system using the typical f and ε_p parameters, as follows:

$$k_{anal} = \frac{A_{sp}}{A_{sp}*} = k_0 \cdot \frac{f + Q_0}{f + Q_0*} \cdot \frac{\varepsilon_p}{\varepsilon_p*} \tag{5}$$

The reference k_0- factors are usually given for the Au comparator, because it only has one stable isotope and one characteristic gamma line, and the nuclear data of the (n,γ) nuclear reaction are well known. However, all isotopes can be used as comparators, if their $k_{0, Au}(komp)$ factors are known exactly or determined earlier:

$$k_{0,komp}(x) = \frac{k_{0,Au}(x)}{k_{0,Au}(komp)}. \tag{6}$$

The concentration of the unknown element c_x in a sample of w weight can be calculated as follows:

$$c_x(ppm) = \frac{\left[\frac{N_{p,x}}{t_m \cdot S \cdot D \cdot C \cdot w}\right]}{A_{sp,Au}} \cdot \frac{1}{k_{0,Au(x)}} \cdot \frac{f + Q_{0,Au}(\alpha)}{f + Q_{0,x}(\alpha)} \cdot \frac{\varepsilon_{p,Au}}{\varepsilon_{p,x}}, \tag{7}$$

where a is the epithermal shape-factor and Q_0 is the resonance integral-to-thermal cross-section ratio.

Any (n,γ) reaction can be applied for analysis, if the $k_{0,Au(x)}$ factors, Q_0 and the half-lives are accurately known. The f flux ratio (thermal/epithermal), the epithermal shape-factor (α) and the exact energy calibration of the detector's efficiency at the time of the activation has to be determined experimentally with great care. Additionally, corrections must be applied in order to take into account the effects of the non-ideal irradiation conditions.

There are several ways (e.g. Cd ratio method) to determine the $f = \Phi_{th}/\Phi_e$ flux ratio. One of the simplest methods is to irradiate a thin Zr foil (so-called flux monitor) together with the samples. Zirconium has favorable features for using as a multi-isotopic flux monitor, because of its two isotopes can be characterized by very different Q_0 values, and they are known to high precision: ^{94}Zr(n,γ)^{95}Zr Q_0=5.31 and ^{96}Zr(n,γ)^{97}Zr Q_0=251.6. The measured gamma-lines have high energies (gamma-absorption is negligible) and are free of true coincidences. Measuring the radiation of the Zr foil and with the exactly known $k_{0,Au}$(^{95}Zr, ^{97}Zr) values, the actual f flux ratio can be expressed as:

$$f = \frac{\frac{k_{0,Au(1)}}{k_{0,Au(2)}} \cdot \frac{\varepsilon_{p,1}}{\varepsilon_{p,2}} \cdot Q_{0,1}(\alpha) - \frac{A_{sp,1}}{A_{sp,2}} \cdot Q_{0,2}(\alpha)}{\frac{A_{sp,1}}{A_{sp,2}} - \frac{k_{0,Au(1)}}{k_{0,Au(2)}} \cdot \frac{\varepsilon_{p,1}}{\varepsilon_{p,2}}}, \tag{8}$$

where (1) ^{95}Zr (724.2+756.7 keV), (2) ^{97}Zr (743.3 keV)

4. The role of the α parameter

The 1/E distribution for the epithermal neutron spectrum is only valid under certain conditions. The $1/E^{1+\alpha}$ function gives a better approximation to the real epithermal neutron flux, where **α is the epithermal shape factor**. Corrections are developed in order to measure the bias from ideal case, as in most (n, γ) reactions there are more than 100 resonances.

The calculation of $I_0(\alpha)$ and $Q_0(\alpha)$ is based on (as I_0 and $Q_0 = \frac{I_0}{\sigma_{th}}$ are available in tables) the E_r effective resonance energy values, which were introduced at reaction rate calculations (Ryves, 1969).

$$Q_0(\alpha) = \frac{Q_0 - 0.429}{E_r^\alpha} + \frac{0.429}{(2\alpha+1)(0.55)^\alpha} \tag{9}$$

The value of α is generally zero or negative in light water moderated reactors, at the poorly thermalized channels close to the zone. In other types of reactors (e.g. graphite, heavy water moderated) the value of α can be up to +0.2. In low-power reactors, the parameters of irradiation channels do not vary for longer periods of time, but the ones with higher power (more intensive fuel-burn-up) they change more significantly because of the frequent core reconfigurations.

Three different methods are developed for simultaneous determination of the thermal/epithermal flux ratio and α: irradiation only with Cd-cover, with and without Cd-cover and without Cd-cover. The latter, without cover version, uses the Bare Triple Monitor method with ^{94}Zr, ^{96}Zr and ^{197}Au isotopes.

5. Analytical applications

- NAA is frequently used to **certify the concentrations of elements** in standard reference materials of environmental, biomedical and geological origin
- In the field of **nuclear energy production,** the corrosion products of structural materials in the primary coolant of nuclear power plants were determined.
- Adsorption-desorption processes on structural **materials of nuclear power plants can be investigated** using the radiotracer technique. The extent of the adsorption of the metal ions of corrosion (Cr, Fe, and Co) and some fission products (Cs, Ce, I) on the surfaces of structural materials (stainless steel and Zr1%Nb alloys) were studied.
- **In the field of environmental chemistry,** NAA is suitable for analyzing the chemical properties of industrial aerosols.
- The associations between the **environmental hazards**, **nutrition-related diseases,** and essential micro and macro elements can also be investigated with this method.
- **Selective irradiation** has an important role in instrumental activation analysis, which enables the determination of many elements with high precision and sensitivity within short turn-around time. Boron filter (B_4C) has been constructed and used for epithermal neutron activation analysis of biological, geological and fiberglass samples. Using a boron shield the NAA method can be used to samples with unfavorable matrices (e.g. Na, Ca, Sc, P) and when the induced activities of major components are high.
- **Monitoring water chemistry parameters** is required for the safe operation of the research reactor. The activity concentrations of characteristic fission and corrosion products in the primary cooling water and the concentrations of different impurity components in various water systems and in the spent fuel ponds of the Budapest Research Reactor (BRR) are measured.
- In the research field of **nuclear waste treatment and disposal**, the radionuclide ^{135}Cs, which is one of the difficult to measure nuclides, was determined in nuclear waste samples. The method based on the selective separation of Cs and the detection of ^{135}Cs by two independent measuring methods, i.e. NAA and ICP-MS.
- **In geological samples** rare earth elements are determined and meteorites can be studied as well.

6. NAA at the Budapest Research Reactor (BRR)

The Budapest Research Reactor is a light-water moderated and cooled tank-type reactor. The thermal power of the reactor is 10 MW, whereas the thermal neutron flux in the core can reach 2.2×10^{14} cm^{-2} s^{-1}. There is a possibility of short, and long term irradiation of samples for instrumental neutron activation measurements.

6.1. Short-term irradiation at the BRR with fast rabbit system

There are 40 vertical irradiation channels in the research reactor, and one of them is equipped with short time irradiation possibility directly from the laboratory (**Figure 2**). The rabbit system ensures that the irradiated sample goes from the reactor zone to the gamma spectrometer in the shortest time possible. With the present parameters of the research reactor (zone design, reactor power, neutron flux parameters: thermal, epithermal, fast) irradiations up to 5 minutes can be carried out while cooling the carrier capsule with CO_2 gas stream.
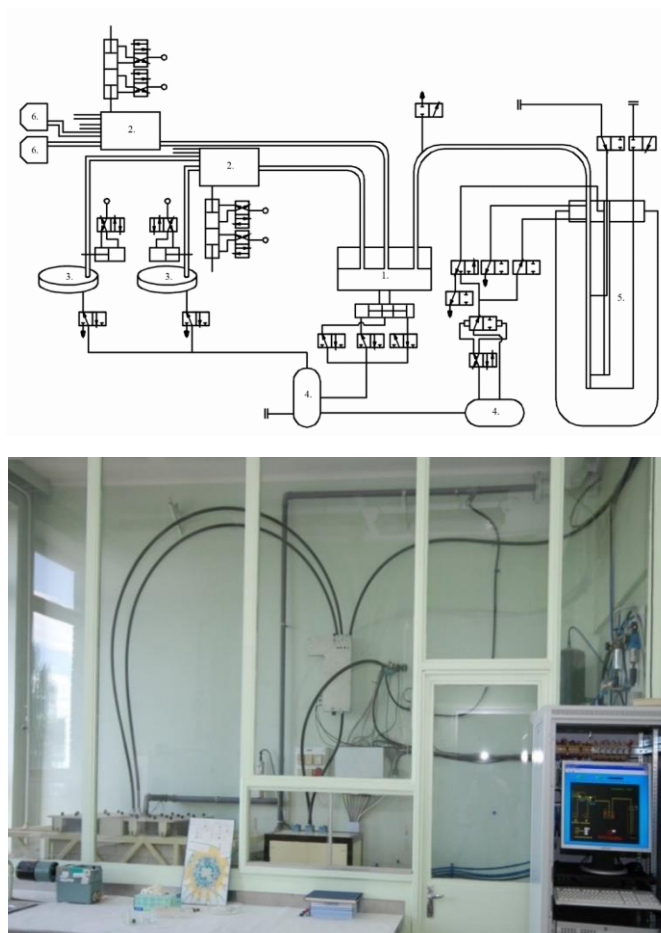

Figure 2. *The block scheme (top) and a photo (bottom) of the fast rabbit system at the BRR. 1. Sender/Receiver Station, 2. Router, 3. Delay Stacker, 4. Air tank, 5. Reactor vessel, 6. Drop Out Station.*

Figure 3. Few mg of powdered samples are wrapped in Whatmann 41 filter paper which is hydraulically pressed for pellet and placed into high purity polyethylene capsules. Larger polyethylene carrier is loaded into VESPEL plastic, ready for irradiation.

Operation of the fast rabbit system:

- Few tens of mg of the samples are weighted into high purity polyethylene capsules or prepared in pellet form of 6 mm diameter using manual hydraulic press and Whatmann 41 filter paper for packing (**Figure 3**), and placed to the loading station in a small polyethylene (PE) capsule (8 mm x 5 mm), and in an inner and outer capsule (1.) (**Figure 3**). In the same irradiation capsule, but separate holder an element comparator of known weight (e.g. Zr, Au, Cu) is co-activated.
- The sample from here gets to the irradiation channel of the reactor with pressurized air.
- The arrival of the sample to the end position in the channel is detected by a sensor that activates the pre-set countdown counter for irradiation time.
- At the end of the irradiation compressed air brings back the capsule to the sample loading station (1.).
- From here, depending on its induced radioactivity the capsule goes either to one of the sample handling glove boxes (6) or one of the delay stackers for decay (3) using compressed air.

An irradiation sheet is electronically stored reporting irradiation conditions, the person responsible for irradiation, sample identifier, sample weight, typical nuclides created in the sample, estimated activity, irradiation time, exact date and time of irradiation. Neutron flux parameters have been measured with the "Bare Triple-Monitor".

6.2. Long-term irradiation at the BRR

Long-term irradiation (typically 1–24 h) is done separately, in the No. 17 rotating, well-thermalized channel located in the Be reflector (thermal neutron flux density is 2×10^{13} $n \cdot cm^{-2} \cdot s^{-1}$; **Figure 4a**). Samples, in dried and powdered form (50–200 mg), are weighted and sealed in high-purity quartz ampoules (**Figure 4b, c**). A set of 6 quartz ampoules are wrapped together using aluminium foils (**Figure 4e**), as well as monitor foils of Au, Zr or

Ni (**Figure 4d**). Samples are irradiated in hermetically closed Al carriers (**Figure 4f**). After irradiation and a typical decay time of 3–4 days, the quartz vials are unpacked and surface cleaning. Each sample is counted for two or three times. The first measurement takes place at about 4-5 days after irradiation (for 10-15 minutes) when the elements As, Br, Ca, K, La, Na, Sb, U can be determined. The second, optional measurement takes place 7-14 days later (for 1–2 h), if the detection limits are needed to be improved, i.e. during this period the ^{24}Na, ^{42}K isotopes decay out. After a cooling period of 15–30 days (when the ^{82}Br, ^{140}La isotope decayed out), the samples can be counted for the third time for 2–6 hours at appropriate distance, when typically Ba, Ce, Co, Cr, Cs, Eu, Fe, Rb, Sb, Sc, Ta, Tb, Yb, Zn, Zr elements are analyzed.
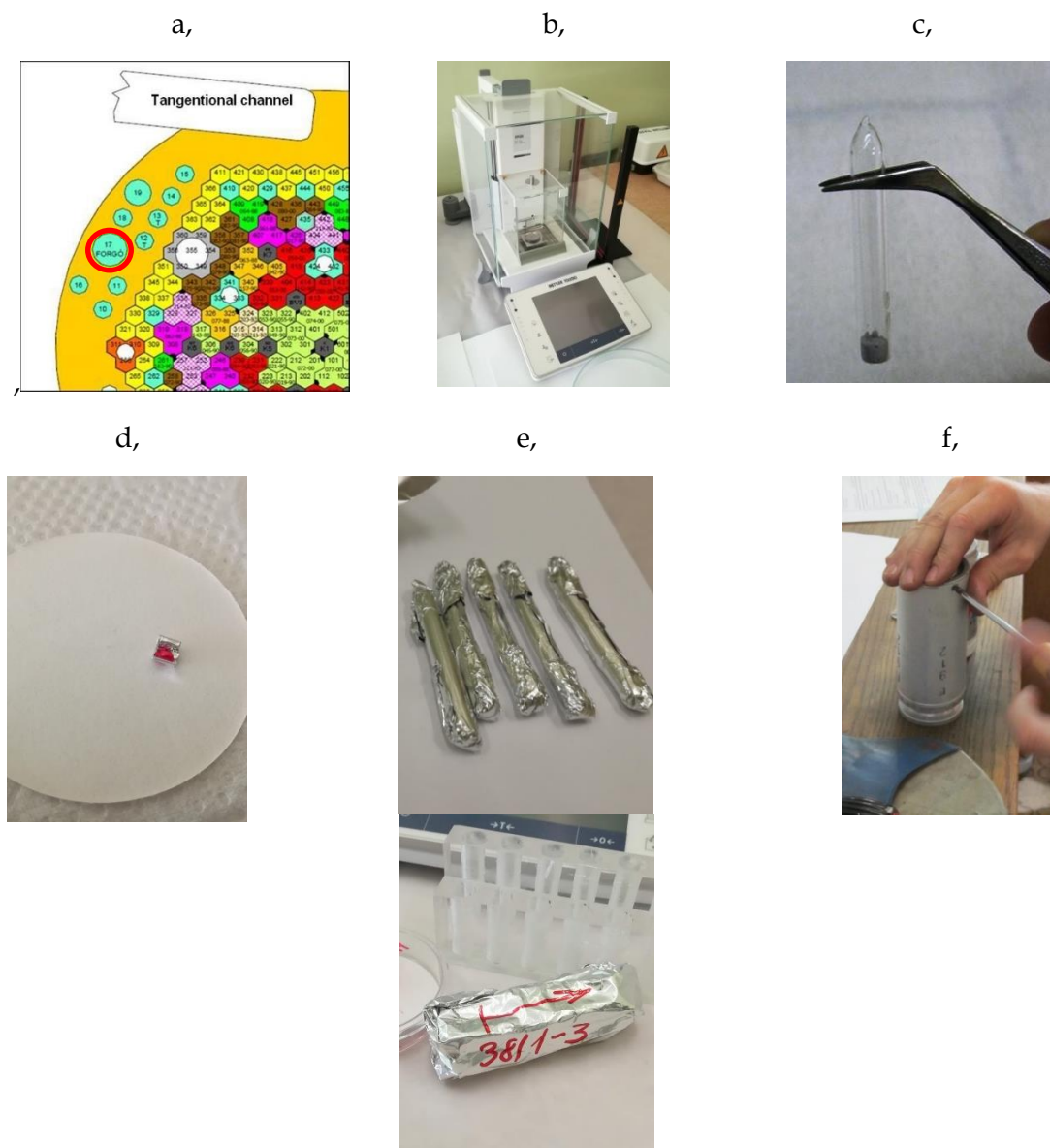
a,

b,

c,

d,

e,

f,

Figure 4. *a, The N⁰. 17 rotating, well-thermalized channel in the Be reflector of the BRR, used for long-term irradiation. b, METTLER TOLEDO XPE microbalance. c, High purity quartz ampules containing powdered rock samples. d, Monitor foil set, wrapped in high purity Al-foil. e, Sealed quartz ampules wrapped separately and as a pack in aluminum foil. f, The pack is hermetically closed in an Al carrier, ready for irradiation.*

The protocol during long-term irradiation NAA:

- 50-150 mg of the powdered, well homogenized, and dried samples are sealed in a surface cleaned high purity quartz ampoules (8 cm long, 6 mm ∅, Heraeus Suprasil ®). A set of 6 quartz ampoules are wrapped together with monitor foils of Au, Zr and Ni/Fe ("Bare Triple-Monitor"). Samples are irradiated in a hermetically closed aluminum container.
- The container containing the samples is manually placed in the 2nd position of the well thermalized, rotating vertical channel of the BRR.
- After the requested irradiation time, the container put out and placed to the hot cell, where the aluminum container is opened up.
- From here, after 3-4 days cooling time, the samples are carried up to the laboratory to be cleaned from alumina foils and surfaced cleaned with acid.

The irradiation parameters are recorded in report sheet containing person responsible for irradiation, exact irradiation time, start and finish, typical nuclides created in the sample, estimated and measured activity after irradiation. Neutron flux parameters have been measured with the "Bare Triple-Monitor".

7. Gamma-spectrometry of NAA

After short- and or long-term irradiation of the sample, the decay gamma measurements are following the same procedure. The hardware and software of the NAA laboratory at BNC had been upgraded (Szentmiklósi et al 2016.) recently. The gamma-rays emitted from the samples are counted in low-level counting chambers (to reduce the external background), with a carefully calibrated p-type Ortec HPGe detector, having an energy resolution of 1.75 keV and relative efficiency of 55 %, in a 50-3300 keV energy range. The detector is connected to a dual-input ORTEC DSPEC 502 spectrometer, and operated by the ORTEC Maestro 7 software. The spectra are recorded with 2×16 k channel and zero-dead time (ZDT) option. The immediate result of a gamma spectroscopy measurement is the raw spectrum, in which full energy peaks appear corresponding to gamma photons of different energies. Channel numbers on the gamma spectra's horizontal axis can be calibrated in gamma energy (keV) based on known energy gamma lines of standard radioactive isotopes. Gamma spectrometers usually have very good linearity, which makes the so-called two-point calibration possible, in combination with the nonlinearity. The radioactive nuclei (chemical elements) can qualitatively be identified by their peak positions (energies) of the measured gamma peaks, while the quantity, i.e. the concentration of isotopes (elements) can be derived from their background corrected net peak areas.

The corrected and uncorrected halves of the spectra are stored in a single SPC file. For spectrum evaluation, HyperLab 2013.1 software is used. For identification of radioactive isotopes and for calculation of the element concentrations, KayZero for Windows 3.06 program (De Corte et al. 2001) is applied, which is able to take into account the thermal-epithermal neutron flux ratio (f), alpha (a), and Fc calculation factors. KayZero calculates concentrations using the k_0-standardization method, according to Ref. (De Corte and Simonits 2003).

7.1. Calibration of the gamma spectrometer

The calibration of the gamma spectrometer is based on the determination of three fundamental parameters: *detection efficiency, channel-energy calibration with nonlinearity and*

the energy resolution. Certified gamma-sources are used to determine these parameters, whose energy and activity data are known to high precision and whose gamma-lines are distributed evenly in the measured energy range (50-3300 keV). The detection-efficiency is measured with ^{241}Am, ^{133}Ba, ^{60}Co, ^{137}Cs, ^{152}Eu, ^{226}Ra sealed radioactive point sources and with additional radioisotopes produced in research reactor or accelerator, like ^{51}Cr, ^{56}Co, ^{65}Zn, ^{198}Au, ^{110m}Ag, ^{75}Se. Calculations are carried out with the EFFICIENCY, NONLINEARITY and RESOLUTION ANALYSIS modules of HyperLab program.

7.1.1. Detection efficiency

One of the most important parameters of γ-detectors is the **absolute full-energy peak efficiency** (ε_p (E_γ)). Its value gives the proportion how much a gamma-radiation with E_γ energy emitted by the source contributes to the corresponding measured full-energy peak in the spectrum. It can be described by a 6-8 degree polynomial on a log-log scale (**Figure 5**). The absolute full-energy peak efficiency of a given detector depends on the source-detector distance, the shape, and extent of the source and its γ-ray energy.
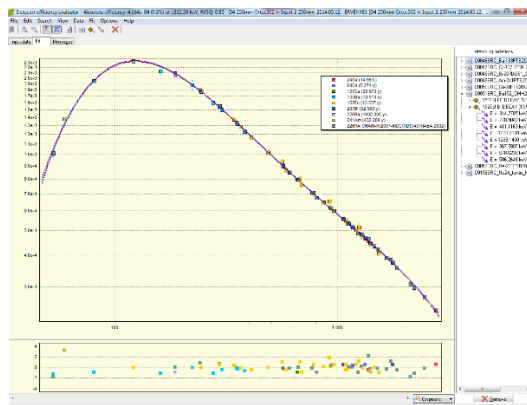

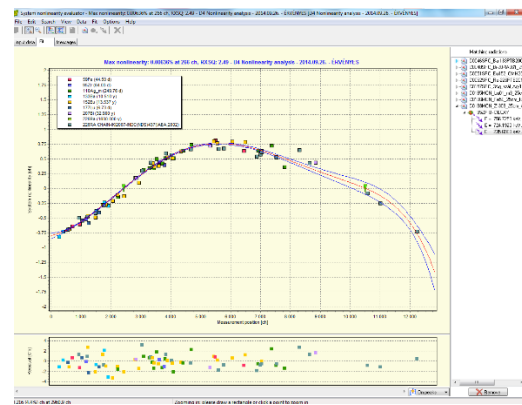**Figure 5.** *The absolute efficiency curve of the NAL NAA D4 spectrometer for point-source geometry*

Figure 6. *The nonlinearity of the NAL NAA D4 spectrometer*

7.1.2. Nonlinearity

The partial processes of the detection and the signal processing are fundamentally linear in nature, thus the channel number of the spectrum is proportional with the energy. In practice, this is not completely true. The linearity of the energy determination can be improved further during the spectrum evaluation by correcting it with its experimentally determined small deviation from linearity, which is caused by the electronics and hence is constant over a period for a given set-up. The systematic, thousandths-level deviation is the so-called **differential nonlinearity**. The nonlinearity calibration is determined from the same set of data as the efficiency when peaks of well-known energies are measured, and the differences of positions and literature data are fitted with a polynomial. Energies measured in the analysis are then corrected with this function (**Figure 6**).

7.1.3. Energy resolution

In gamma-spectroscopy, the **energy resolution of the detector** plays a key role. It is characterized by the *FWHM*: (*full width at half maximum*), which is about 1.8 keV for the ^{60}Co peak at 1332.5 keV (**Figure 7**). The spectrometer's resolution is determined by the electronics and the detector together and can be given as the square sum of the 3 terms as a function of energy. These are the contributions from the electronics, the statistical fluctuation of charge production and the effects of the imperfect charge collection of the detector, respectively.
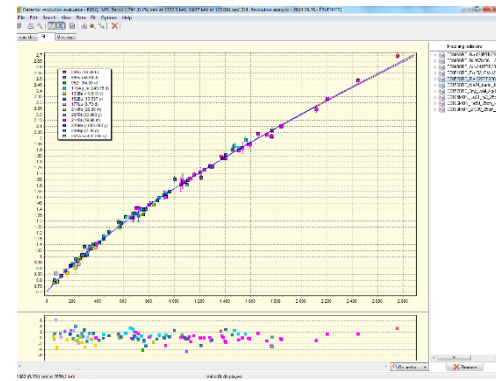

Figure 7. The energy resolution of the NAL NAA D4 spectrometer

7.2. Evaluating gamma spectra, calculating the concentration

The analytical information of the spectra is in the full energy peak positions and their area. The goal of the spectrum evaluation is the most precise determination of these parameter couples for every peak.

For spectrum evaluation, the *HyperLab* program is used. At first, a low- and a high-energy intense peak of a known nuclide is chosen to calibrate the energy axis and peak-widths. Next, the program runs through the spectrum, identifies the peaks significantly above the background, determines the optimal limits of the regions and fits the model function in each region. From these, peak positions, peak areas, and their uncertainties can be determined. After the **automatic fit**, results shall be revised regarding the χ^2 values and the residuum. Where it is necessary, peaks should be added or removed, region boundaries or the model functions have to be modified in order to make the fit better.

Figure 8 shows a fit of a region from a geological sample by the *HyperLab 2013* program. The step function is clearly visible under the asymmetric peaks with the so-called 'tail' on the right-hand side. The fitting is finished after the **nonlinearity and efficiency** are loaded. The former is transformed to zero value at the energy calibration base points. The last task is the creation of a **peak list (PTF)** file, which contains peak positions, their energies, half-width values, area, their uncertainties and the χ^2 values of the fits in a tabulated form.
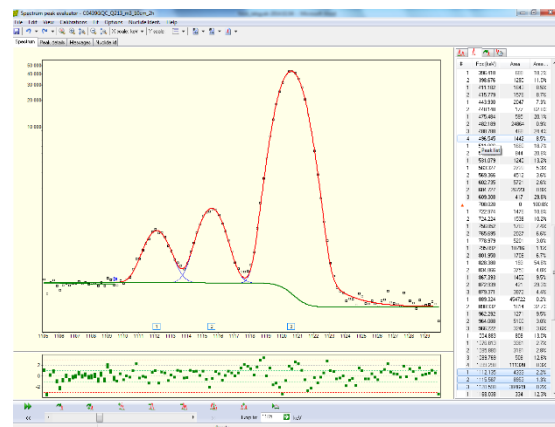

Figure 8. A region of a geological sample's spectrum fitted with HyperLab 2013 program.

7.3. Calculating the concentration

KayZero for Windows 3.06 program is used for the identification of radioactive isotopes and for element concentration calculations, that is based on the k_0-standardisation (**Figure 9**). There are is a possibility to make a working folder to each and every irradiation/measurement package and fill up the data of monitor set and also the measured samples, reading in the *.spe* and *.ptf* files of the spectrum and peak lists (**Figure 9a**). From the data corresponding to **Zr and Au monitors** the *f* **flux ratio** and **α parameter**

can be calculated with the Bare-Triple Monitor method (**Figure 9c**). Fission neutron flux can be calculated from **Fe and/or Ni monitor data** for the corrections of nuclear interferences. The resulting elemental concentrations must be corrected for those of the blank samples. In the case of short-time irradiations, the Na, Al, Cl and Br content of the filter paper, while in case of long irradiations the Na content of the quartz ampoules has to be taken into account. Reaction interferences caused by fast neutrons are corrected by the program if the interfering nuclear reactions result in the same radioisotope, e.g. $^{23}Na(n,\gamma)^{24}Na$ interferes with $^{27}Al(n,\alpha)^{24}Na$ and $^{24}Mg(n,p)^{24}Na$. During quantification of Al, Mg, and Na, corrections for the fast-neutron-induced interfering nuclear reactions of Si and Al have to be carried out. The Cr and Mn concentrations have also been corrected with the sample's Fe content. Because of the interferences originating from the neutron-induced fission of ^{235}U, corrections have been applied depending on the uranium content of the sample (>10 ppm) when determining Zr, Mo, Ba, La, Sm, Nd and Ce elements.
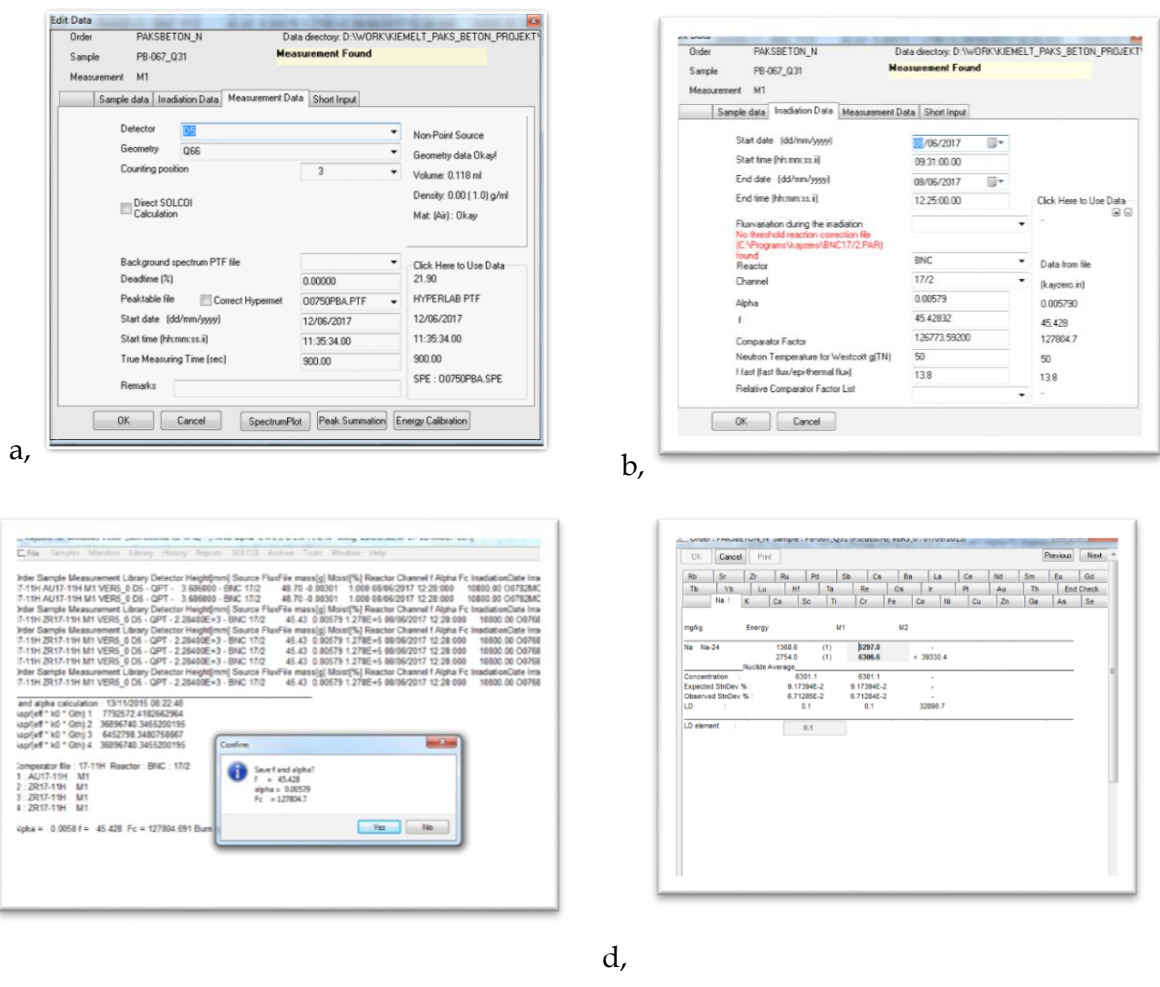

a,

b,

c,

d,

Figure 9. a, KayZero for Windows 3.06: reading in the.ptf files of peak lists. b, All parameters of irradiation, containing information about the irradiation channel and its parameters are uploaded. c, KayZero for Windows 3.06 program: calculating f and a parameters with the Bare-Triple Monitor Method. d, Major gamma-peaks of the measured elements, and concentrations calculated from them. The analyst can enforce its experience.

8. The laboratory exercise

During the laboratory exercise, geological standards and reference materials are prepared by the participants into high-purity quartz ampoules for long-term irradiation at the sample preparation room, using METTLER TOLEDO XPE microbalance. A Bare-Triple monitor set is also prepared and packed together for co-irradiation. One sample will be also prepared for short-term irradiation and irradiation will be demonstrated in the rabbit-system laboratory. Unpacking of long-term irradiated sample pack can be experienced behind lead shielding by the participants (for safety reasons on inactive samples). Previously irradiated geological standard and monitors will be measured in one of the low-level counting chambers of the laboratory. The collected spectra will be fitted with HyparLab 2013 software, and afterward, concentrations will be calculated with the Kayzero for Windows program. The results can be compared to the certificate of the measured sample.

8.1. Workflow of the laboratory exercise:

1. Sample preparation: weighting the powdered standard geological samples into quartz ampules and also making pastilles out of them.
2. Visiting the fast rabbit system lab, and theoretically irradiating the prepared sample. In the same lab wrapping out (inactive) quartz ampules from aluminum foil and surface cleaning of quartz.
3. Previously activated samples are placed in a low-level counting chamber for recording gamma spectrum.
4. Fitting the collected spectra with HyperLab program. Energy calibration, and generating of the peak list file.
5. Elemental concentrations are to be calculated with the Kayzero for Windows program. Loading in the sample parameters and peak list file, and recalculated with previously collected spectra from the same sample.
6. Comparison of results with reference data.

References

De Corte F, van Sluijs R, Simonits A, et al.: Installation and calibration of Kayzero-assisted NAA in three Central European countries via a Copernicus project Appl. Radiat Isot 55, 347–354. (2001)

De Corte F., Simonits A., Recommended nuclear data for use in the k0 standardization of neutron activation analysis. Atomic Data and Nuclear Data Tables 85, 47 (2003).

De Corte F.: The k0-standardization method. Habilitation thesis, Rijksuniversiteit Gent, Gent 1987. http://www.kayzero.com/k0naa/k0naaorg/Links_files/The%20ko-Standardization %20Method.pdf

Ryves, T. B., 1969, Metrologia 5, 119 (1969).

Simonits, A., De Corte, F., Hoste, J., Zirconium as a multi-isotopic flux ratio monitor and a single comparator in reactor-neutron activation analysis. J. Radioanal. Chem. 31, 467 (1976).

Simonits, A., De Corte, F., Moens, L., Hoste, J., Status and recent developments in the k_0-standardization method. J. Radioanal. Chem. 72, 209 (1982).

Szentmiklósi, L., Párkányi, D., & Sziklai-László, I. (2016). Upgrade of the Budapest neutron activation analysis laboratory. Journal of Radioanalytical and Nuclear Chemistry, 309(1), 91–99.

Szentmiklósi, L., Maróti, B., Párkányi, D., Harsányi, I., Révay, Zs.: High-energy detector calibration data for k_0-neutron activation analysis, Journal of Radioanalytical and Nuclear Chemistry (2018) 315: 743-750

Prompt Gamma Activation Analysis

A practical guide

László Szentmiklósi, Zsolt Kasztovszky

1. Introduction to prompt-gamma activation analysis (PGAA)

1.1. Development of the PGAA technique

All activation analytical methods are based on nuclear reactions, in which the atomic nuclei in the sample are excited. By detecting of the emitted radiation qualitative and quantitative analysis is possible. Thanks to their advantages (high selectivity, high sensitivity, non-destructive-, matrix-free- and panoramic features) they are competitive with the more common analytical methods.

The first neutron activation experiment has been performed by György Hevesy and by Hilde Levi in 1936, just four years after the discovery of neutron (Chadwick, 1932). Already in the mid-1930s, prompt gamma radiation was incidentally observed when hydrogen-containing material was irradiated by slow neutrons.

Two basic types of neutron activation analysis exist. If the irradiation and the detection of γ-photons are separated in space and time, and only the decay γ-photons are detected, this is the "traditional" **Instrumental Neutron Activation Analysis (NAA)**. In case of **Prompt Gamma Activation Analysis (PGAA)** and **Neutron Resonance Capture Analysis (NRCA)** the activation and the detection of γ-photons are simultaneous. For PGAA the analytical signals are usually originating from the radiative capture of lower energy neutrons, while for NRCA from a resonance-like capture of more energetic neutrons into atomic nuclei.

The first PGAA experiment at a research reactor was performed at the Cornell University, US in the 1960s. Although the principles have been already known for some time, it became more widespread only in the 1980s, and was started to be applied as a routine multi-element analytical method since the 1990s.

Until recent times, a crucial limitation of the method was the lack of reliable spectroscopic data. At the turn of the Millennium, significant efforts were made to develop a suitable PGAA spectroscopic library (Molnár 2004).

At present, only a handful of reactor-based PGAA facilities operate all over the world. Besides Hungary, the most important ones are in Germany, Japan, the United States, South Korea and India. A new instrument is under construction in Morocco and Egypt. The Budapest PGAA laboratory is in operation since 1996.

1.2. Production and classification of neutrons

Neutrons can be classified according to their energies. Neutrons, which are in thermal equilibrium with the environment, are referred to as **thermal neutrons**. Thermal energy is

equivalent to $kT = 25.26$ meV[2] as a characteristic energy at room temperature, or with 2198 m s^{-1} as a most likely velocity. The thermal neutron energies follow Maxwellian distribution. Neutrons having lower energies (~5 meV) are called **cold neutrons**, while those with an energy over 0.1 eV are called **epithermal**. Neutrons with energies of MeV order are called **fast neutrons**. However, these threshold limits are not definite; it is more precise, if we differentiate according to energy distribution, i.e. energy spectrum of neutrons. In the epithermal energy range, the energy distribution can be approximated with an $1/E$ function on log-log scale, while fast neutrons show the features of a fissile neutron spectrum, and can be fitted with the Watt-formula.

In a nuclear fission, fast neutrons are produced, but the probability of the neutron capture is the highest for thermal and for cold neutrons. Therefore, fast neutrons are slowed down by multiple collisions with suitable moderators made of light elements. This process is called thermalization. At a research reactor, a so called **cold neutron source**, an additional liquid hydrogen or deuterium containing cell in the path of the neutrons can be applied in order to produce external beam(s) of cold neutrons.

The probability of the interaction between neutrons and the atomic nucleus is characterised by the quantity called **cross-section**; it has the unit of **barn**[(3)]. In case of slow (i.e. cold and thermal) neutron capture, most practically relevant nuclei follow the so-called **1/v-law**. It means that the neutron capture cross-section (σ) is inversely proportional to the velocity of neutrons, i.e. with the square root of neutron energies. In this energy range, σ is easy to calculate from the σ_0 values, a cross-section corresponding to v_0=2200 m s^{-1} neutron velocity:

$$\sigma = \sigma_0 \frac{v_0}{v} \tag{1}$$

where $\sigma_0 = \sigma_0(v_0)$ is the so-called **thermal neutron capture cross-section**. For characterisation of the chemical elements, the average of isotopic cross-sections weighted by isotopic abundances (Θ) is used:

$$\sigma = \sum_i \Theta_i \, \sigma_i \tag{2}$$

1.3. Main features of PGAA

-   PGAA is based on the **radiative neutron capture**. Based on the energy and intensity of the **γ-radiation** arising from the reaction one can determine the exact composition of an unknown sample. Neutron capture occurs on every nucleus except ^{4}He, thus the method is in principle applicable to the simultaneous **determination of every chemical element**.
-   Typically, well measurable are some light elements (H, B, Cl), heavy metals with environmental significance (Cd, Hg), and some rare earth elements important in geochemistry (Nd, Sm, Gd and Eu).
-   PGAA is suitable for **panoramic analysis**, i.e. when the concentration or detection limits of every component in an unknown sample are determined at once.

---

[2] 1 eV=1,602 176 462 (63)×10^{-19} J
[(3)] 1 barn = 10^{-28} m^2

- The most important advantage of PGAA is the **simplicity or absence of sample preparation**. In most cases, powders or liquid samples packed in Teflon foil or in Teflon vial are irradiated. Solid samples (e.g. rocks, artefacts) can be investigated without packaging.
- During the analysis, the number of transmuted nuclei is much less than those in case of NAA, thus the isotopic composition is practically not affected (no burn-up effect) and the induced radioactivity is negligible in most cases. Consequently, the method is considered as **absolutely non-destructive** and suitable to study valuable or unique samples.
- The energies and intensities of the emitted photons are determined exclusively by nuclear parameters, and thus are independent of chemical environment of the samples. Therefore, in most cases, PGAA is considered to be **matrix-free**.
- Both impinging neutrons and emitted gamma photons can penetrate through a few cm thick layers, therefore PGAA – contrary to many other analytical methods – provides the **average bulk composition of the irradiated and observed volume**. With the help of collimated neutron beam, elemental distribution in an inhomogeneous sample can be determined, too.
- **Detection limits** of PGAA vary within a wide range from one element to another, and usually, they are significantly higher than those of NAA or of ICP-MS (inductively coupled mass spectrometry). The best detectable elements can be measured at 0.1-1 ppm level, while those with low neutron capture cross-sections can be quantified only if they are major components.
- PGAA has a **broad dynamic range**. It means that from the minimum detectable amount of element *A* in *B* and from the minimum detectable amount of element *B* in *A*, the *A/B* ratio can vary within an order of 6 to 8. This interval may not be symmetric.
- The uncertainty budget of the measurement and of the evaluation can be rigorously described with statistical methods, and thus the uncertainty of a single measurement can be estimated with a high confidence. The intensity of signals (i.e. the count rate or counts per unit time) from prompt-γ photons is constant, thus **the accuracy of the results can be improved with increasing acquisition time**.
- The PGAA method does not require standardisation measurements for each sample types; a common nuclear data library is suitable for all kinds of samples.
- On the other hand, PGAA is not competitive with the mainstream element analytical techniques in aspects of availability, productivity, cost and simplicity.

1.4. How is the analytical signal produced?

When a slow neutron is captured, a **compound nucleus** is formed first. The excitation energy of the compound nucleus is equivalent to the binding energy of the neutron (7–9 MeV), as the kinetic energy of the neutron is negligible. The compound nucleus can decay through various de-excitation channels, followed by the emission of γ-photons or charged particles.

So, the primary source of the analytical signal is the radiative neutron capture, with other words, the (n, γ)-reaction (**Figure 1**). During the (n, γ)-reaction, the daughter nucleus emits prompt **γ-photons**, starting from the capture state and in one or several steps it reaches the ground state ($\gamma_1 \ldots \gamma_5$, **Figure 2**). The energies and intensities of the γ-photons are

characteristic to the de-excitation of the daughter nucleus of (A+1) mass number, and thus indirectly to the parent nucleus. This nuclear reaction takes place mostly within 10^{-12} s, that's why the reaction called "prompt". When the $^{A+1}_{Z}X$ daughter nucleus is stable, the reaction ends with the emission of prompt-γ photons. However, in some cases **radioactive** daughter nucleus is produced that transforms further to a stable one – mostly emitting $β^-$particle with a definitive $T_{1/2}$ half-life. In much less cases, $β^+$-decay or electron-capture may occur. During PGAA, both prompt- and **decay-γ photons** ($γ_6$ in **Figure 2**) are detected and can be utilised in the analysis.
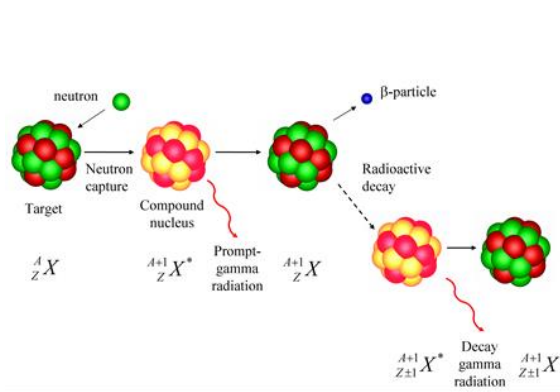

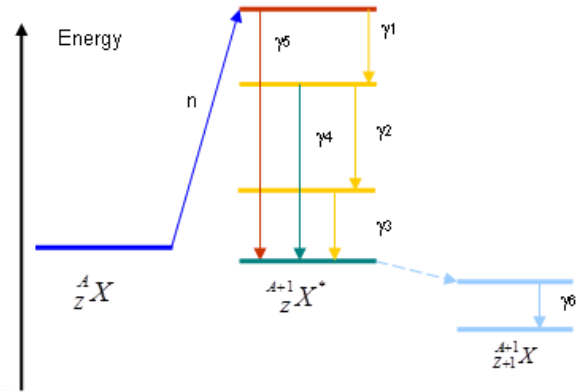**Figure 1.** *The origin of the analytical signal in PGAA*

Figure 2. *The decay scheme of radiative neutron capture and a subsequent $β^-$-decay*

1.5. Quantitative analysis

The number of the emitted prompt-γ photons at a given gamma-ray energy, relative to the number of neutron captures, gives the quantity called **emission probability** ($P_γ$). This emission probability multiplied by the neutron capture cross-section and by the isotopic abundance ($θ$) is the **partial gamma-ray production cross-section** ($σ_γ$), a compound nuclear quantity of the fundamental importance in PGAA.

$$σ_γ = σ_0 P_γ θ \tag{3}$$

The basis of the quantitative analysis is that the **count rate $\frac{dN_P}{dt}$ of a peak with $E_γ$ energy is proportional to the number of atoms emitting γ-photons of the given energy**. In general, a sample with volume V, irradiated with a neutron beam, will produce a count rate of:

$$\frac{dN_P}{dt} = \int_V \int_{E_n=0}^{\infty} \frac{μ(r)N_{Av}}{M} σ_γ(E_n) Φ'(E_n, \boldsymbol{r}) ε'(E_γ, \boldsymbol{r}) dE_n d\boldsymbol{r} \tag{4}$$

in an $E_γ$ peak, where N_P is the peak area, $μ(\boldsymbol{r})$ is the mass density of the analyzed element as a function of position vector **r** in the sample, N_{Av} is the Avogadro number, M is the relative atomic mass of the element, $Φ'(E_n, \boldsymbol{r})$ is the neutron flux as a function of neutron

energy and the position within the sample, $\varepsilon'(E_\gamma, \mathbf{r})$ is the counting efficiency of the detector. With the help of these position-dependent quantities, the inhomogeneous composition of the sample, the spatial inhomogeneity of neutron beam intensity, as well as the gamma absorption and other geometric effects can be in principle taken into account. The general **Equation 4**, however, can be simplified in most practical cases, as follows:

- With proper design of the equipment, the position dependence of the detector efficiency can be avoided,
- Self-shielding and self-absorption in the sample is taken into account by means of integral correction factors,
- In case of small and thin samples, the effect originated from the spatial inhomogeneity of the neutron beam is negligible,
- In case of homogeneous samples, volumetric integral of the density function is replaced by the mass of the sample,
- Regarding the dependence of capture rates from neutron velocity, a convention is introduced:

The neutron capture cross-sections are calculated as equivalent to monochromatic neutrons with 2200 m s^{-1} (σ_0), according to **Equation 1** (supposing the validity of $1/v$ law). **Thermal equivalent flux** (Φ_0) is defined so as that the product of the two would give the observed reaction rate:

$$R \equiv N \int_{E_n=0}^{\infty} \Phi(E_n)\sigma(E_n)dE_n = N \int_{E_n=0}^{\infty} v \cdot n(E_n)\frac{\sigma_0 v_0}{v} dE_n =$$

$$= N \cdot \sigma_0 \int_{E_n=0}^{\infty} v_0 \cdot n(E_n) dE_n = N \cdot \sigma_0 \cdot \Phi_0 \tag{5}$$

where n is the neutron density, N is the number of atoms in the analysed volume.

As a result of the above simplifications, the counts in one single peak (N_P), collected in t_m time can be calculated as follows:

$$N_P = m \cdot S \cdot t_m = \frac{m\, N_{Av}}{M} \Phi_0 \sigma_\gamma \varepsilon(E_\gamma) t_m \tag{6}$$

where m is the mass of a given element in the sample, S is the analytical sensitivity (cps mg^{-1}).

When ratios of peak areas are studied and concentrations are calculated, the above described effects concern every component. Therefore, many sources of uncertainties, for instance the actual value of neutron flux, can be eliminated.

When the produced nucleus is radioactive, decay-γ photons are also utilised in the analysis. (γ_6 photon in **Figure 2**). In this case, it must be taken into account that the count-rates for decay peaks varies in time: it approximates the saturation value of $m \cdot S$ during the neutron irradiation.

1.6. Analytical applications of PGAA

The major fields of applications are as follows.

- Together with other (radio)analytical methods, PGAA is often used for **quality assurance** of standard reference materials and for **certification** in environmental chemistry and industry.

- **Some industrial applications** are the investigations of metals (fuel cells, hydrogen in alloys), impurities in semiconductors, analysis of borosilicate glass, control of heavy metal emission in power plants, as well as analysis of fossil fuels.

- In the **nuclear technology**, analysis of reactor graphite and beryllium, study of reactor poisons, analysis of fuel rods, nuclear waste and water from primary cooling loop was carried out.

- Composition of **foods**, plants and seeds were determined; moreover, **biological**, medical (BNCT) and physiological investigation were carried out. The boron, which has an important role in the growth of the plants and the Ca-metabolism of living organisms, could easily be measurable in matrices containing H, C, N, O and S.

- Exploiting the non-destructive feature of PGAA, various **archaeological** and other **cultural heritage** related objects (stones, pottery, metal, glass, precious stone, etc.) are studied.

- In **geology, environmental science and cosmo-chemistry,** various rocks, meteorites, etc. can be studied for their major and trace components.

- PGAA is perfectly applicable to investigate the composition of various **catalysts**, when small amounts of samples are available, even under the operation conditions (*in situ*)

- Other applications in **material sciences**: cements, amorphous alloys, fullerene, nanotubes, etc.

2. The Budapest PGAA instrument

2.1. The neutron source and the neutron guides

The Budapest Research Reactor (BRR) is a tank-type, light water cooled and moderated reactor. The reactor has a thermal power of 10 MW; the thermal neutron flux in the core can be as high as 2.2×10^{14} cm^{-2} s^{-1}. A **cold neutron source** is built in to the end of the tangential channel No. 10. This is a 400 cm^3 volume cell, filled with liquefied hydrogen. From the cold source, the neutrons are transported to the various experimental stations by neutron guides. The PGAA station is situated about 33 m away from the reactor. At the end of this guide, the neutron beam is split into two parts to serve two independent stations: on the upper beam, the **PGAA** (*Prompt-Gamma Activation Analysis*) instrument, while on the lower beam, the **NIPS-NORMA** (*Neutron-Induced Prompt-Gamma Spectrometry/Neutron Optics and Radiography for Material Analysis*) instrument are operated.
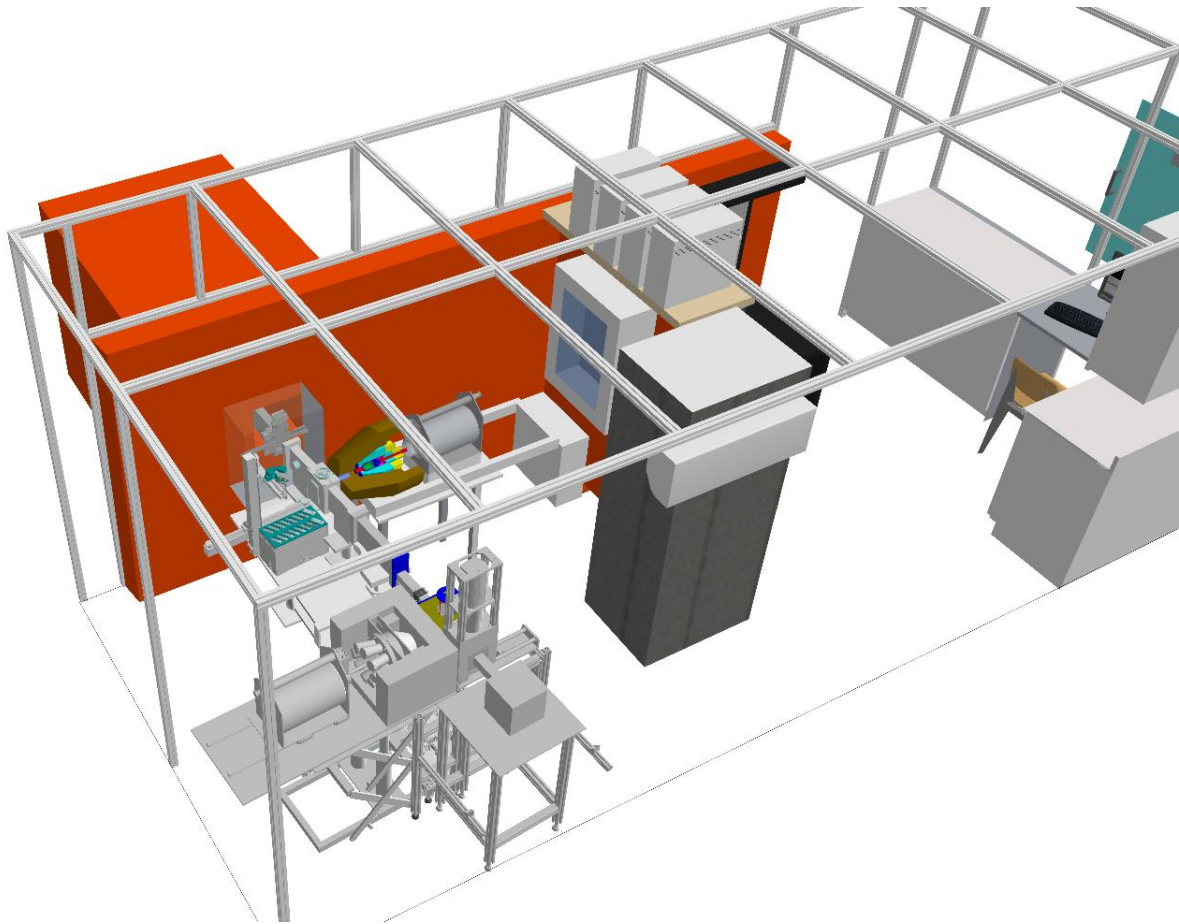
Figure 3. *The 3D view of the PGAA and the NIPS-NORMA stations*

2.2. The PGAA spectrometer

The central part of the PGAA instrument is a **HPGe detector**. In our setup this central detector is surrounded by a **bismuth-germanate** (*BGO*) scintillator annulus segmented in 8 parts. The so-called "cold finger" and two more „*catcher*" detectors are placed to its rear side. When the γ photons, which scattered out from the germanium crystal, are absorbed by one of the BGO's segments or by the catchers, the scintillations are detected by photomultiplier tubes. Summing up the scintillation signals, the so-called **Compton-suppressed** detection mode is implemented: signals of the HPGe detector that coincide in time with signals in any scintillator segments are selectively rejected by an **anti-coincidence** gating. This way, single escape peaks are reduced by a factor of 5, double escape peaks are reduced by a factor of 100, and the Compton-plateau is suppressed by a factor of 5–40, while keeping the useful full-energy peak areas. The first two effects simplify the spectrum, while the Compton-suppression improves the detection limits and decreases the counting uncertainties of the peak areas. The detector assemblage is surrounded with a 10 cm thick **lead shielding,** i.e. the γ-photons can reach the HPGe detector only through a narrow lead **collimator**. This arrangement limits the solid angle of the detector, and ensures that γ-photons cannot interact directly with BGO, only after being scattered out from HPGe crystal.

2.3. Main characteristics of the detector system

A) Efficiency

One of the most significant parameters of a γ-detector is the **absolute detection efficiency**, defined as the ratio between the number of detected "events" in the full energy peak and the number of given energy photons emitted from the radiation source. The efficiency curve is a 6 to 8 order polynomial on log-log scale (**Figure 4**).
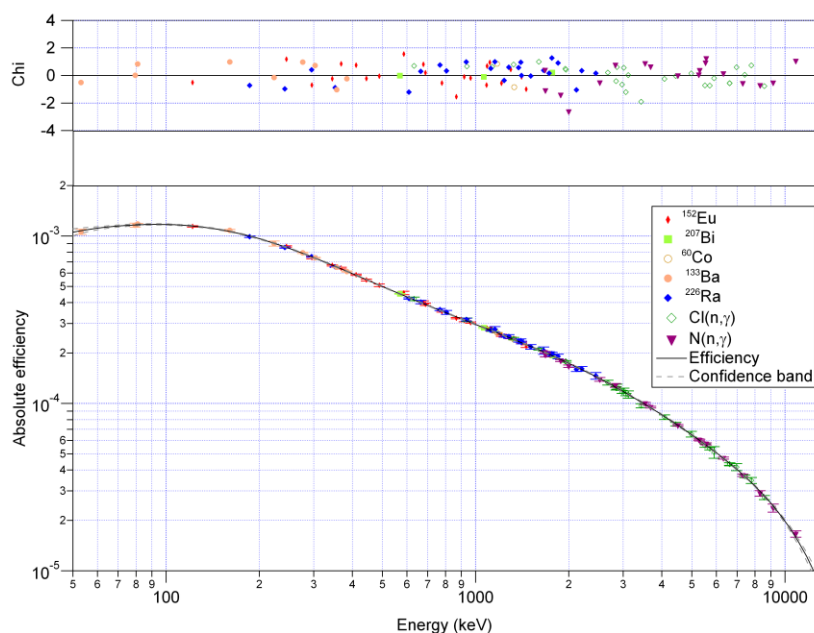

Figure 4. *Absolute efficiency of the Budapest PGAA system*

B) Nonlinearity

The γ-photons create electron-hole pairs in the sensitive volume of the semiconductor material. Since only about 3 eV is transferred during a single interaction, a photon of a few MeV can produce more than 1 million pairs of positive and negative charges. As the steps of signal detection and processing are basically linear, there is a theoretically linear correspondence between channel numbers and energies. In practice, this linear function is not perfect. The systematic deviation from linearity is in the order of 0.1% and can be characterized by the **differential nonlinearity**. In the wide energy range of PGAA, 1–2 channel shift can result in about 1 keV energy bias, which leads to false peak identification; therefore, nonlinearity must be taken into correction. According to our experiences, there is only a slow change in the nonlinearity function during a period of a few months. It means that **nonlinearity calibration,** along with the efficiency measurements, must be regularly repeated. In this procedure, radioactive sources with known γ-energies are measured and the peak positions are compared to their literature energies. A polynomial function is fitted on the data set, and the obtained nonlinearity function is used for correction during the spectrum evaluation stage (**Figure 5**).
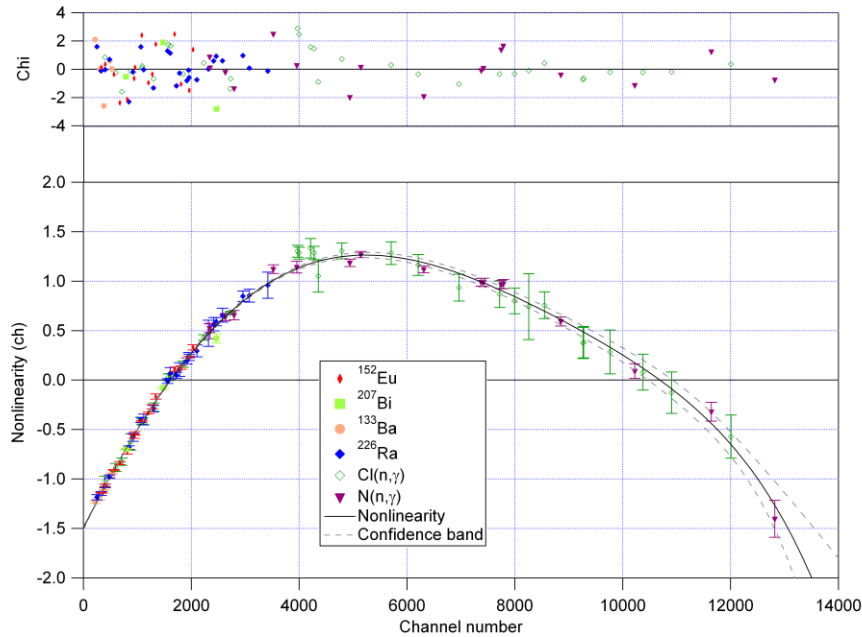
Figure 5. *Nonlinearity of the Budapest PGAA system*

C) Energy resolution

The other important factor in PGAA is the **energy resolution of the detector**. It can be characterised by the *full width at half maximum (FWHM)* of known γ-lines. In case of 1332 keV line of ^{60}Co, FWHM is about 1.8–2.2 keV.

The energy resolution of the spectrometer is determined by the characteristics of the detector and the associated electronics. As a function of energy, the overall peak broadening effect can be calculated in quadrature from contributions of the electronics, the statistical fluctuation of charge creation and the imperfect charge collection.

D) Calibration of the spectrometer

In order to determine the above discussed calibration functions, we use γ-sources of accurately known energies and intensities, which cover the whole energy range used in PGAA. At low energy, commercial **radioactive sources** (^{152}Eu, ^{207}Bi, ^{60}Co, ^{133}Ba and ^{226}Ra) are used, while for the 2–11 MeV region **prompt-γ lines of** N and Cl are measured. For the determination of absolute efficiency curve, the absolute activity of the most precisely calibrated radioactive source is used, and the rest are normalised to this. The EFFICIENCY, NONLINEARITY and FWHM ANALYSIS modules of the HYPERMET-PC software are used for such calculations.

2.4. The signal processing

The first step of signal processing is done by the **preamplifier**. Our RC-feedback type preamplifier creates an exponential pulse with 10–30 ns rise time and a decay constant of 45 μs for each detected event. The further steps of the signal processing are to transform this long pulse to a shorter one, and to derive a quantity still proportional to the original amplitude, i.e. this is proportional to the charge created (and therefore to the deposited energy) in the sensitive volume of the detector.

For this purpose, **analogue** spectroscopic amplifiers were in use for several decades. These units filter and amplify the exponential signal and form them to a semi-Gaussian shape. The amplitude of the semi-Gaussian is read by an analogue-digital converter (ADC) and the event is placed to the appropriate channel of the multichannel analyser (MCA). The digitization step here is at the end of the signal processing chain.

Some years ago a new generation of electronics was commercialized that rely on **digital signal processing**. Here a sampling ADC digitizes already the incoming detector signal and the signal processing is carried out on the numerical data stream by mathematical algorithms. This approach has certain advantages and can even dump the energies and time stamps of individual events into a file on the hard drive for off-line data analysis.

3. Practical aspects of PGAA

3.1. Sample preparation and data acquisition

Sample preparation for prompt-γ activation analysis is very simple. Depending on the composition, approximately 0.5–2 g of sample is necessary, which can be solid or liquid. Measurement of smaller samples, i.e. with some tens of mg masses, is still possible, but it requires longer acquisition time. When it is allowed, inhomogeneous and rough samples are powdered and homogenised, then packed into FEP- (fluor ethylene-propylene) bags. The typical dimensions of such filled bags are 20×30 mm^2, while the thickness is about 1–3 mm. Self-supporting samples can be directly mounted by Teflon monofilament strings into the beam. Pellets can be pressed from powder samples if needed. Liquid samples are irradiated in Teflon vials. Teflon and FEP are favourable, because they do not contribute to the spectrum significantly, and they are chemically resistant.

After packaging, sample is mounted on an aluminium frame to ensure the reproducible positioning, and the frame is placed into the neutron beam. We open the beam shutter, and start the **prompt-γ counting** with the Budapest PGAA Data Acquisition Software (**Figure 6**). In practice the acquisition time needed can vary within a very wide range, depending on the elements to be identified. According to our experiences, in most cases 30 to 120 minutes are enough to quantify major components in a geological matrix. (In many practical cases, we analyse geological samples: rocks, sediments, soils, minerals. Furthermore, glass or ceramics are very similar to geological samples in composition.) When only a small amount of sample is available, or detection of a low sensitivity element is requested, acquisition can take up to several days.

When sufficient events have been collected, we save the spectrum and close the beam. For further data treatment, the spectrum in Genie 2000 format (with *.CNF extension) is converted to S100 format file with *.MCA extension.

Following the experiment, the samples are stored behind lead shielding for a few days, in order to let the **induced radioactivity decay below the exemption level**. After that, the sample can be **returned** to the owner **or sent to further analysis**.
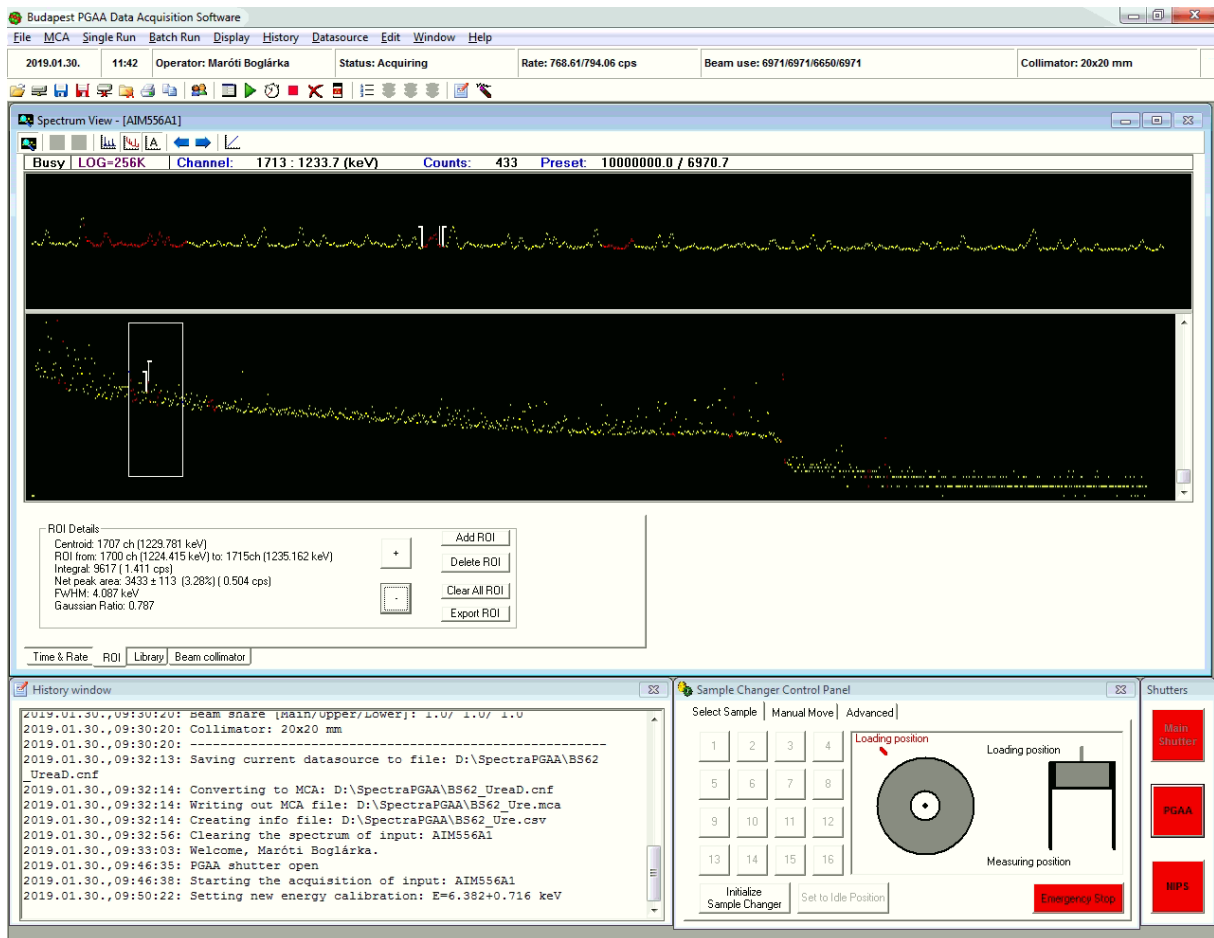
Figure 6. *Screenshot of the* B<small>UDAPEST</small> *PGAA DAQ acquisition software*

3.2. The spectrum evaluation

The useful spectroscopic information is carried by the full-energy peak positions and by the peak areas. The main goal is to determine these quantities as precisely as possible. A typical PGAA spectrum usually consists of hundreds of peaks. For the evaluation, we divide the spectrum to **regions**, each containing up to ten peaks.

For routine spectrum evaluation, H<small>YPERMET</small>-PC is adequate software. At the beginning, a well-known low-energy and a high-energy peak are chosen for **energy and FWHM calibrations**. Then, the software automatically searches and finds the peaks throughout the whole spectrum, sets up the optimal limits of the regions, and fits the model function in each region to the measured histogram values. As a result, an output peaklist with the peak energies, areas and their uncertainties is generated. Finally, the result of the **automatic fit must be revised**, and if necessary, corrected observing the residuals and χ^2 values. In many cases, the fit must be improved by modification of the fit parameters or by adding or deleting peaks in the given region.

Figure 7 demonstrates a typical fit by H<small>YPERMET</small>-PC. When the fit of the entire spectrum is finished, prepared **efficiency and nonlinearity corrections** are loaded, and a final PKL **peaklist** is generated that contains the peak positions, energies, FWHMs, areas, and their estimated uncertainties, as well as χ^2 of the fit for every peak.
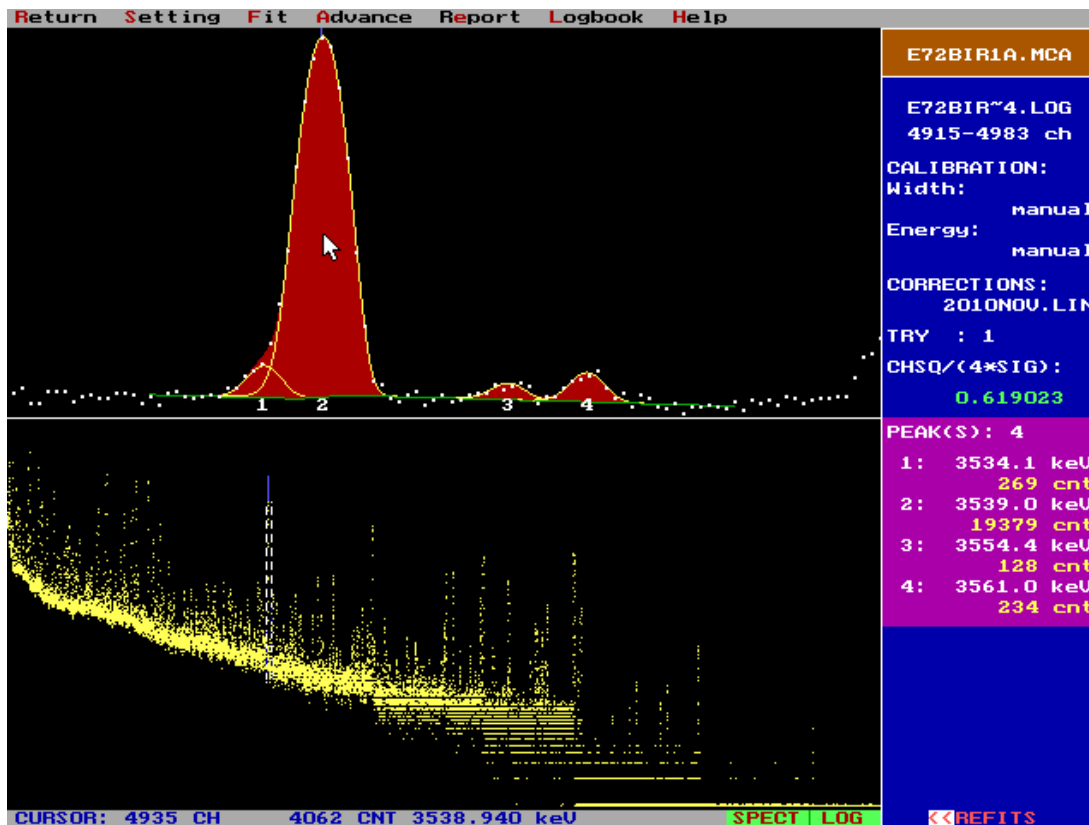
Figure 7. The fit of the most intense silicon peak with HYPERMET-PC

3.3. Calculation of the elemental composition

The calculation of the elemental composition is done by means of a MICROSOFT EXCEL **macro, ProSpeRo** (**Figure 8**), which requires the peaklist from HYPERMET-PC as an input. Steps like identification of prompt-γ peaks, comparison with the PGAA library, statistical evaluation are done automatically. The first results however must be revised, on the basis of our *a priori* knowledge about the sample.

In the first step, the macro loads the peaklist file and the PGAA library, which contains up to 25 of the strongest prompt-γ lines for each element, as well as the γ-lines attributed to the background radiation. Each line in the peaklist, which energy matches with ($\chi_E < 3$) is assigned from the library, and the equivalent masses are calculated according to Eq. (6). In the next step, gamma lines are sorted by chemical elements, and the outliers are rejected by statistical tools. Finally, a **weighted average** of the mass and an overall uncertainty are calculated from the peaks. The statistical (or accidental systematic) uncertainty of the weighted mean is usually much smaller than if the analysis would have been done on the basis of only a single peak. Furthermore, a **quality factor** is calculated, too, that depends on the number of the identified peaks and their relative emission probabilities. The absence of the strongest lines strongly affects the quality number, while the absence of weak lines has little effect.

If the energies of certain peaks significantly deviate from the database value, or the individual masses do not agree with average mass, the given peak is discarded by the macro or by the analyst, i.e. it will not be used in further calculations, and the final mass and uncertainty values are recalculated. On a **result sheet**, the macro collects the "real"

identified components, and calculates their **concentrations** after background correction. The results are given in various units (atomic % and mass %).

*Figure 8. Part of the mass table from the ProSpeRo EXCEL macro. * in the yellow column means that the given peak is included in the mass calculation. The mass value in column "AJ" gives the average mass of an element, next to it, one can find the "internal error" (calculated from individual errors of mass values, applying error propagation) and the external error (experimental spread around the average). Columns „AN" and „AO" contain the normalised deviation of mass and energy values from the average (μ) ($\chi = \frac{x-\mu}{\sigma}$), while in column AR one can find the quality factor for a given element.*

3.4. On the detection and quantification limit of PGAA

One chemical element is considered to be present in the sample, when at least its most intense peaks are identified in the spectrum. The peak search algorithm of HYPERMET-PC is able to identify a peak in the spectrum if its amplitude is greater than three times the standard deviation of background counts in its neighbouring channels. Supposing that the peak can be described with Gaussian curve, the peak area is: $N_p = \Gamma \delta \sqrt{\pi} = \Gamma W / 1.6551 \sqrt{\pi} \approx \Gamma W$, where Γ is the peak amplitude and W is the peak width (*FWHM*, full width at half of the maximum). Due to the Poisson statistics the standard deviation of background (b) equals to $\sqrt{b}$. The amplitude of the minimum detectable peak is therefore $\Gamma = 3\sqrt{b}$, thus the **lower limit of detection** (m_{DL}, *Limit of Detection, LOD*) for an element is:

$$m_{DL} = \frac{N_{P,DL}}{S \cdot t} \approx \frac{3 \cdot \sqrt{b}\, W(E_\gamma)}{S \cdot t} = \frac{3 \cdot M \cdot \sqrt{b}\, W(E_\gamma)}{N_A \cdot \Phi_0 \cdot \sigma_\gamma \cdot \varepsilon(E_\gamma) \cdot t} \tag{7}$$

where $N_{P,DL}$ is the minimum detectable peak area of an E_γ energy line, S is the analytical sensitivity (count rate originates from unit mass of a given element, cps/mg). The lower limit of detection depends on the background related to the sample matrix, thus it can differ even orders of magnitude for different kinds of samples. Typical detection limits for the Budapest PGAA facility are shown in **Figure 9**. **Limit of quantification** (*Limit of Quantitation, LOQ*), in addition, depends on the tolerable uncertainty of the analytical results.
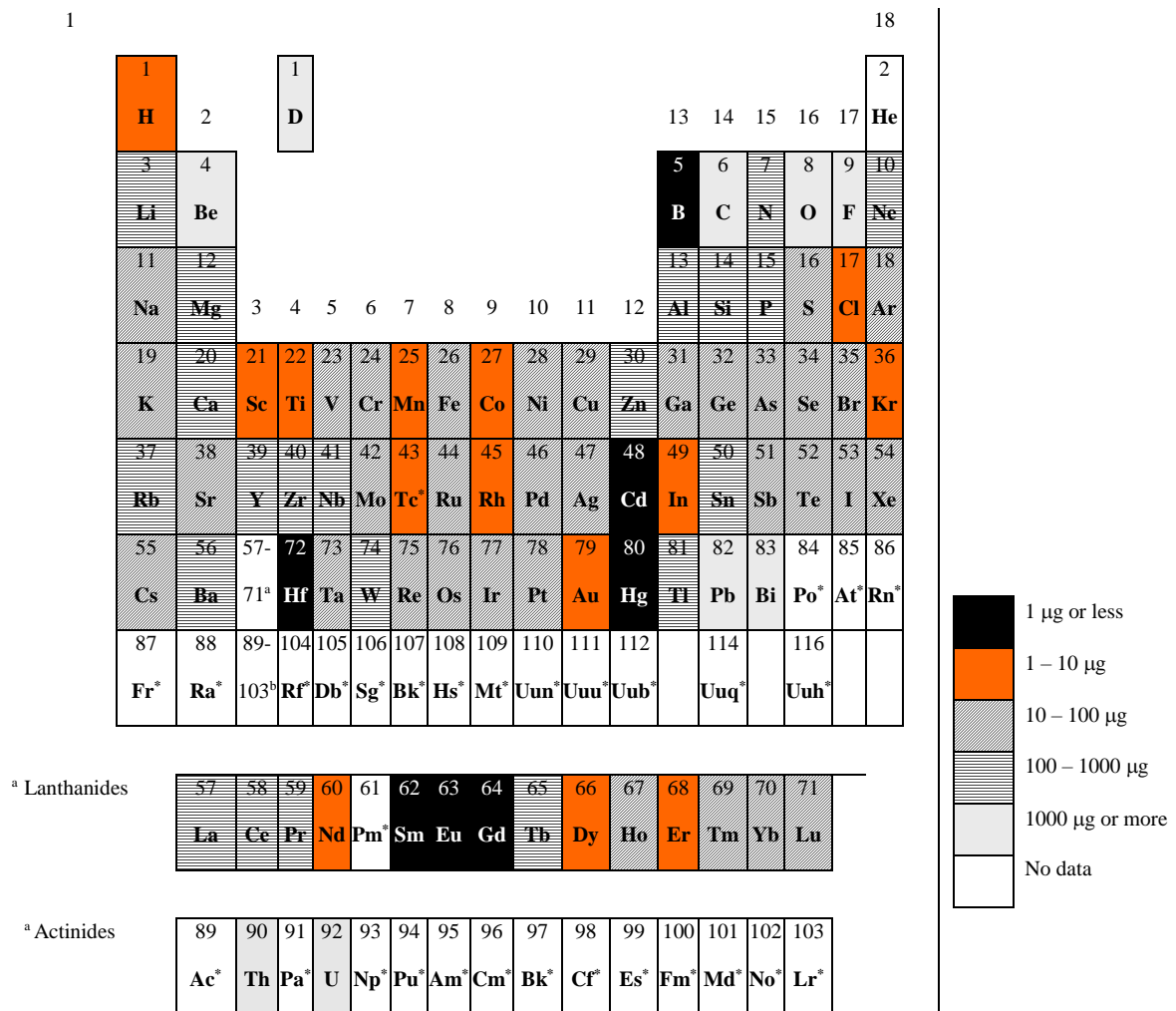

Figure 9. Lower limits of detection at the Budapest PGAA system. The best conditions of detection and 30000 s acquisition times are assumed.

4. Main steps of the lab exercise

1. Measure the provided unknown sample at the PGAA station. Determine the main components during data acquisition by identifying the most intense peaks in the spectrum. Use the PGAA analytical library.
2. Evaluate the PGAA spectrum with Hypermet PC.
3. Draw conclusions about detectable elements, as well as about the accuracy and precision of the analytical results

References

G.L. Molnár, 2004, Ed., *Handbook of Prompt Gamma Activation Analysis* (Dordrecht: Kluwer Academic Publishers ISBN: 978-1-4757-0997-1).

R.M Lindstrom, Zs. Révay, J. Radioanal. Nucl. Chem. (2017) **314** 843-858

Z.B. Alfassi, C. Chung, 1995, *Prompt Gamma Neutron Activation Analysis*, (Boca Raton: CRC Press).

L. Szentmiklósi et al, J. Radioanal. Nucl. Chem. (2016) **309** 71–77

L. Szentmiklósi et al, J Radioanal. Nucl. Chem. (2010) **286**:501–505

Zs. Révay, Analytical Chemistry (2009) **81** 6851-6859.

Zs. Révay, Nucl. Instr. Meth A (2006) **564**(4-6) 688-697.

T. Belgya, J. Radioanal. Nucl. Chem. (2014) **300**(2) 559-566.

IAEA Database of Prompt Gamma Rays from Slow Neutron Capture for Elemental Analysis (2007), https://www-nds.iaea.org/pgaa/

PSD Neutron Diffractometer

Margit Fábián

1. Structure determination of amorphous samples by neutron diffraction

Neutron powder diffraction is a standard technique for studying atomic and magnetic structures. The technique has become particularly powerful since the advent of the profile analysis technique (Rietveld, 1969; also reviewed by Albinati &Willis, 1982) [1, 2]. As powder techniques are applied to new and more complex problems, the standard compromise between intensity and resolution becomes an experimental limiting factor. We describe here a neutron diffractometer with a position sensitive detector system used for structural studies of amorphous materials.

Materials can have varying degrees of disorder. The neutron diffraction technique can be used to measure the structure of atom clusters and molecules in disordered materials. Glasses lack long-range order, but may have medium range ordering over several atomic lengths. The measured diffraction pattern is related to the positions of the atoms relative to each other in the glass.

In this section an elementary introduction to the method of structure determination by neutron diffraction is given. Particular focus is devoted to the structural characterization of amorphous materials. In an ideal case, the structure of a given system is completely determined when one is able to determine the equilibrium position of all atoms. This is quite straightforward in the case of crystalline solids, for which these equilibrium positions are not only well defined but also periodically repeated. For these systems the diffraction experiments produce diffractograms with the characteristic Bragg reflexions evidenced by well-defined narrow peaks at given angular positions, corresponding to the scattering vector matching a vector in the reciprocal lattice.

In the case of an amorphous material, clearly defined equilibrium positions are no longer present. Instead of having well defined atomic positions, one must refer to a distribution of atoms as a function of distance, i.e. to the probability of finding an atom at a distance *r* provided there is another atom at the origin. The so-called pair distribution function *g(r)* is proportional to this probability and it is the function that one usually intends to obtain from the experiment.

A measurement of the neutron diffraction pattern from an amorphous solid involves the determination of the scattered intensity as a function of the elastic scattering vector

$$Q = \frac{4\pi}{\lambda}\sin\theta \qquad (1)$$

in which λ is the incident neutron wavelength and 2θ the scattering angle. In the steady state reactor two-axis experiment, the flux $\Phi(\lambda)$ of thermal neutrons extracted from the moderator has a Maxwellian distribution of velocities and is time independent. The beam of wavelength λ, selected by the monochromator crystal, is incident on the sample and

scattered into the detector through an angle 2θ. The experiment thus entails a measurement of intensity as a function of 2θ.

In diffraction experiments intensity as a function of scattering vector Q is investigated. For an amorphous solid $S(Q)$ is a continuous function, tending to unity $Q \to \infty$. After taking into account appropiate factors such as beam intensity, number of atoms in the sample and detector efficiency, and making corrections for absorption, the scattered intensity measured in the detector is reduced to a fundamental quantity, the differential cross section per atom:

$$\frac{d\sigma(Q)}{d\Omega} = \sum_{ij} \frac{\sqrt{n_i n_j}}{n} \, \bar{b}_i \, \bar{b}_j \, S_{ij}(Q) \tag{2}$$

where n_i is the number of atoms of type i in the sample and $S_{ij}(Q)$ is the partial structure factor for the atom pair (i,j). In glasses the structure factors only depend on the scalar variable Q. The structure factors are related to the structure in real space through a Fourier transform:

$$S_{ij}(Q) = \delta_{ij} + \frac{4\pi}{Q} \, \sqrt{n_i \, n_j} \int_0^\infty [g_{ij}(r) - 1] \sin Qr \cdot r dr \tag{3}$$

where $g_{ij}(r)$ is the partial pair correlation function is real space. The latter quantity has a direct physical interpretation, namely that $4\pi r^2 n_j g_{ij}(r)\Delta r$ is the average number of j atoms in a range $(r, r+\Delta r)$ from an i atom.

The total reduced atomic distribution function, $G(r)$, was calculated from the structure factor, $S(Q)$, (or more precisely from the interference function, $I(Q)$) by Fourier transformation:

$$G(r) = \frac{2}{\pi} \int_o^{Q_{max}} Q[S(Q) - 1] \sin Qr \, dQ, \quad I(Q) = Q[S(Q) - 1] \tag{4}$$

where Q_{max} is the upper integration limit. Relation between $G(r)$ and total atomic pair correlation function, $g(r)$ which characterizes the one-dimensional average atomic pair correlation is:

$$G(r) = 4\pi\rho_0 r[g(r) - 1] \tag{5}$$

where ρ_0 is the average number density. The partial atomic pair correlation functions $g_{ij}(r)$ can be calculated by the following basic relations:

$$S_{ij}(Q) = 1 + \frac{4\pi\rho_0}{Q} \int_0^{r_{max}} r[g_{ij}(r) - 1] \sin Qr \, dr \tag{6}$$

$$S(Q) = \sum_{i,j}^k w_{ij} S_{ij}(Q) \tag{7}$$

$$w_{ij}^{ND} = \frac{c_i c_j b_i b_j}{\left[\sum_{i,j}^{k} c_i b_j\right]^2} \qquad (8)$$

$$g(r) = \sum_{i,j}^{k} w_{ij} g_{ij}(r) \qquad (9)$$

where r_{max} is the simulation box half edge-length, w_{ij} the weighting factor, c_i, c_j the molar fractions of components, b_i, b_j the coherent neutron scattering lengths. In the investigated glasses k = 2, thus k(k + 1)/2 = 3 different atom pairs are present. In the calculation procedure all $g_{ij}(r)$ components take part, although their weights are rather different, depending on the concentration and the scattering length of the actual atoms [3].

The coordination number CN_{ij}, we can calculate from the radial distribution function, $RDF_{ij}(r)$:

$$RDF_{ij}(r) = 4\pi r^2 \rho_0 g_{ij}(r) \qquad (10)$$

by integrating the RDF in a coordination shell between radius r_1 and r_2

$$CN_{ij} = c_j \int_{r_1}^{r_2} RDF_{ij}(r) dr \qquad (11)$$

2. PSD - Neutron Powder Diffractometer

The instrument that is capable of recording neutron powder diffraction patterns is also called 'two-axis' neutron spectrometer, the two principle axes being the monochromator and the sample axis. This is a very popular and useful instrument and therefore virtually every reactor source has at least one of them. Here the 'PSD' powder diffractometer, installed at the Budapest Research Reactor is introduced briefly [Sváb, 1996] [4-6]. A top view of PSD is shown in **Figure 1**. The PSD diffractometer is placed on a tangential thermal neutron beam of a medium flux reactor source. Primary collimation is done before the monochromator.
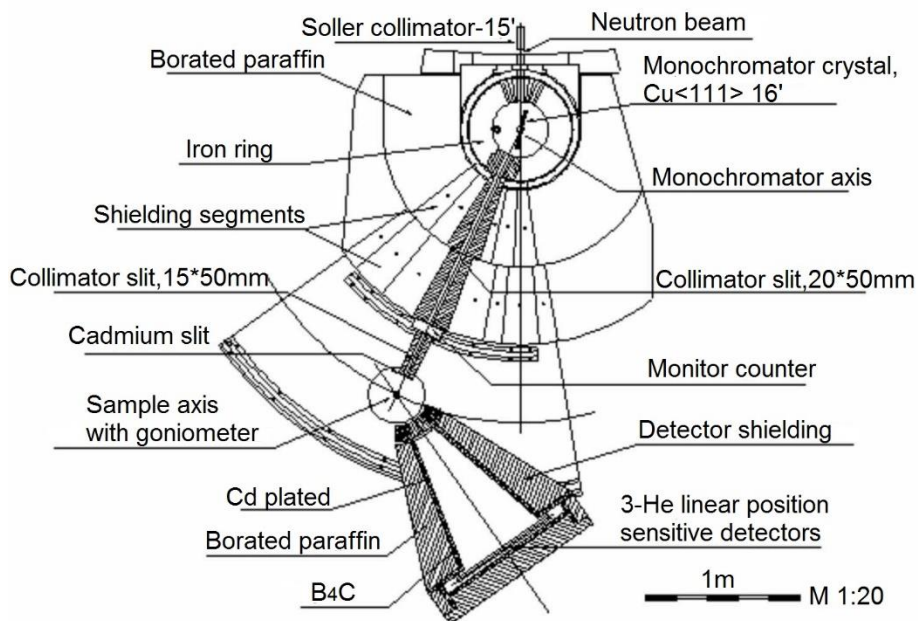
a)

b)

Figure 1. a) Schematic view and b) photo of the PSD neutron diffractometer

The diffractometer is suitable for structural studies of powder, liquids and amorphous materials in the range of momentum transfer Q=0.45-9.8 Å^{-1}. The wavelength selected from the primary neutron spectrum is around 1 Å (now is λ=1.068 Å), for which, in the case of Cu(111) monochromator single crystal (with a mosaic spread of 16') a neutron flux density of about 10^6 n cm^{-2} s^{-1} can be achieved at the sample position. Scattered neutrons are detected at a distance of 1.2 m from the sample by 60 cm position-sensitive ^{3}He detector tubes (placed within appropriate shielding- the system is based on three ^{3}He filled linear position sensitive Reuter-Stokes detectors, 600 mm long, 25 mm diameter each, the three

detectors are placed in the scattering plane above each other), which span a scattering angle range of 25°. In order to cover the whole scattering-angle range up to 110°, data are collected at five different positions of the detector system. The resolution that can be routinely achieved by such a setup about is 10^{-2}, in terms of $\Delta d/d$.

Data transfer and instrument control has been done by PC-AT (Master PC) with Eagle I/O card. A Windows based instrument software program package and the interface electronics have been upgraded. A new dedicated electronic device has been constructed, which serves for the electronic control of the movements and data transfer of the diffractometer. Recently a new sample environment element has been added. An in-situ sample conditioning cell has been designed and built for the PSD diffractometer. The High Temperature and Pressure (HTP) cell may be operated at pressure ranging from ambient to about 300 bar and at temperatures from RT to 900°C.

PSD instrument details:

Channel	Thermal, 9T tangential
Primary collimator	Soller-type: 20′
Take-off monochromator angle facility	$-5° < 2\Theta_M < 45°$
Monochromator/Mosaicity	Cu(111) / 16′
Monochromatic wavelength	1.069 Å
Resolution, $\Delta d/d$	$1.2 \cdot 10^{-2}$
Flux at the sample position	$10^6 \ n \cdot cm^{-2} \cdot s^{-1}$
Beam size at the specimen	10 mm x 50 mm
Scattering angle, 2Θ	$5° < 2\Theta < 110°$
Momentum transfer interval, Q	$0.45\text{-}9.8 \ Å^{-1}$
Monitor counter	fission chamber
Detector system	- 3 linear position sensitive ^{3}He detectors - the detector assembly spans 25° scattering angle at a given position
Data collection	Xilinx preprogrammed unit
Data transfer and control	PC-AT with Eagle I/O card and a dedicated electronic device
Remote control and file transfer	Windows programme package

For powder specimens of about 3-4 g we use thin walled cylindrical vanadium sample holders with 8 mm diameter.

3. Neutron diffraction measurements

At the PSD neutron diffractometer we use a special measurement program, named WinNda 1.0 developed by our engineers and beam line scientist. The program interface is shown in **Figure 2**. Several menus help with programing and starting the measurements. As the first step the detectors are programed, using the *Detector* menu. The second step is to start the program, from *Functions* menu, choosing *Auto Measurement* submenu. **Figure 3** shows the empty program window, where the boxes need to be filled with the sample parameters and data regarding the actual measurement plan.
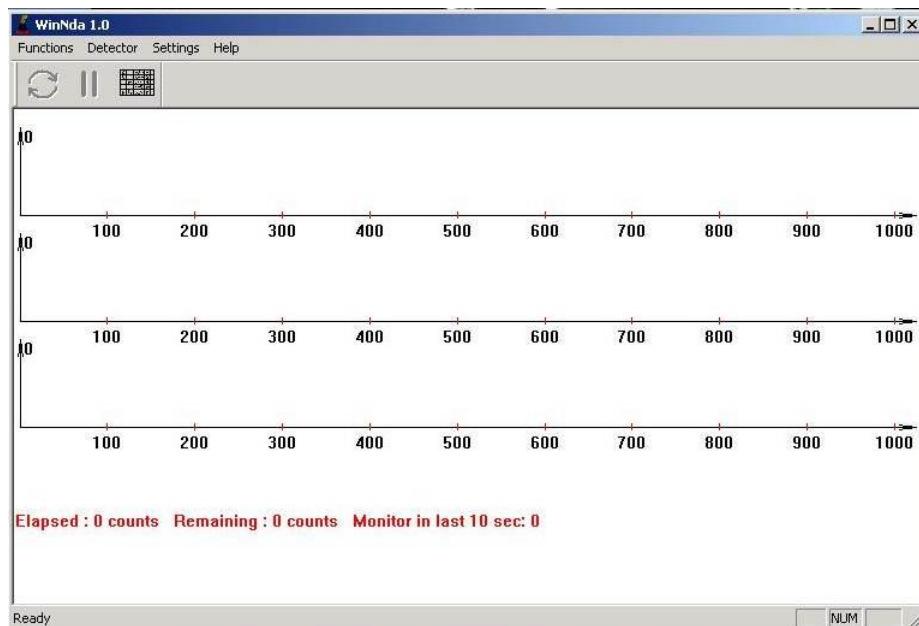
Figure 2. *Interface of the measuring program*
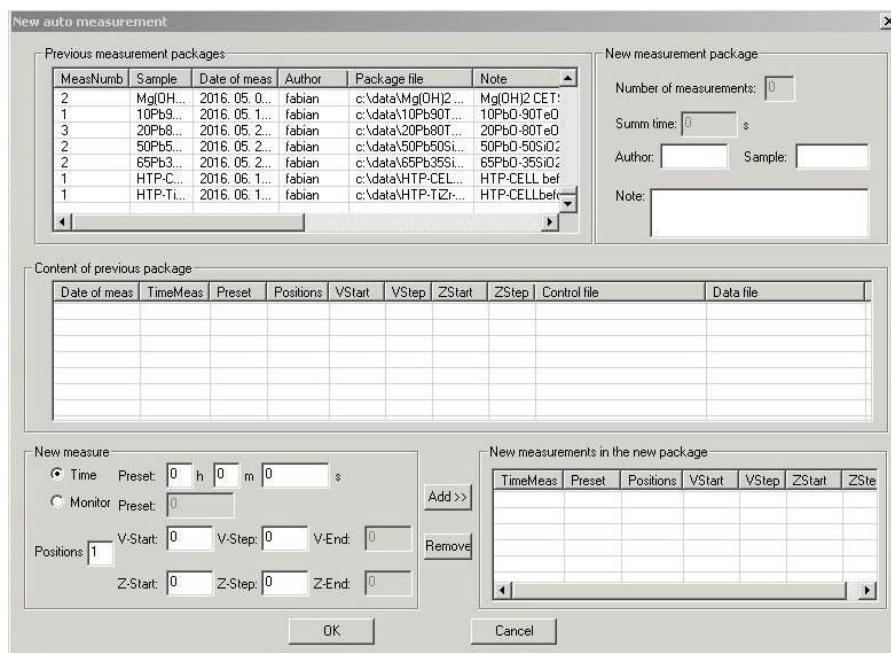
Figure 3. *Empty program interface*

Measurement programming proceeds as follows:

- information regarding the sample. Use a short name for identification, and fill the *Note* with all data which can help identify our measurement, like detailed sample composition, mass, height of the sample in the holder.

- write the measurement time and number of repetitions if required. When poorly scattering samples are measured or there is not enough material to fill the holder, we need to repeat the measurement in order to obtain data with good statistics;

- start-end positions which more or less cover the 2θ = 8-115° range in 5 steps;.

To start one run, composed of 5 steps, repeated 4 times, we need to use the ADD button. When boxes are filled, we can start our experiment. **Figure 4** presents an example of filled measuring program interface, for an As$_2$Se$_3$ chalcogenide sample.
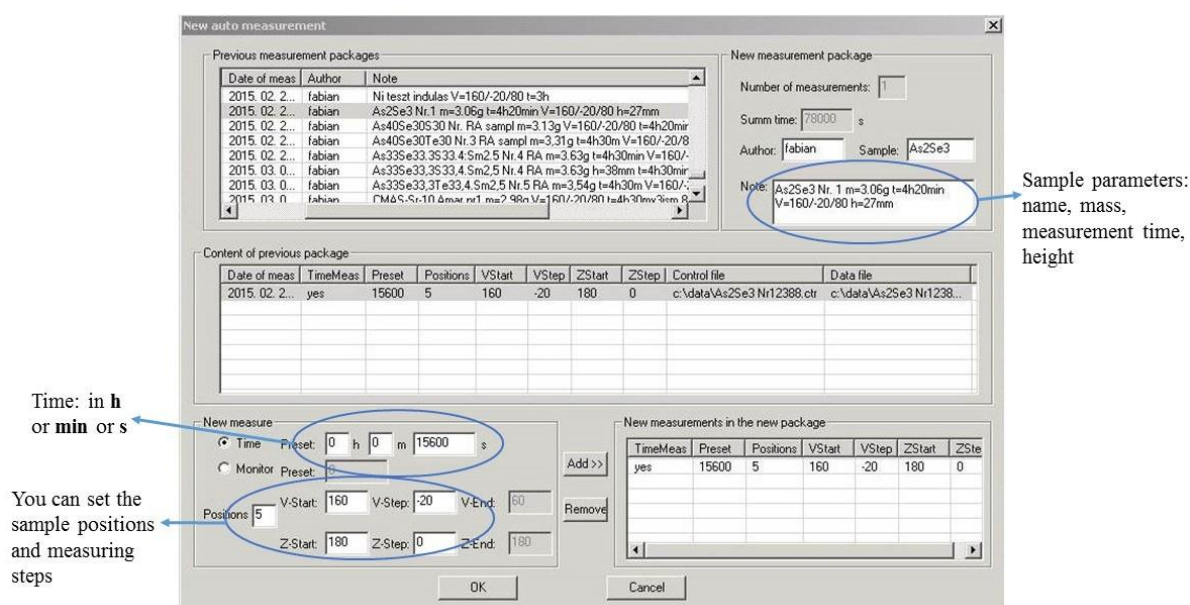

Figure 4. Filled Measurement program

With the *OK* button we can start our measurements. From time to time the runs can be checked by means of the Refresh icon. The measuring steps, like changing of measurement position included in the program, are performed automatically. After a successful experiment, when the measurement time is over, the program will stop automatically. Typically several output files are generated, the most important being the ones which contain the datasets and those, where the sample parameters and measurement conditions are recorded. **Figure 5 a** and **b** display examples of these files.

Figure 5. a) Obtained ctr file, containing information from the measurements

Figure 5. b) Data file, with measured data points. Column1: nr. of channel, column 2: data from detector 1, column 3: data from detector 2 and column 4: data from detector 3

At the conclusion of the experiment the program can be stopped by closing the WinNda window. During the experiment, the measurements can be suspended in order to check something. Subsequently, the measurements can be resumed from the position/time of interruption.

4. Selected example: Chalcogenide sample

This sample is chosen to illustrate some of the above discussed calculations. From the diffraction measurements the following data files are obtained:
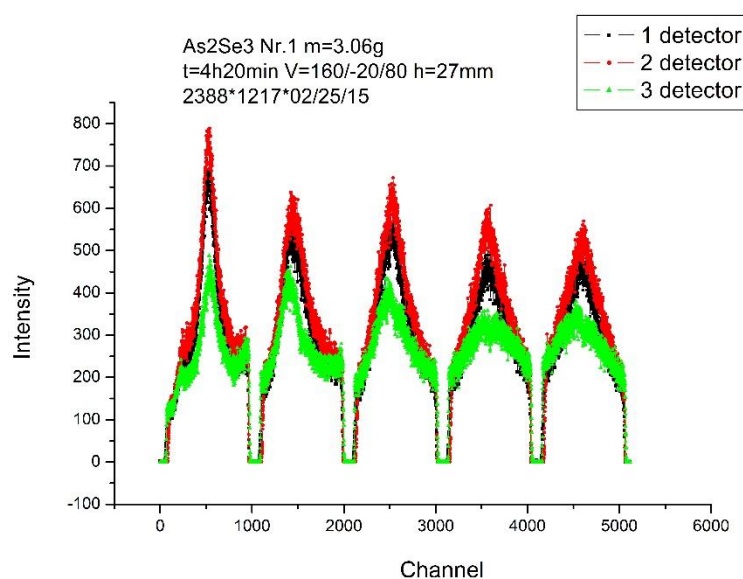
As2Se3Nr12388.dat
As2Se3Nr12388.ctr
As2Se3Nr12389.dat
As2Se3Nr12389.ctr

The first information about the structure of chalcogenides comes from the plotting of the datasets, which will show first raw data, plotted in Origin, As2Se3Nr1.OPJ

Figure 6. Raw structural information about the As2Se3 samples.
Broad distributions show that we have amorphous structure

4.1. Data processing

By means of a dedicated program – SLADCONV – the structure factor of the sample is calculated in 3 steps. The required operations are illustrated here for two measurements on an As_2Se_3 sample, named 2388 and 2389.

4.1.1. Windows-DOS conversion

This step is required because the instrument data processing computer runs with DOS operation system. Under DOS we rename the files with numbers: As2Se3Nr12388.dat to 2388.dat; As2Se3Nr12388.ctr to 2388.ctr; As2Se3Nr12389.dat to 2389.dat and finally As2Se3Nr12389.ctr to 2389.ctr.

Running the Sladconv.exe program, the file Sladconv.txt is generated. The name SLADCONV comes from, SLAD - Studsvik Liquids and Amorphous materials Diffractometer + Conversion.

The SLADCONV.txt file contains the measurement numbers, sample data and measurement time:

2388
2389
As2Se3 m=3.06g, V=160/-20/80, t=4h20min...plus other parameters of interest.

The standalone Sladconv.exe file, converts dat -> daf and ctr -> ctf, yielding 2388.ctf, 2388.daf, 2389.ctf and 2389.daf, which are suitable formulations for the DOS programs.

4.1.2. Sum of the measurements, using the following commands:

Msum.txt
Msum.exe

The Msum.txt file contains summation instructions:

2
 '2388.daf' '2388.ctf'
 '2389.daf' '2389.ctf'
 'sumAs2Se3.daf' 'sumAs2Se3.ctf'
As2Se3 m=3.06g, V=160/-20/80, t=4h20min

Running Msum.exe performs the summation.

4.1.3. Scaling of the data, using the following commands:

Skala03.exe
Skala03.txt
and the background files:
hprof03.dat
hprof03.par
Skala03.txt looks like:

Line number	Text
01	1
02	1 1 1
03	sumAs2Se3.ctf
04	sumAs2Se3.daf
05	V8mm.ctf
05	V8mm.daf
07	sumAs2Se3.neq
08	sumAs2Se3.dat
09	sumAs2Se3.rit
10	sumAs2Se3.q
11	0.8670 0.8670 0.8670 0.8670 0.8670
12	As2Se3 m=3.06g, V=160/-20/80, t=4h20min

01 - number of measurements
02 - nr. of detectors which are working
03 - sum up of our data, from previous steps

05, 06 - data from empty sample holder - we used 8mm Vanadium can
07-10 - after the calculation we get several output data how is .neq (tracking file), .dat (income spectrum), .rit (spectrum for Rietveld analysis) and .q (spectrum in Q).
11 - transmission data, for each of the 5 positions
12 - information about the sample and the measurement conditions

4.2. Structural details from diffraction measurements

The structure factor $S(Q)$ for the As_2Se_3 sample was measured at the PSD neutron diffractometer, the datasets were calculated using the program existing at the facility. We obtained a typical amorphous spectrum with broad distributions, specific to the amorphous state.

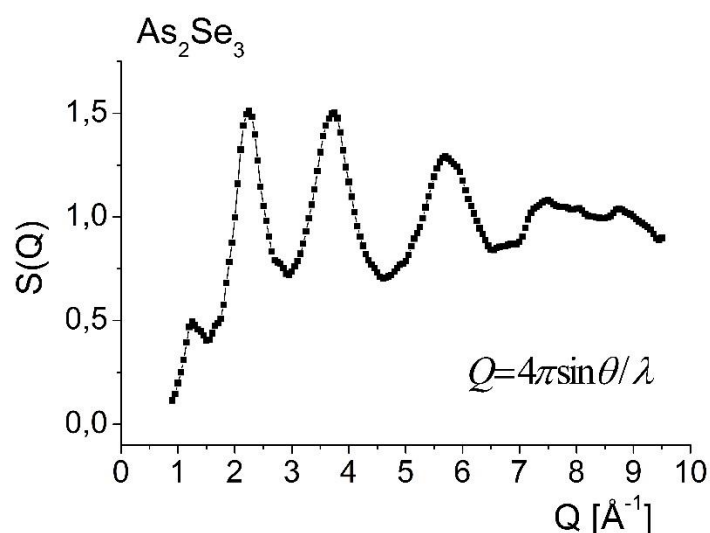**Figure 7** presents the plot $S(Q)$, obtained from neutron diffraction measurements.

Figure 7. S(Q) from neutron diffraction measurements

The structure factor is Fourier transformed to obtain the total radial distribution functions (**Figure 8**) and their corresponding pair correlation functions.

The interpretation of the partial pair correlation functions is done by means of numerical simulations. Reverse Monte Carlo modelling is applied (RMC)[7], which provides significant information about the local structure of the amorphous matrix. Use of such model allows to determine many of the atomic structural parameters, in particular to calculate the partial pair correlation functions ($g_{ij}(r)$) and average coordination number (*CN*). In this way it was possible to identify the presence of As–Se, Se-Se and As-As correlations. The partial atomic correlation functions, $g_{ij}(r)$ obtained from RMC modelling for As-Se, As-As and Se-Se network former atomic pairs are presented in **Figure 9**.
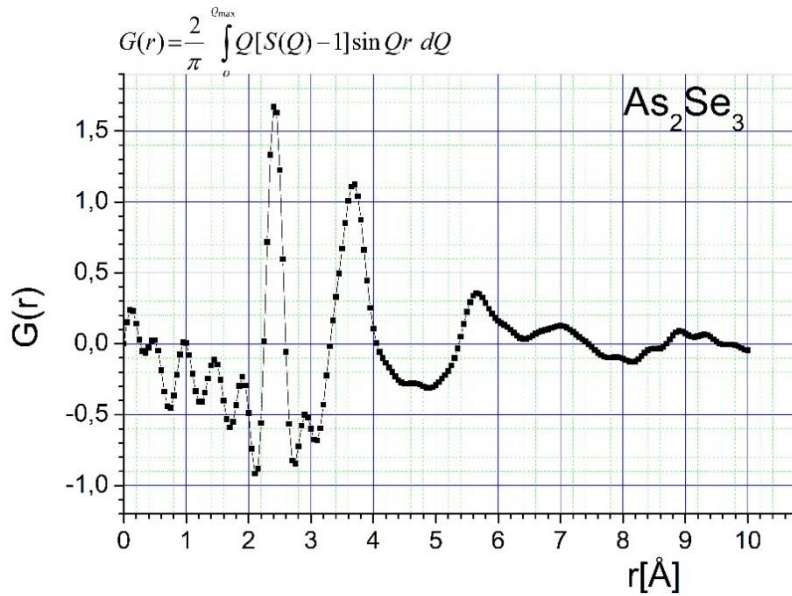
$$G(r) = \frac{2}{\pi} \int_{o}^{Q_{max}} Q[S(Q) - 1] \sin Qr \; dQ$$

Figure 8. *G(r) Total radial distribution function*
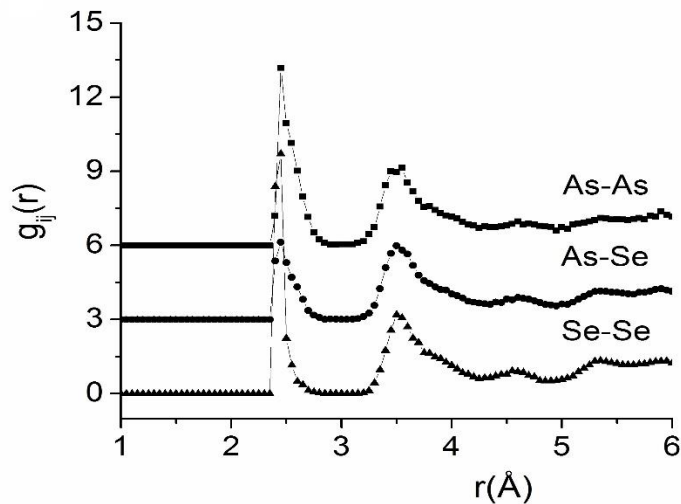
Figure 9. *The partial pair correlation functions, obtained from RMC modelling of As_2Se_3 composition*

The As-As and As-Se correlations show a strong and sharp first peak at 2.45±0.01 Å and two broad and much less intense peaks at 3.50±0.1 and 4.6±0.1 Å, related to 2nd neighbour distance and 3rd neighbour distance of the As-As, As-Se bonds, respectively. The characteristic peaks for the possible Se-Se homopolar bonds appear at 2.35±0.1 Å in the binary As_2Se_3 glass.

The total coordination numbers yielded by RMC modelling are CN_{As} = 3.02±0.05, CN_{Se} = 2.02±0.05 (**Figure 10**). The obtained total coordination number for As is close to 3, while for Se it is close to 2, showing that As atoms are surrounded by 3, Se atoms by 2

neighbours. From these results it can be concluded that there is a covalent network formed by threefold coordinated As and twofold coordinated Se atoms.
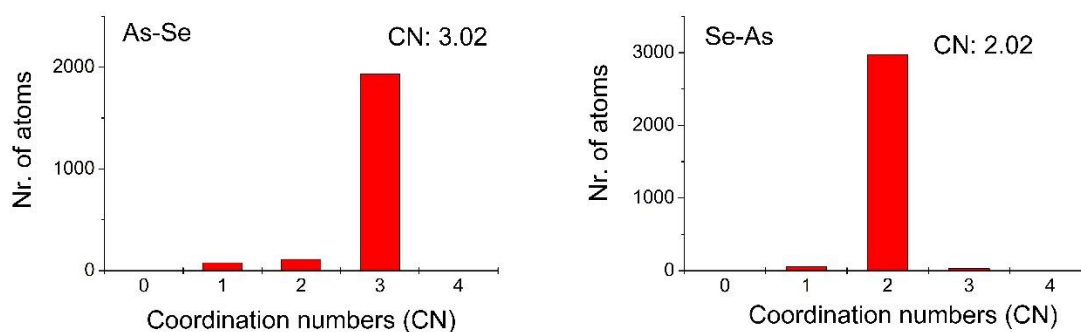
Figure 10. Coordination number distributions from RMC calculations, As atoms are surrounded by 3.02 Se atoms; Se atoms are surrounded by 2.02 As atoms

In general, neutron diffraction is the main tool to study the structure of glasses. The local structure of As_2Se_3 glass is investigated by using neutron diffraction methods, on the PSD powder diffractometer at the Budapest Research Reactor. Applying the software package developed at the facility, we can get the main structural information for the As_2Se_3 amorphous sample.

References

[1] H.M. Rietveld, J. Appl. Cryst. 2 (1969) 65-71

[2] A. Albinati, B.T.M. Willis, J. Appl. Cryst. 15 (1982) 361-374.

[3] M. Fábián - PhD. Dissertation, 2009.

[4] E. Sváb, Gy. Mészáros, F. Deák, Materials Science Forum 228-231 (1996) 247-252.

[5] L. Temleitner, Gy. Mészáros, L. Pusztai, E. Sváb, Physica B 350 (2004) e865-e867.

[6] www.bnc.hu

[7] R.L. McGreevy, L. Pusztai, Mol. Simul. 1 (1988) 359-367.

Powder diffraction measurements on the MTEST diffractometer to reveal the structure of ordered and disordered materials

László Temleitner

1. Introduction

What kind of information is provided by the MTEST diffractometer?

Determines short-range order positional correlations between atoms or molecules of bulk disordered crystalline, amorphous or liquid materials through measuring total scattering powder diffraction patterns.

It helps to localise equilibrium atomic position(s) of light elements in a crystalline lattice.

Contributions to magnetic structure determination.

Residual stress determination on engineering materials.

1. 1. Theoretical introduction

In this chapter, we restrict the discussion to powder neutron diffraction using constant wavelength technique. It is also supposed, that you are acquainted to fundamentals of crystallography. In the following sections, we examine the right-hand side of the following equation:

$$\frac{d\sigma}{d\Omega} = \frac{1}{N} \left\langle \left| \sum_{j=1}^{N} b_j\, e^{i\vec{Q}\vec{r_j}} \right|^2 \right\rangle$$

The left-hand side is a quantity, which we are going to determine by measurement: the differential cross-section. It provides the expected number of scattered neutrons into a $d\Omega$ solid angle over 1 second of time, if the incoming neutron flux is 1 neutron/s/cm^2. The right-hand side contains the description of scattered intensity of scattering vector ($Q=4\pi/\lambda*\sin(\theta)$, momentum transfer) over N number of particles on average, each possesses its scattering length (b_j) and instantaneous position vector (r_j).

1.2. Powder diffraction measurement on crystalline samples

Crystalline materials are built up by periodically repeated units in the 3 dimensional space: as a result, *crystalline lattice* is formed. The name of the smallest meaningful unit among all of the possible repeating units is called *unit cell*. These two elements: the lattice and the content of the unit cell describe the *average structure* of the crystal; determining them is the main task of the diffraction experiments. So, instead of describing all of the coordinates, we need to focus only on the unit cell.

If we imagine the scattering process on a lattice, we can construct planes parallel to each other passing through the lattice points: these are the lattice planes. The regular distance

between the planes is indexed by the *hkl* Miller indices. The distance between planes provides the length of (1/h, 1/k, 1/l) vector in the coordinate system of unit cell. In the case of cubic lattice it is ('a' being the lattice constant):

$$d_{hkl} = \frac{a}{\sqrt{h^2 + k^2 + l^2}}$$

The scattering angle is obtained from Bragg-equation, taking into account constructive interference condition ('n' is the order of harmonic):

$$n\lambda = 2d\sin(\theta)$$

Mathematically, a crystal structure is formed by convolving the (point) lattice by the unit cell. According to theorem of convolution, in reciprocal (or Fourier) space, the differential cross-section can be calculated by multiplying the Fourier-transform of the content of the unit cell and the Fourier-transform of the unit cell:

$$\frac{d\sigma}{d\Omega} = \frac{1}{N} \left| \left\langle \sum_{j \in unitcell} b_j \, e^{-i\vec{Q}\left(\vec{R_j} + \vec{R_j}(t)\right)} \right\rangle \right|^2 \delta\left(\vec{Q} - \overrightarrow{q_{hkl}}\right) + incoherent\ scattering$$

Here q$_{hkl}$ represents the reciprocal lattice vector. The instantaneous position of the atom is separated into equilibrium and oscillating parts. Averaging this oscillating part over time gives the Debye-Waller factor (<u^2> is the mean square displacement):

$$\frac{d\sigma}{d\Omega} = \frac{1}{N} \left| \left\langle \sum_{j \in unitcell} b_j \, e^{-i\vec{Q}\vec{R_j}} \right\rangle \right|^2 e^{\frac{-Q^2\langle u^2\rangle}{3}} \delta\left(\vec{Q} - \overrightarrow{q_{hkl}}\right) + incoherent\ scattering$$

If we look at the previous equation, we can observe, that we get intensities only at reciprocal lattice points. As it is connected to the lattice, we can determine the lattice parameters simply by the positions of Bragg-peaks. Moreover, the intensities of the Bragg-peaks determine the content of the unit cell.

The equation seems feasible for studies, except that it should contain instrumental resolution function instead of Dirac-delta, and should take into account, that we deal with powder diffraction and not single crystal diffraction. We are going to use the following resolution function assuming Gaussian profile (Caglioti form):

$$FWHM^2(2\theta) = U\tan^2(\theta) + V\tan(\theta) + U$$

If resolution were not too bad, we do not have to take care about incoherent scattering in most cases.

Crystal structure determination starts usually with peak finding and looking for definable lattice and its parameters. After success, the peaks can be indexed with proper Miller indices belonging to one scattering angle. Therefore, the procedure of looking for lattice parameters is named indexing. The lack of intensities at some specific lines might help to discover the right space group (describes the combined symmetry of the lattice and unit cell: there are 'only' 230 in three dimensions) or restrict to a few.

The following step is to determine the content of the unit cell – numerous methods exist to reach our final aim: determine the atomic coordinates (Wyckoff-site) within the space group and mean square displacement parameters. One technique is Rietveld refinement, which starts from an initial model and modifies positional, displacement, instrumental, etc. parameters in order to minimize the following sum over the whole pattern:

$$COST = \sum_j weight_j \left(I_{measured,j} - I_{simulated,j}\right)^2$$

Another technique is simulated annealing, where parameters are varied on trial-and-error basis. If the above cost function is decreased, the algorithm accepts the change of the parameters, otherwise only with the following probability:

$$exp\left(-\left(COST_{now} - COST_{previous}\right)/(2kT)\right)$$

If the "temperature" is decreased, it accepts less number of 'worse' configurations. Doing the annealing process several times might help to find the global minimum.

It is interesting to note, that diffuse scattering appears if correlation of atomic pairs in time is not independent of each other. Recently total (Bragg + diffuse) scattering diffraction measurements are abound. This way, not just long, but short range order correlations can be captured as well.

1.2. Diffraction studies of amorphous and liquid materials

In contrast to the crystalline materials, liquids and amorphous materials have not got long range translation symmetry. We cannot find Bragg-, but only diffuse scattering pattern, if we would like to study them by neutrons (or X-rays). To describe them, we have to take into account instantaneous *correlations between pairs of atoms*, instead of average positions like in crystals.

The basic quantity, which would be the ultimate aim to determine by a diffraction measurement is the *radial distribution function (g(r))*. This quantity provides the *ratio of local density* (in a thin sphere of radius r around the central particle) *and average density of atoms.* As these materials have a lack of long range order, g(r) tends to 1 further away from the centre. At low distances, it is 0 due to atomic radius. Its first low r peak marks the most probable first neighbour distance. If we would like to know the number of neighbours (the coordination number), we should integrate up to the distance of the first minimum (about 8.5 Å in **Figure 1**) over the maximal position of the peak:

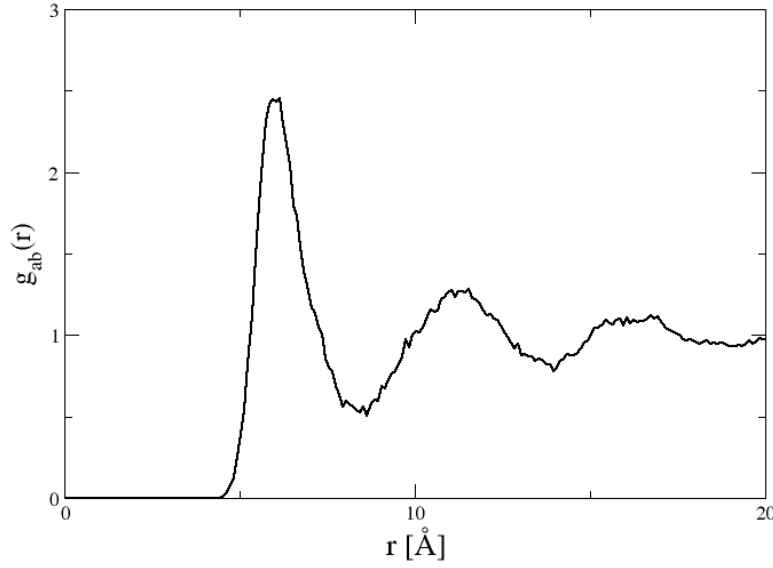$$C = 4\pi\rho \int_{r_0}^{g_{min}(r)} r^2\, g(r) dr$$

Figure 1. *The carbon-carbon partial radial distribution function of liquid carbon tetrabromide*

For an *N*-component system, it is possible to extend the previous definition as we are interested to find the ratio of local and average density of 'B' type atoms from the central 'A'-type atoms: this is the partial radial distribution function ($g_{AB}(r)$). Its Fourier-transform is the so-called Faber-Ziman partial structure factor:

$$Q(S_{AB}(Q) - 1) = 4\pi\rho \int r\,(g_{AB}(r) - 1)sin(Qr)dr$$

$$r(g_{AB}(r) - 1) = \frac{2\pi^2}{\rho} \int Q\,(S_{AB}(Q) - 1)sin(Qr)dQ$$

Knowing the concentration (c_A), scattering length (b_A) and incoherent scattering cross-section (σ^A_{incoh}) of each element, the differential cross-section can be written as:

$$\frac{d\sigma}{d\Omega} = \frac{1}{N}\left\langle \left| \sum_{j=1}^{N} b_j\,e^{i\vec{Q}\vec{r_j}} \right|^2 \right\rangle = \underbrace{\sum_{A,B} c_A\,c_B b_A b_B S_{AB}(Q)}_{\bar{b}^2 S(Q)} + \sum_A c_A \frac{\sigma^A_{incoh}}{4\pi}$$

Due to symmetries, we should perform "only" N(N+1)/2 experiments by changing b_A's to derive each partial radial distribution function, which is generally not possible solely by experimental means. This is the reason, why computer modelling techniques: molecular dynamics, reverse Monte Carlo modelling are essential in this field.

The molecular dynamics simulation proceeds the evolution of atomic configuration using interaction potential by solving Newton equations. After successful simulation, the trajectories can be analysed. This way both dynamic and structural properties can be derived. The reverse Monte Carlo procedure performs the simulation of an atomic

configuration by randomly moving atoms and determines the corresponding scattering pattern. The move will be accepted, if the new simulated pattern is approaching the measured one better, than before (if not, it might be accepted with less than 100% probability, similarly to the simulated annealing method). As a result, set of configurations are obtained, which are consistent with the measured data. The atomic coordinates can be analysed geometrically.

In the majority of measurements, usually S(Q) – the structure factor – is published because it contains information on coherent scattering. If the sample provides well separated distances in r space, a common habit is the transformation of S(Q) to r space, where the weighted sum of $g_{AB}(r)$'s, the G(r) is obtained:

$$G(r) = \sum_{A,B} \frac{c_A c_B b_A b_B}{\bar{b}^2} g_{AB}(r) = 1 + \frac{2\pi^2}{r\rho} \int Q\,(S(Q) - 1)sin(Qr)dQ$$

As a general point of view, to reach good resolution in r-space, you should measure as wide as possible Q-range. The instrumental resolution is not an issue this case. Specific studies, which use r-space information obtained by other sources, might differ from this rule of thumb.

2. The general purpose 4 circle Material TESTing diffractometer – an overview

The MTEST two-axis diffractometer is installed at the 6th radial thermal beamport of the Budapest Research Reactor. The beam provides thermal neutrons according to the Maxwell-Boltzmann distribution with highest probability of 25 meV neutrons. However not only thermal, but higher energy neutrons and gamma photons come from the core of the reactor as well. In order to attenuate the contribution of the former one, an oriented sapphire single crystal is installed in the beamport, while the gamma contribution is attenuated by the biological shielding of the monochromator.

The first axis consists in the monochromator crystal, where the wavelength is selected according to Bragg's law. Three kinds of monochromator crystals are installed, which allows to optimize the intensity, wavelength (in the 0.089 – 0.227 nm range) and resolution (typically 0.6° in 2Θ) of the monochromatic beam on demand.

The monochromatic beam might pass different kinds (from 60' to 12') of Soller collimators in order to improve spatial resolution. Then it goes through the ^{235}U coated ionization chamber, which serves as monitor counter, measuring the intensity of the incoming beam. Before reaching the second axis, where the sample sits, slits limit the originally 4 cm high x 1 cm wide beam to the required size. The neutron flux here is about $2 \cdot 10^6$ neutron/(cm^2 sec) at a wavelength of 0.133 nm.
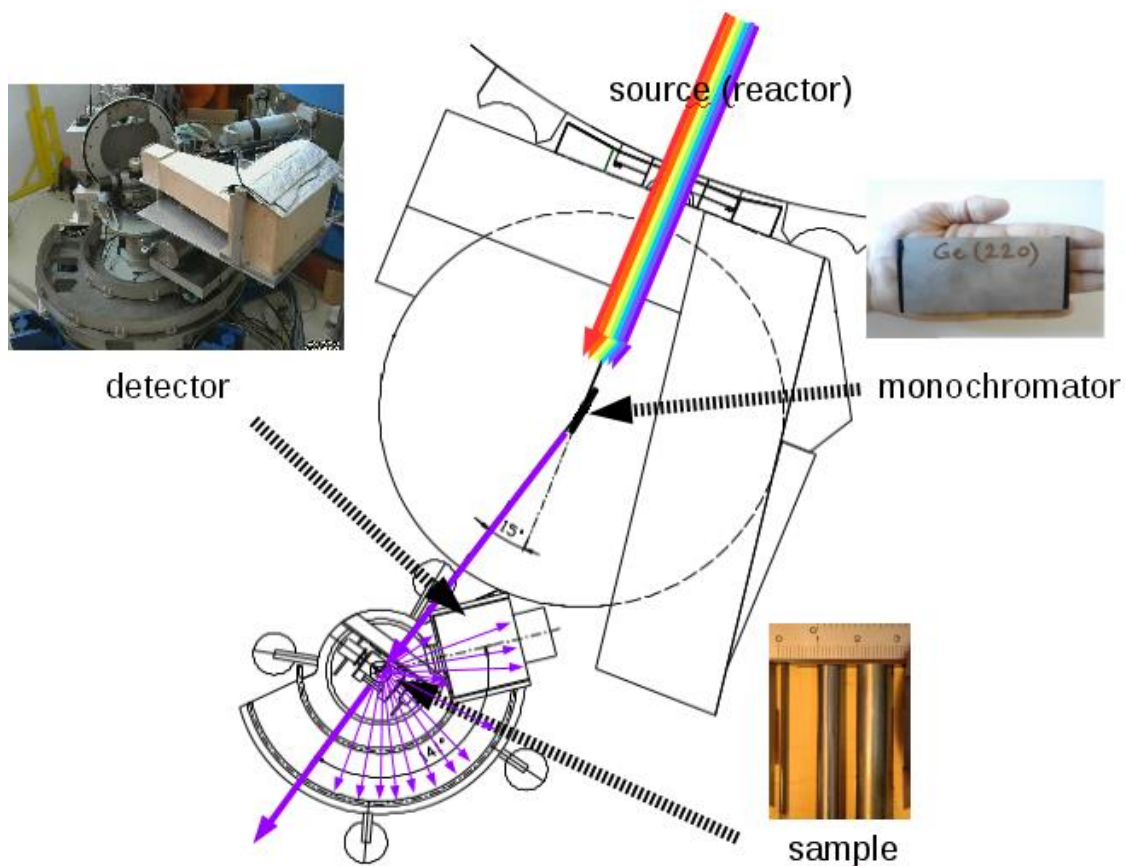
Figure 2. Overview of the MTEST ver 3.0 diffractometer (Modified from ver 2.0 layout, whose source: L. Temleitner, L. Pusztai, Sz. Pothoczki: Tetraéderes molekuláris folyadékok – Egyszerű anyagok, fejfájást okozó problémák [in Hungarian: The structure of neat liquids consisting of tetrahedral molecules – Simple materials that have caused a lot of headache], Természet Világa, 147(2016,8) 346.)

The second axis contains the sample, which is usually sealed in a 6 or 8 mm diameter, thin-walled (order of 0.1 mm) vanadium can. Thus, a sample amount of 1.25 or 2.5 cm^3 is required in optimal case. At room temperature a sample changer for 4 cans (controlled by the "Phi" axis), liquid N_2 operated cryostat and vanadium furnace (up to 1000°C) are available as ancillary equipment. For single crystal studies Eulerian cradle (3 circle+the 2Θ circle) is available.

The scattered neutrons are detected by a detector system placed in three well-shielded banks, making the system suitable to studies of disordered materials. Each low and high-angle banks consist of at least two pieces of 61 cm long 1 inch diameter Reuter-Stokes ^{3}He 1D position sensitive detectors. In the central bank the 20 cm width, 2 inch high ORDELA ^{3}He 1D position sensitive detector is placed. This arrangement allows to record the 5°-142° range of diffraction pattern by 2 frames and medium (0.6°). resolution.

3. Laboratory practices using the MTEST diffractometer

The first part of the practice is addressed to provide first-hand experience on absorption, coherent and incoherent scattering on some commonly used materials in neutron diffraction. The second part consists of a measurement of a liquid or a crystalline sample.

3.1. How to do measurement using the control system?

First of all, do not panic! You need to take care about maximum 2 axes during the whole practice: the "Phi", which rotates the sample changer and the "2Theta", which moves the detector into the required central position.

The measurement is controlled through command lines using the "./mtest" program in the home directory of "mtestuser".

If you want to:

- get the actual angular position of a motor: "**./mtest MOTOR**", e.g. "**./mtest 2Theta**" provides the actual angular value of the detector.
- move the detector to a given angular position: "**./mtest MOTOR TO**", e.g. "**./mtest 2Theta 90.0**" moves detector approximately perpendicular to the incoming beam.
- start a measurement "**./mtest FILENAME MOTOR NO_OF_RUNS START_RUN_NO INITIAL_DEGREE START_DEGREE FINAL_DEGREE STEP_DEGREE MEASUREMENT_TIME_SEC COMMENT**", e.g. "**./mtest ccl4 2Theta 1 2 23 24.5 57.5 33 1200 ccl4_measured_at_RT**" performs the measurement only once at 24.5° and 57.5° of 2Θ axis spending 20 minutes for each. Before doing it, the detector moves to 23°. In each measurement the datasets are saved into the ccl4_2_... files writing the comment into it (note the lack of spaces in the comment!). We refer the "**23 24.5 57.5 33**" sequence as standard setup in the following.

During the measurement at regular intervals the already measured datasets are recorded into file using "**FILENAME_RUN_POSITION_SNAPSHOT.dat**" kind of format, e.g. "**ccl4_2_2_3.dat**" will be created at the third snapshot at 57.5°according to the example shown above. The file contains the full description of the setup, actual positions of each motor, elapsed time, monitor counter count and number of detected events for each channel. I have to note here, that the "**defaults**" file contains some non-frequently changing parameters like the setup of incoming slits and at other than room temperature measurements the temperatures also recorded in regular intervals.

3.2. Absorption, coherent and incoherent scattering

In this part, we are going to investigate the following materials: cadmium (one of the best absorber for thermal neutrons), PMMA (a polymer that contains lots of hydrogen), nickel powder (frequently used for calibration), vanadium (only incoherent scattering – even though it is crystalline, Bragg-peaks are hardly seen).

Steps of the practice:

a) We do measurement for 1 min at low 2Θ degrees to provide some reference.

b) Mount the previously prepared samples to the sample changer.

c) Rough centring of the sample: move the "Phi" motor by manual control, until the required sample becomes more-less centred. The next position follows by 18°.

d) We start with cadmium: let's move the detector to the previous angle, and measure intensity for 1 min again! You should observe, that the intensity is less in comparison with step "a".

e) Then, set up the PMMA and perform two measurements at low 2Θ angles, 1 min for each. We can experience, how high the incoherent scattering intensity is. This feature makes challenging to measure the coherent scattering part of protonated samples.

f) Rotate the sample changer to set the nickel powder for measurement. Move the detector to a position specified in practice and start 1 min measurement. You should observe intense Bragg peaks: this is the reason, why nickel is used for calibration purpose.

g) The last sample will be the vanadium rod. Determine, at which angle we should observe Bragg-peaks, then perform measurement for 1 min. We should find that the scattered intensity comes almost only from incoherent scattering. This is the reason, why it is used to correct efficiency of detectors placed at different angles.

3.3. Measuring the crystal structure of calcite

Calcite is one of the most frequently appearing mineral on Earth, consists of $CaCO_3$ – we are going to determine its crystal structure. During the measurement, the next steps are followed:

- Remove PMMA, cadmium, vanadium from the sample changer and mount the can containing the calcite powder into the sample changer.
- Adjust the position of the changer using the two microscopes at the detector: move 2Θ to 57.5 degrees and centre it.
- Perform the measurement using standard setup: set the 23 as initial degree and measure from 24.5 to 57.5 degrees in 2Θ, by 33 degrees step spending 600 seconds time for each.

We are going to evaluate the datasets, according to section 3.5.

3.4. Measuring the liquid structure of carbon tetrachloride

Carbon tetrachloride (CCl_4) is a tetrahedral-shape non-polar solvent, regular item in chemistry lab. Within the last 10 years it has been found, that orientation correlations between pairs of molecules show relatively long range (several nm) order. During the measurement, the next steps are followed:

- Remove PMMA, cadmium, vanadium from the sample changer and mount the can containing CCl_4 into the sample changer.

- Adjust the position of the changer using the perpendicular microscopes at the detector: move 2Θ to 57.5 degrees and centre it.

- Perform the measurement on the full range by standard setup: set the initial degree to 23 and measurement from 24.5 to 57.5 degrees in 2Θ, by 33 degrees step and 600 second measurement time for each.

We are going to evaluate the datasets, according to section 3.5.

3.5. Evaluation of the measured datasets

At first glance, it seems to be easy to reach differential cross-section working simply by definition, but detection of incoming scattered neutrons requires different efficiency of the detectors, the sample might absorb or it is necessary to put the sample in a holder, etc. To avoid the possible errors, the following measurements should be performed (E_x means normalized intensity measured experimentally):

- sample, typically in a container: E_S

- container: E_c

- background (you might omit it, if absorption were negligible): E_B

- vanadium standard (almost fully incoherent scatterer, it might not be necessary, when a crystal is measured): E_V

- calibration standard to determine the wavelength

Using the above measurements, you can determine non-attenuated measured intensity using transmission coefficients ($A_{S,1}$, $A_{C,1}$, $A_{C,2}$ – where letters mean Container/Sample, no. refers to the measurement written above):

$$I_S = \frac{1}{A_{S,1}}\left[E_S - \frac{A_{C,1}}{A_{C,2}}E_C - \left(1 - \frac{A_{C,1}}{A_{C,2}}\right)E_B\right]$$

$$I_V = \frac{E_V - E_B}{A_V}$$

Finally, the differential cross-section is obtained by taking into account *atomic number densities* of vanadium and the sample (ρ_V and ρ_S, respectively):

$$\frac{d\sigma}{d\Omega} = \frac{\rho_V}{\rho_S}\frac{I_S}{I_V}\frac{\sigma_{V,incoh}}{4\pi}$$

Note that this is a simplified description: multiple scattering and inelastic (called Placzek correction) contribution are also necessary to be subtracted.

The evaluation of the measured datasets is performed with custom made programs. It proceeds according to the following procedure:

a) Pre-evaluation: we would like to use the last saved dataset, but sometimes incidents happen during the measurement (e.g. the sample might evaporate)

b) Normalizing the raw dataset by the monitor counts and performing dead-time correction. Then the program averages the datasets measured at the same detector position, applies the efficiency of each tubes and converts the channel numbers to degrees in 2Θ and to Q in Å^{-1}.

c) Absorption correction: subtract the previously measured empty container/ background

d) Finally, the full pattern is created by merging the frames

4. Interpretation of the measured datasets

4.1. Measuring the crystal structure of calcite

For interpretation, we intend to use two softwares. The FullProf program is regularly used for Rietveld refinement purpose and the Fox program, which implements simulated annealing.

a) During the measurement, we are going to determine the wavelength and refine instrumental parameters by means of Rietveld-method using FullProf software.

b) In FullProf, we are going to set an approximate wavelength and vary the intensities. Then, gradually allow variation of the following parameters: 'W', then 'V' of the instrumental resolution function with Gaussian shape; constant background; zero shift; wavelength; the mean-square displacement related B factor. After good agreement is reached, check the actual value of the wavelength!

c) At this point you have a freedom to use your favourite Rietveld refinement/simulated annealing code – during the practical work we are going to use Fox.

d) We would like to determine lattice type and lattice parameters: this step is called indexing. Open the data by Fox using the known wavelength and automatically look for peaks. Then start indexing: we are going to choose the suitable lattice.

e) By the help of *International tables for Crystallography A* and the lack of lines, determine the possible space groups.

f) Perform the LeBail-fit of the pattern: it refines positions of the Bragg-peaks by changing lattice parameters and instrumental parameters as well. Also, integrated intensities belonging for each Bragg-peak are obtained.

g) We expect, that Ca^{2+} and CO_3^{2-} ions are well separated in the lattice. Due to symmetry reasons, we should look for at least 3-fold symmetry places for carbon atoms and also high symmetry positions for calcium. We can also use as a starting hypothesis, that the distance between carbon and oxygen in CO_2 is 0.116 nm – here it should be surely longer. You can follow several strategies. The simplest one is to create an initial structure and perform short simulations using Fox, which looks for the best configuration by simulated annealing technique. After 2-3 simulations, check the best candidates and increase/decrease the CO bond distance. In the ideal situation, you will get the crystal structure of calcite. If you choose the other way, after you placed calcium and carbon atoms look at the difference Fourier-map, which shows the real-space representation of the difference between measured and simulated dataset. The maximum difference sites show where the oxygen atoms should be positioned.

h) Try to reach good agreement with the measured data: the R_{wp} factor should be less than 10%!

i) Compare, what we have got with earlier published results using Open Crystallography Database!

4.2. Measuring the liquid structure of carbon tetrachloride

We are going to interpret the results using three different techniques:

a) First of all, we are going to use the **MCGR** program to check, what kind of information we can see solely by the diffraction data. This program implements the reverse Monte Carlo method without atomic configuration: it varies the intensity of G(r). Is it really tetrahedral shaped? We are going to determine carbon-chlorine and chlorine-chlorine bond distances and investigate the molecular structure. By gradually constraining G(r) to be zero below and after the carbon-chlorine bond distance, we are trying to filter out possible systematic errors of the measurement.

b) We are going to compare S(Q) obtained from large scale molecular dynamics simulation with the measured dataset.

c) Reverse Monte Carlo demonstration using the **RMC_POT** software: without knowing anything about the applied potential, we are going to try to model our system and reach good agreement with the measured dataset.

d) Analysing both MD and RMC configurations: we are going to determine angular distributions between molecular neighbours, which would be impossible solely by G(r). Also, analysis of Rey's will be demonstrated to show nanometre range positional correlations in this liquid.

References

MTEST diffractometer: visit the BNC homepage at www.bnc.hu

About the different kind of corrections: Fischer et al. Rep. Prog. Phys. **69** (2006) 233. and its references

Crystal structure determination:
FullProf: https://www.ill.eu/sites/fullprof/
Fox: https://fox.vincefn.net/
Crystallography Open Database: http://www.crystallography.net/cod/
International Tables for Crystallography A or Bilbao Crystallographic server:
http://www.cryst.ehu.es/

Selected papers about carbon tetrachloride:
Rey, Journal of Chemical Physics **126** (2007), 164506.
Pothoczki et al., Journal of Chemical Physics **130** (2009), 064503.
Pothoczki et al., Chemical Reviews **115** (2015), 13308.

Reverse Monte Carlo programs:

    MCGR: part of win_NFLP package:

    http://www.szfki.hu/~temla/rmcpow_tutorial_win_nflp.zip

    RMC_POT: http://www.szfki.hu/~nphys/rmc++/opening.html

Molecular dynamics by GROMACS:

    http://www.gromacs.org/

    Good tutorial for beginners: http://wbarnett.us/gromacs-tutorials/

    https://www.svedruziclab.com/tutorials/gromacs/

Small Angle Neutron Scattering

Adél Len, László Almásy

1. Introduction

The method of small angle neutron scattering (SANS) is based on the coherent and elastic scattering of neutrons from the atomic nuclei at angles smaller than 20 degrees.

SANS reveals structural details in the size range between *1nm* and *1000nm*, giving information about size, shape, orientation of structures in the sample. In the following discussion we consider relatively simple sample morphologies: particles in a continuous medium, where the coherent neutron scattering length density of the particle differs from that of its surroundings (this difference is called contrast, *K*). In general, systems to be studied by small angle scattering can be materials containing two or more phases, such as crystallites, pores, cracks, or solid and liquid materials having composition and density inhomogeneities and fluctuations.

The following example is a system that is suitable for SANS studies: a potassium doped tungsten wire (**Figure 1**), where the potassium bubbles are the scattering objects (size: *10 nm -500 nm*), and the tungsten grains are the matrix.
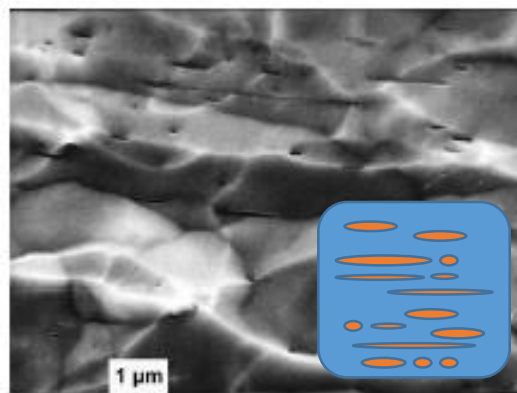

Figure 1. SEM picture and constructed model of
potassium bubbles (orange) in tungsten matrix (blue)
(SEM picture from: L. Bartha, P. Harmat, O. Horacsek, T. Grósz, L. Rosta:
Proceedings on 4th International Conference on Tungsten (1998) 203-210)

The scattering length densities (SLD) and contrast (K) for the potassium – tungsten system:

$$A_W = 3.066 \times 10^{10} \ cm^{-2}$$
$$A_{Ksolid} = 0.484 \times 10^{10} \ cm^{-2}$$
$$K = A_W - A_{Ksolid} = 2.582 \times 10^{10} \ cm^{-2}$$

If the scattering object is bigger than several tenths to hundreds of nanometres, SANS gives information about the interfaces within the scattering object.

Besides the general advantages of neutron methods, such as non-destructivity, isotopic substitution, sensitivity to the magnetic structure etc., the method of SANS shows several special advantages:

- gives average information about the entire volume of the sample placed into the neutron beam (not only about its surface)

- needs no sample preparation, therefore sample-preparing artefacts can be avoided

- makes possible the in-situ following of various processes in function of physical or chemical parameters, such as temperature, concentration, annealing, enlightening, strain or stress etc.

Comparing it to the small angle X-ray scattering (SAXS), because of the difference between the X-rays and neutrons interaction with the matter, SANS and SAXS usually provide different information; often the neutron and X-ray small angle scattering are used as complementary methods.

The main disadvantage of SANS method is its indirect character, therefore mathematical model analysis has to be used for evaluation and interpretation of the experimental data. Such analysis can often be complex and can provide not unique solutions.

2. Theoretical basis

2.1. Scattering vector

The interaction of the neutron with the matter is described by its particle and wave nature.

The wave vectors of the incoming and scattered neutrons are denoted with $\overrightarrow{k_0}$ and $\vec{k}$ (**Figure 2**). $\vec{Q}$ is the change of the wave vector after scattering, and it is called scattering vector. Its absolute value is given by **Equation 1**, where θ is the half of the scattering angle, λ is the wavelength of the neutrons.

Figure 2. Geometry of scattering of the neutron from the nucleus

$$|\vec{Q}| = |\vec{k} - \overrightarrow{k_0}| = \frac{4\pi}{\lambda} sin\theta \qquad (1)$$

$$\left|\vec{k}\right| = \frac{2\pi}{\lambda} \qquad (2)$$

2.2. SANS basic equation

The coherent scattering intensity is given by the superposition of the plane waves which are coherently scattered from the nuclei. The coherent scattering intensity is given by **Equation 3**, and is the Fourier transform of the distribution of neutron scattering length densities (*S(r)*), inside the volume of the sample.

$$I(Q) = \int_{V_i} \int_{V_j} S(r_i)S(r_j) \exp\left(-iQ(r_i - r_j)\right) dV_i dV_j \qquad (3)$$

where *i* and *j* indexes denote the ith and j^{th} atomic nuclei.

2.3. Scattering intensity

The intensity of the scattered neutrons ($I(\lambda,\theta)$) is measured by the detector as the number of neutrons per second in the unit solid angle (**Equation 4**). It depends on the flux of the neutrons at the sample position (neutrons/cm² s), the efficiency of the detector, the volume of the sample irradiated by the neutron beam, transmission of the sample, number of particles in unit volume, and the macroscopic differential cross section.

$$I(\lambda, \theta) = I_0(\lambda)\Delta\Omega\eta(\lambda)TVN\frac{d\Sigma}{d\Omega}(Q) \qquad (4)$$

where:

$I_0(\lambda)$ - incoming neutron flux
$\eta(\lambda)$ - detector efficiency
T - sample transmission
V - sample volume
N - number of the particles in unit volume
$\Delta\Omega$ - solid angle, independent from 2θ scattering angle for angles smaller than 5°
$\Delta\Omega = \frac{dxdy}{L_{SD}^2}$
L_{SD} - sample to detector distance
$dxdy$ - cell size of the detector

The $\frac{d\Sigma}{d\Omega}(Q)$ macroscopic differential cross-section (**Equation 5**) contains the useful information about the structure of the sample. For a system, consisting of uniform particles distributed in a homogeneous matrix, $\frac{d\Sigma}{d\Omega}(Q)$ can be written in the following form:

$$\frac{d\Sigma}{d\Omega}(Q) = NV_p^2 K^2 F(Q)S(Q) \qquad (5)$$

where:

V_p - the volume of one scattering particle
K - contrast
$F(Q)$ - form factor
$S(Q)$ - structure factor

The form factor *F(Q)* describes the shape of the scattering object, having uniform scattering length density, and is similar to **Equation 3**, but the integration is limited to the particle volume:

$$I(Q) = \int_{V_i} \int_{V_j} \exp\left(-i\mathbf{Q}(\mathbf{r_i} - \mathbf{r_j})\right) dV_i dV_j \qquad (6)$$

Several examples of analytically expressed form factors are given in the **Table 1**.

The *S(Q)* structure factor describes the local ordering of the particles in the sample. It is related to the probability distribution function of the inter-particle distances through the *g(r)* pair correlation function (**Equation 7**). When the scattering objects are far from each other, the value of *S(Q)=1*.

$$S(Q) = 1 + \frac{4\pi N}{QV} \int_0^{\infty} [g(r) - 1] r \sin(Qr)\, dr \qquad (7)$$

Table 1. *Form and structure factors*

F(Q) - sphere of radius *r*	$\left[\dfrac{3(\sin(Qr) - Qr\cos(Qr))}{(Qr)^3}\right]^2$
F(Q) - cylinder *r* – radius *L* - length *L* *J₁(x)* – first order Bessel function *a* – angle between the axis of the cylinder and *Q* vector	$\int_0^{\pi/2} \left[\dfrac{2J_1(Qr\sin\alpha)}{Qr\sin\alpha} \dfrac{\sin(QL\cos\alpha/2)}{QL\cos\alpha/2}\right]^2 \sin\alpha\, d\alpha$
S(Q) - concentrated polymer solution with ξ correlation length	$I(0)\dfrac{1}{1 + (Q\xi)^2}$

2.4. Porod approximation

Debye (Debye 1949) and later Porod (Porod 1951) have shown, that in a two phase system the SANS curve can be characterized by a constant value, called Porod invariant (denoted by *C*, (**Equation 8**), which does not depend on the form of the interface.

$$C = \int_0^{\infty} \frac{d\Sigma}{d\Omega} Q^2 dQ = 2\pi K^2 O_S \qquad (8)$$

where:

$\frac{d\Sigma}{d\Omega}$ – macroscopic differential cross section
K – contrast
O_S - specific surface

If the surface between the various domains is sharp, the O_S specific surface can be calculated from E**quation 9**. The asymptotic law that is valid for large Q values, where *Q>>1/size of the scattering object*, is attributed to Porod.

$$O_S = \frac{S}{V} = \pi \frac{[I(Q)Q^{-4}]_{Q\to\infty}}{C} \qquad (9)$$

The logarithm of the intensity represented as function of logarithm of Q gives a line of slope of -4.

If we represent $I(Q)Q^{-4}$ as function of Q^{-4}, the slope of the curve will give the level of the incoherent background scattering and the intersection with the vertical axis will give the value of the Porod invariant.

Determining the specific surface is of great interest for cases when the size of the scattering objects is equal or larger than the maximal size attainable for the instrument, or in case of random phase containing structures, where the phases grow randomly into each other, but the surface between them is sharp.

When this surface is diffuse, that is, the scattering length density changes continuously across the surface, the exponent is lower than *-4* (in the range *-5 - -4*), and if the surface is fractal-like, the exponent value is larger than *-4*.

Figure 3 represents various systems that exhibit power law behaviour.
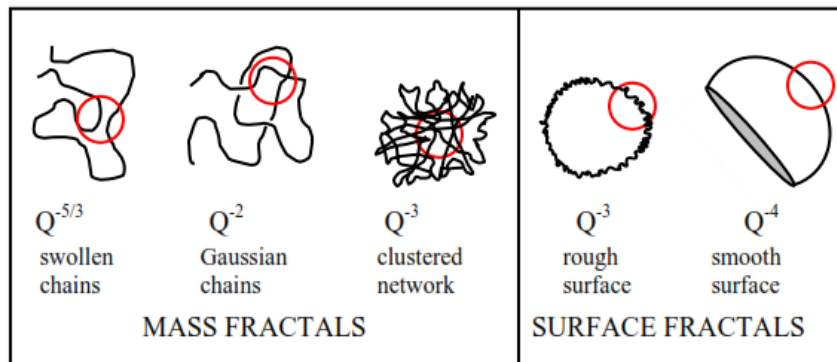

Figure 3. Assortment of fractal exponents
(https://www.ncnr.nist.gov/staff/hammouda/distance_learning/chapter_33.pdf)

2.5. Guinier approximation

If we analytically unfold **Equation 6** to a power series for values *Qr < 1*, and neglect the higher order terms, the scattered intensity will take the form of E**quation 10**.

$$I(Q) = K^2 V^2 exp\left(\frac{-Rg^2 Q^2}{3}\right) \qquad (10)$$

where *Rg* is the gyration radius (Glatter 1982).

In practice the natural logarithm of the measured intensity is plotted versus Q^2 , and if the data look like a straight line, then its slope will be equal to the gyration radius. If the

scattering objects have simple shapes, their dimensions can easily be calculated with the formulas given in **Table 2**.

Figure 4 illustrates the scattering curve of a cylinder with the Guinier and Porod regions.

Table 2. Radii of gyration

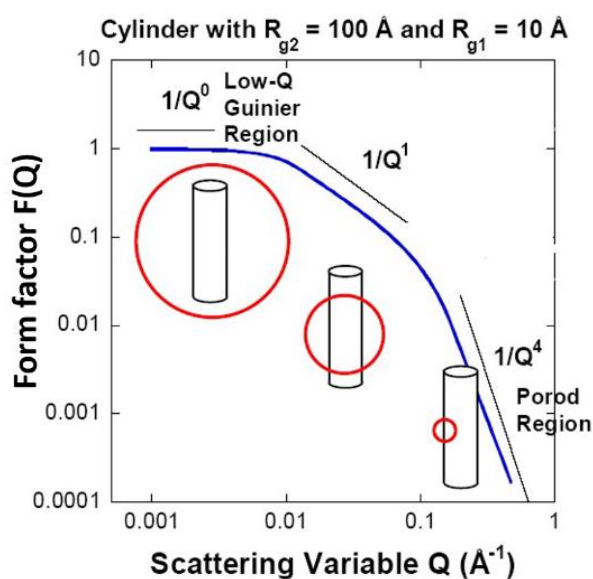| Sphere (radius *R*)	$Rg^2 = \dfrac{3}{5}R^2$
Ellipsoid (*a, b, c* half-axes)	$Rg^2 = \dfrac{a^2 + b^2 + c^2}{5}$
Rod (length *L*, radius *r*)	$Rg^2 = \dfrac{L^2}{12} + \dfrac{r^2}{2}$
Spherical shell (radii R_1, R_2)	$Rg^2 = \dfrac{3}{5}\left(\dfrac{R_2^5 - R_1^5}{R_2^3 - R_1^3}\right)$

Figure 4. Illustration of the Guinier and Porod regions

(https://www.ncnr.nist.gov/staff/hammouda/the_sans_toolbox.pdf)

3. *Yellow Submarine* SANS instrument at Budapest Research Reactor

The SANS instrument named *Yellow Submarine* (YS, **Figure 5**) is a pin-hole type instrument, where the beam is defined by slits and holes on the collimator tube, and the wavelength is defined by means of a velocity selector. The *Q* resolution can be varied by varying the divergence - by setting the slit sizes - and collimation length, and varying the

wavelength. The covered *Q* range is relatively wide (*0.006 – 0.4 Å⁻¹*). The scattered neutrons are detected by two-dimensional (2D) position sensitive detector.

YS is installed at the cold neutron channel number *10/2* of the BRR, and has been in operation in its actual configuration since year 2000. It uses cold neutrons produced by the liquid hydrogen cold source. Its overall length is *33m* (Scheme shown on **Figure 6**).

Figure 5. *Image of the detector tank and sample environment of Yellow Submarine*
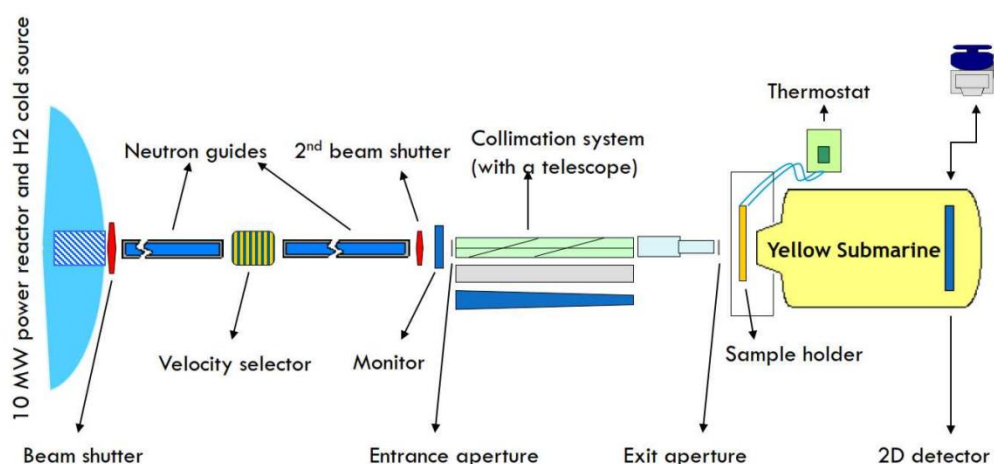

***Figure 6***. *Scheme of Yellow Submarine*

3.1. Reactor

YS is operating at the VVR type *10MW* power research reactor at Budapest Neutron Centre (see chapter "Introduction to neutron beam experiments").

The neutrons produced in the reactor core have energies around *1-2 MeV* and they are slowed down in the light water moderator in the reactor vessel. For the purpose of SANS further slowing is needed, which is achieved in a cold source consisting of a helium cooled cell filled with liquid hydrogen (see chapter "Introduction to neutron beam experiments"). By collisions with hydrogen nuclei having temperature of *20K*, the neutrons are slowed down to wavelengths between *3-25Å*.

3.2. Velocity selector

The mechanical velocity selector (designed and built in Budapest) serves to select a monochromatic neutron beam from the cold neutron spectra, by allowing neutrons of defined velocity to pass, while absorbing others. It consists of a turbine with several disks whose windows form helical channels (**Figure 7**). The disks are coated with a strongly neutron-absorbing material, gadolinium-oxide. The rotation speed is variable between *700 rpm* and *7000 rpm*. By changing the rotation speed, the velocity – thus the wavelength – of the passing neutrons can be varied from *3Å* to *25Å*. The relation between the rotation speed and the wavelength can be determined by measuring the time of flight of the neutrons (de Broglie equation – see **Equation 11**).
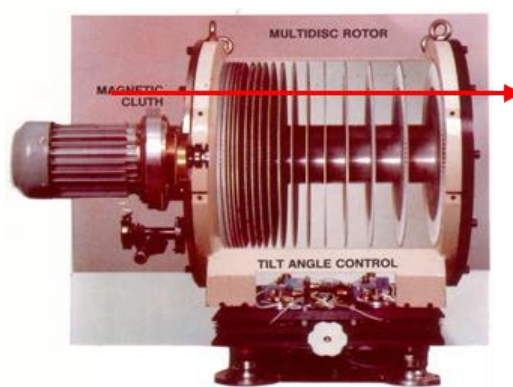
Figure 7. *Schematic representation of a multi-disk velocity selector.*
The red arrow represents the direction of the neutron beam

$$\lambda_n = \frac{h t_n}{m_n d_n} \qquad (11)$$

where:

λ_n – selected wavelength of the neutrons
t_n – flight time
m_n = 1.6749286 $\cdot 10^{-27}$ kg, mass of the neutron
h = 6.625 $\cdot 10^{-34}$ Js, Planck constant
d_n – selector-detector distance

The wavelength spread can be tuned between *10* and *30%* FWHM, by varying the rotor tilt angle (the angle between the beam and the selector axis).

3.3. Neutron guides

The role of the neutron guides is to direct the neutrons to the sample with the smallest possible loss. The neutron guides are boron containing glass plates, coated with nickel-titanium layers. The layers reflectivity can be tuned up to *0.8 – 0.9* (see chapter "Introduction to neutron beam experiments").

3.4. Collimator

The easiest way to collimate the neutron beam is to guide it through a vacuumed tube that contains diaphragms made out of neutron absorbing material. The diaphragms define the diameter, and the divergence of the beam. Their form can be circular or rectangular. The shorter collimation length will lead to higher neutron intensity and more divergent beam, while the large collimation distance will decrease the divergence, but will lower the neutron intensity. For an optimal intensity-resolution combination, usually the collimation length is chosen to be similar to the sample to detector distance. On the YS usually *4.7 m* collimation length is used. The beam diameter at the sample position can be chosen from *2 mm* to *16 mm*.

3.5. Detector

For monitoring the incoming neutron flux variation in time a uranium fission chamber with *0.1%* efficiency is used, placed between the neutron guide and the collimator entrance slit.

For detecting the thermal neutrons scattered from the sample, nuclear reactions are used. The detector at the YS instrument uses the: $n(^{10}B,\alpha)^7Li$ reaction. The alpha particles ionize the gas and induce a current impulse, which is registered and its position is determined. by a specially designed electronics.

The YS detector contains $^{10}BF_3$ gas, its pixel size is *10 mm x 10 mm*, and it has *64 x 64* pixels. It can be moved in a *6 m* long vacuumed tube, the smallest sample to detector distance is *1.3 m*, the largest *5.4 m*. Before the detector house a Cd - B plate is placed, with the purpose of absorbing the high intensity direct neutron beam transmitted through the sample (**Figure 8**). The Cd - B plate is called "beam-stop", and its size can be varied according to the size of the beam defined by the collimator.
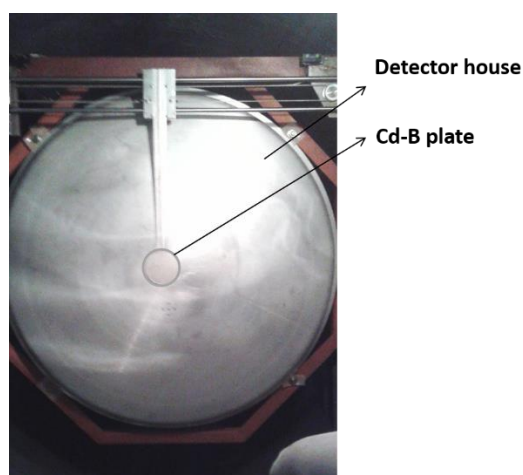

Figure 8. Cd plate (beam-stop) at the centre of the detector

3.6. Sample environment

Usually, three types of sample holders are used: a sample holder with temperature regulation – from *15°C* to *90°C* (**Figure 9**), a room temperature sample holder with and a vertical sample changer, designed for samples to be measured in magnetic field. All holder

types have several sample positions. An electromagnet of max *1.8T* magnetic field is available.

Larger (max. *0.5m* diameter) samples can be measured by removing the sample changer.

Solid compact samples are placed into the sample holder without any preparation. For powder and liquid samples quartz cuvettes of various sizes (**Figure 10**), or other holders made of low neutron absorbing and scattering material are used.

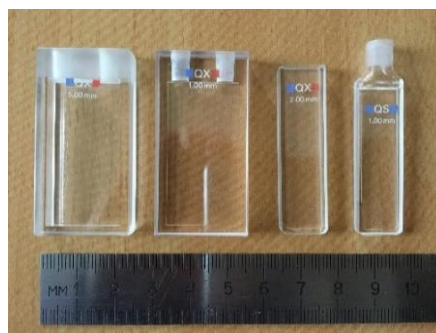*Figure 9.* 6 position sample holder with temperature regulation

Figure 10. Quartz cuvettes

4. Experiment description

4.1. General considerations

SANS experiments are performed on a great variety of samples, with many different objectives. In spite of that, several common considerations exist, that have to be taken into account when the experiment is planned.

1. The multiple scattering limits the thickness of the sample, which can vary from micrometres to several millimetres depending on sample characteristics (scattering cross sections) and wavelength. High transmission value (*>60%*) should be used to decrease or avoid the multiple scattering.

Examples for maximum thicknesses:

- metal samples: *1-2 mm*
- solid foams: *5-10 mm*
- ceramics, marbles: *1-5 mm*
- polymers: *1-2 mm*
- H_2O based solutions: *1 mm*
- D_2O based solutions: *5 mm*
- concentrated D_2O solutions: *1-2 mm*
- dilute D_2O solutions: *5 mm*

2. SANS is an indirect method, mathematical modelling is used to evaluate the measured data, and ideal models do not always describe perfectly the real structures. Therefore at choosing the samples it is useful to consider the preparation and analysis of a series of

samples, by varying their physical or chemical characteristics. It is also useful to measure one or more reference samples.

3. Most successful measurements require previous knowledge about the samples, obtained by methods other than SANS. Useful complementary information can often be obtained by electron microscopy measurements.

4. The scattered neutrons are detected with 2D area detectors. The scattering from a sample can be isotropic or anisotropic (**Figure 11 a)** and **b)**). For randomly orientated scattering objects the measured intensity distribution is isotropic around the beam centre, while samples with oriented structure produce anisotropic scattering. Randomly oriented samples show the same scattering intensity at same scattering angles, while for scattering objects oriented along a given direction in the sample the scattering intensity depends on the azimuth angle for a constant scattering angle. Therefore the isotropic and anisotropic scattering has to be evaluated in different ways.
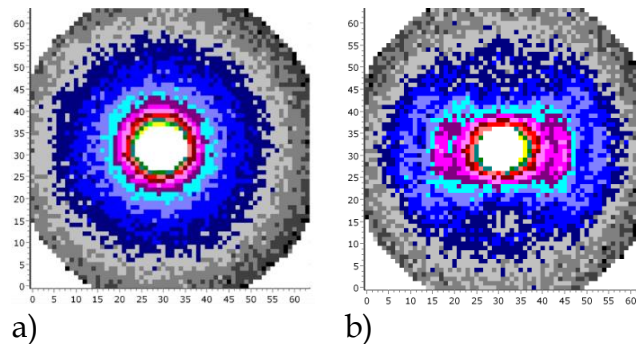

a)   b)

Figure 11. a) Isotropic scattering b) Anisotropic scattering

4.2. Measurement

1. SANS measurements on YS take from few minutes to few hours depending on the sample. The sample preparation means filling the liquid or powder samples into cells or placing the solid samples into the sample changer.

2. Measurement of the thickness (and/or density) of the samples is needed, especially in those cases where quantitative information from the measurement is needed.

3. The optimal Q range is selected by choosing the sample to detector distance and wavelength, usually with the aid of the instrument scientist. **Table 3** contains the Q range for several wavelengths and the two limiting sample to detector distances for YS. When a wide overall Q range is required, the measurements are performed at two different detector positions and/or different wavelengths, allowing an overlap between the individual Q ranges. Choice of the sample to detector distance, wavelength, wavelength spread and aperture sizes are influenced by the desired instrumental resolution (sharp scattering features require good resolution) and flux on sample which is higher at lower resolution settings.

Table 3. Q range for various instrument configurations

Selector rotation speed	Wavelength	Sample to detector distance: 5.54m		Sample to detector distance: 1.5m	
		Qmin (6cm)	Qmax (30cm)	Qmin (6cm)	Qmax (30cm)
2000 rpm	12.07 Å	0.0059	0.0297	0.0271	0.1325
2500 rpm	9.70 Å	0.0074	0.0369	0.0338	0.1648
3000 rpm	8.12 Å	0.0088	0.0440	0.0403	0.1969
3500 rpm	6.99 Å	0.0103	0.0512	0.0469	0.2288
4000 rpm	6.14 Å	0.0117	0.0583	0.0533	0.2604
5000 rpm	4.95 Å	0.0145	0.0723	0.0662	0.3230
6000 rpm	4.16 Å	0.0172	0.0860	0.0787	0.3844
7000 rpm	3.60 Å	0.0199	0.0994	0.0910	0.4442

4. In case of neutron experiments the main part of the neutron beam is transmitted through the sample without any change. For calculating the transmission of a sample two measurements are needed: the attenuated direct (non-scattered and non-absorbed) intensity measured at the centre of the detector with and without the sample, with the same conditions. The ratio of the two intensities gives the transmission of the sample. A transmission measurement takes several minutes. In order to avoid multiple scattering effects, sample transmissions are usually kept above *60%* (controllable by adequate choice of sample thickness).

5. For a complete set of data the following measurement are necessary:

- the sample
- an incoherent scatterer (light water, graphite, polymer) that yields a flat (Q-independent) signal, used for correction for the detector pixels efficiency differences
- the empty cell (or other sample container)
- a calibrated (absolute standard) sample. As absolute standard a *1mm* thick precalibrated light water sample is usually used; this way two measurements – of the incoherent scatterer and of the absolute standard - are reduced to one

6. Count rate: usually a relative error between *1%* and *3%* is expected. If the counted number of neutrons in one pixel is *N=1 000*, then the standard deviation: *Error =* $\sqrt{1\,000}$ = 31,6, that means a relative error of about *3%*; in case of *N=10 000* counts, the standard deviation : *Error =* $\sqrt{10\,000}$ = 100, and the relative error is *1%*. If 3% relative error (*1 000* counts) at a given Q value is achieved in 1 hour measurement, then the 1% relative error (*10 000* counts) at the same Q value would be achieved in *10* hours. For isotropic scatterers the scattering data are circularly averaged, therefore these measurements can be shorter than for the anisotropic samples.

Depending on the sample characteristics (sample size, contrast, density, nanostructure) and of the desired resolution (instrument set-up) a given count rate can be achieved in shorter or larger times, and the relative error can be optimized according to the desired

precision. As a thumb rule, for isotropic scattering, *500 000* counts over the whole detector are sufficient to obtain a smooth scattering curve, which can be analysed by least squares fitting.

4.3. Practical example

1. **Sample:** iron-oxide nanocrystallites grown in silica gel.

- form of the sample: powder

- the matrix is the silica gel, the scattering objects are iron-oxide crystallites and pores, present in the system. The contrast (*K*) values are the following:

$$A_{Fe_2O_3} = 10.785 \times 10^{10} \; cm^{-2}$$
$$A_{SiO_2} = 4.186 \times 10^{10} \; cm^{-2}$$
$$K = A_{Fe_2O_3} - A_{SiO_2} = 6.599 \times 10^{10} \; cm^{-2}$$

2. Sample preparation: sample is put into a powder cuvette of *2mm* thickness

3. Q range: *0.017 - 0.084Å⁻¹*; in this range it is expected to get scattering from the crystallites of about *100Å* diameter

For the chosen *Q* range:

- sample to detector distance: *5.5m*
- wavelength: *4.16Å (6000 rpm)*
- beam diameter: *12mm*
- collimation length (fixed): *4.7m*

4. Measurements:

- sample
- sample transmission
- empty beam "transmission"
- cuvette
- background (noise) – with a Cd plate (absorber) in the beam
- water (H_2O) of *1mm* thickness

5. Counting time has to be determined.

6. 2D raw data on the detector is obtained. 2D scattering intensity of the iron-oxide crystallites embedded in silica gel matrix is shown on **Figure 12**.
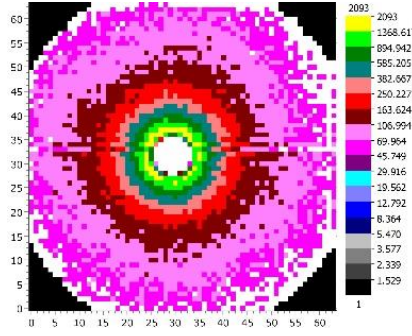
Figure 12. *2D scattering from iron-oxide crystallites in silica gel matrix*

4.4. Data evaluation

SANS data are corrected and rescaled to obtain the macroscopic differential cross section (units of *cm⁻¹*) then circularly averaged for isotropic scattering (1D data treatment). Reduced data are finally plotted using standard linear plots (Guinier, Zimm, Kratky, etc.) in order to extract qualitative trends for sample characteristics (radius of gyration, correlation length, persistence length, etc.) or fitted with models for more detailed data analysis. For anisotropic scattering samples, averaging over azimuthal sectors is performed, or the 2D treatment is used (see chapter "Two dimensional data treatment in SAS").

1. Transmission, sample volume. The sample volume is the volume that is irradiated by the neutrons. The transmission is calculated as the rate of the intensities measured at the centre of the detector with and without the sample: $T = \frac{I_{sample}}{I_{beam}}$

2. Normalization – absolute intensity. The measured macroscopic differential cross section (absolute intensity) is given by the **Equation 12**.

$$\left(\frac{d\Sigma}{d\Omega}\right)_S = \left(\frac{d\Sigma}{d\Omega}\right)_W \frac{\frac{I_S - bg}{d_S T_S} - \frac{I_{cuv} - bg}{d_S T_S}}{\frac{I_W - bg}{d_W T_W} - \frac{I_{cuv} - bg}{d_W}} \qquad (12)$$

where:

$\frac{d\Sigma}{d\Omega}$ – macroscopic differential cross section
I – measured intensity
d – thickness (in *cm*)
bg – measured counts for Cd plate
T – transmission
s – sample
w – water
cuv – cuvette

The value for $\left(\frac{d\Sigma}{d\Omega}\right)_W$ is obtained in a precalibration procedure (water calibrated with vanadium), and its values for various wavelengths are given in **Table 4**.

Table 4. *Water macroscopic differential cross section values (multiplying factor)*

Selector rotation speed	2000 rpm	2500 rpm	3000 rpm	3500 rpm	4000 rpm	5000 rpm	6000 rpm	7000 rpm
Wavelength	12.07 Å	9.70 Å	8.12 Å	6.99 Å	6.14 Å	4.95 Å	4.16 Å	3.60 Å
Factor	0.93	0.91	0.88	0.86	0.83	0.77	0.71	0.66

The data format used at YS is the BerSANS data format. BerSANS is a software developed by Uwe Keiderling, and is freely available at the *https://www.psi.ch/sinq/sansii/bersans* website. The data files used by BerSANS are of ASCII type, and contain all the information about the settings of the instrument and the measured count rate at each detector pixel. The normalization is made with the aid of BerSANS.

3. Radial averaging. The radial averaging is made by the aid of the BerSANS software as well; as result, the intensity, scattering vector data set is obtained. The radially averaged absolute intensity (*I=f(Q)* curve) is shown on **Figure 13**.
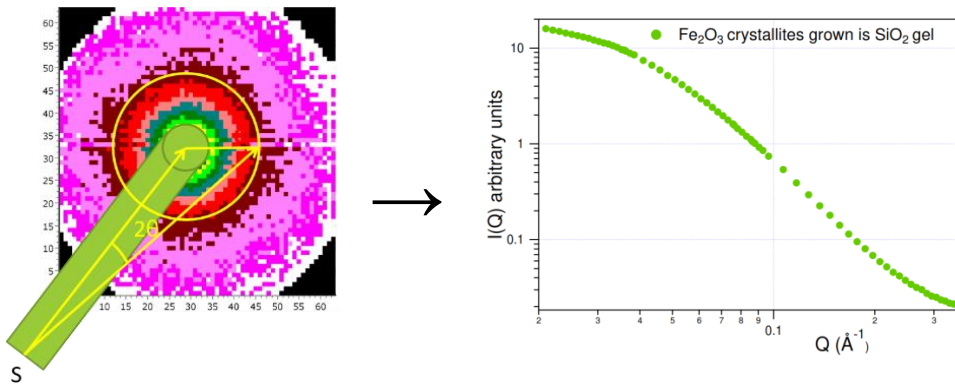

Figure 13. *Radially averaged (I=f(Q) curve) of the iron-oxide crystallites embedded in silica gel matrix*

5. Model fitting. The model fitting can be done by using various available, general purpose or SANS-specific software, such as *Origin, Wavemetrics Igor Pro, Gnuplot, SASfit, SASView* etc.

In the least squares fitting procedure the minimum of χ^2 is searched (**Equation 13**).

$$\chi^2 = \frac{1}{N-p}\sum_{i=1}^{N}\left(\frac{I_i - Y_i}{\Delta I_i}\right)^2 \qquad (13)$$

where:

I$_i$ - ith pixel intensity
N - number of pixels

p - number of free parameters
Y_i - the intensity fitted in the ith pixel
ΔI_i - the error of the ith pixel intensity

If I_i has normal distribution, and the corresponding error bars are correctly estimated, then $\chi^2 \rightarrow 1$. χ^2 values around 1-2 are usually acceptable, while larger χ^2 indicates that the used model is not the true scattering function.

Choosing the adequate model is not always easy, a previous knowledge about the sample is needed (see analytical models in **Table 1**).

In the case of the iron-oxide - silica gel system the scattering from the pores surfaces of the silica matrix and the scattering from the iron-oxide crystallites are not distinguished, therefore the combination of the Guinier model and the Power law model described previously (**Equations 9 and 10**), is used (**Equation 15**):

$$I(Q) = A_1 exp\left(-\frac{Q^2 Rg^2}{3}\right) + A_2 \hat{Q}^{-p} + bg \qquad (15)$$

where:

$$\hat{Q} = \frac{Q}{\left[erf\left(\frac{QRg}{\sqrt{6}}\right)\right]^3}$$

A_1, A_2 - are adjustable parameters, which depend on the contrast and particle number density
Rg - radius of gyration
p -power law exponent describing the scattering surfaces
bg –background

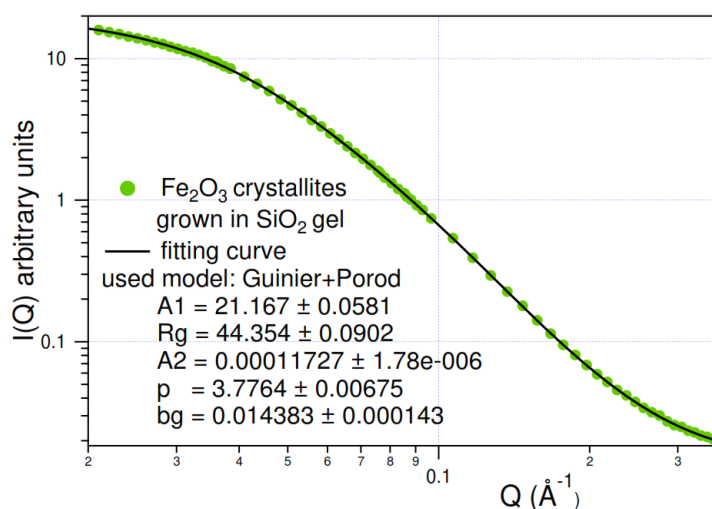**Figure 14** shows the measured data and the fitted model.

Figure 14. 1D model fitting curve for the iron-oxide grown in silica gel

The gyration radius of the iron-oxide crystallites was obtained as 44 Å, the power law exponent was obtained as 3.77, showing an apparent fractal like structure of the scattering of the silica matrix.

Suggested readings

https://www.e-neutrons.org

https://www.ncnr.nist.gov/programs/sans/tutorials/index.html

References

O. Glatter, O. K. (1982). London: Academic Press INC.

P. Debye, A. B., 20 (1949), *J. Appl. Cryst.*, 518.

Porod, G., 124 (1951), *Kolloid Z*, 83.

Two dimensional data evaluation in Small Angle Scattering

Gérard Pépy

1. Introduction

The Small Angle Scattering (SAS) experiment data are usually obtained from a two dimensional (2D) Position Sensitive Detector (PSD); most of the time they depend of the scattering angle only; therefore, the experimentalist is happy to gather these data versus the scattering angle (or scattering vector) in a one dimensional (1D) file and make the data treatment with one of the many appropriate software. However, many experiments exhibit anisotropy or features not centred on the incoming beam: they cannot be reduced to 1D data because the model cannot be split in 1D functions or it may be advantageous to make a full 2D treatment, for instance to have a single pre-factor for the x dependent and the y dependent parts of the model.

Many fields provide anisotropic data: a non-limitative list would include soft matter submitted to an external field, either shear, or stress, or magnetic field, of course magnetic materials ranging from nanolayers to nuclear industry alloys, and also stressed metallic alloys. A specific domain includes experiments on single crystals, which display non centred feature rather than centred anisotropy.

The domain of 2D data treatment has already been reviewed comparing the existing software by that time [1]. On the contrary this chapter will be devoted to the main problems of 2D data treatment, and illustrated by examples treated with the HWXY software developed by the author during a very long time [2].

In the next section we shall review how to display and select 2D data, and we shall remind what means "fitting" a model and how to avoid some traps.

The problem of bad statistics (low counting rates) will be addressed next.

Finally, we shall review a full data treatment case.

2. Display of 2D data

The first idea to display 2D data is to draw them in a 3D frame and to rotate the picture in order to appreciate its shape. This is certainly very attractive to the observer. Meanwhile it is a dead end once the next steps are considered: how to select the most significant pixels and how to compare a model to the experimental data? Therefore, we found that a better way to display 2D data is to make a flat map with various colours according to the intensity. For complex pictures a rainbow palette or a single colour palette with shades are not appropriate; palettes with colour changing fast versus the intensity will much better enhance details.
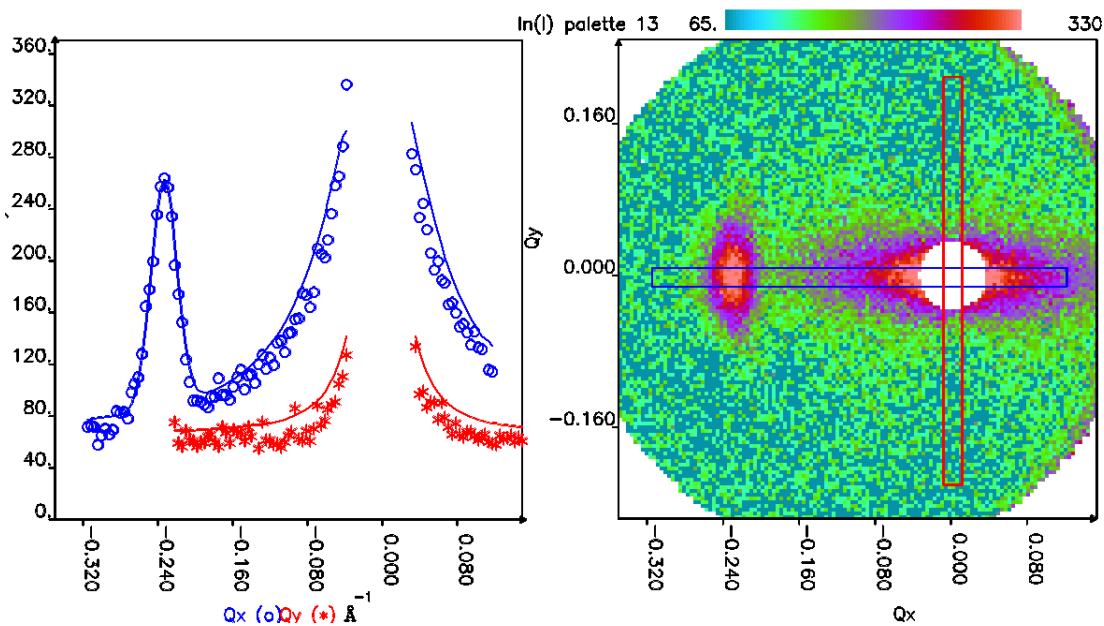
Figure 1. *A fully oriented side chain liquid crystal polymer in the smectic phase (PAXY spectrometer, LLB, Saclay) [3]. The director is along the horizontal axis. On the right is the flat map of all the data. An anisotropic central scattering is observed due to the contrast between protonated and deuterated main chains and a Bragg peak due to the smectic structure. The intensity of the pixels inside two rectangular filters is projected on the relevant axis and displayed on the left. The continuous line is the fitted model; a flat background + a double centred Lorentzian function + a Gaussian-Lorentzian function for the Bragg peak*

At the beginning of a data treatment a small part of the data will be treated, because it is easier to appreciate the intensity shape and also because the fit calculation will be faster. Indeed, the author never found a good way to directly compare a model to 2D data. As a human being the experimentalist is so much used to a 1D representation to compare data points to a model curve that it seems impossible to escape it. For this purpose, the flat colour map allows easily to select the most relevant pixels in filters. The pixel intensity is then projected on one axis. The result is finally displayed on a specific drawing. Then a 2D model function can be calculated for each of the selected pixels, and the projection process can be applied in the same way. In this manner it is easy to compare the model to the data. Let us note, that the projection process alters the function shape. For instance, if the filter is a narrow rectangle it will be easy to recognize a Lorentzian or a Gaussian function; the shape will more and more differ from the classic shape as the rectangle is widened. The shape becomes not familiar at all if the rectangle includes the beam catcher hole!

Many times 2D data exhibit different properties versus x and y axis. Therefore, the most common representation uses rectangular filters (**Figure 1**). They may be horizontal and/or vertical, possibly symmetric versus one axis; there may be several of them.

However, it may happen that the classic display of the projected intensity is not enough to appreciate the quality of the fit. In **Figure 2**, while the model is apparently good, the fit did not converge correctly. A representation of the data – calculated intensity difference

(weighted by the uncertainty) exhibits a misset of the centre position. Using a free centred double Lorentzian function (**Figure 3**) allowed a better fit convergence.
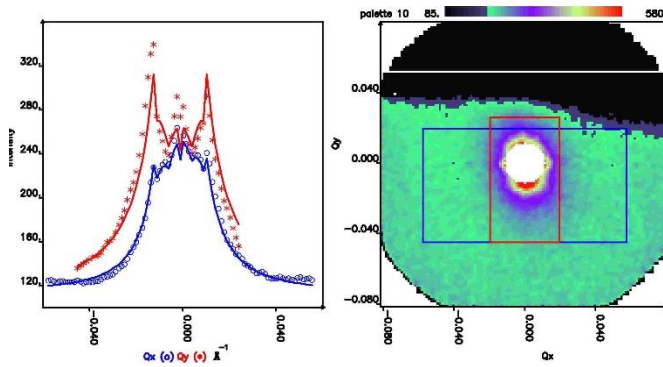

Figure 2. A nematic liquid crystal sheared in a cone-plane apparatus (which produces the shadow on top, PAXY spectrometer, LLB, Saclay) [5]. The model is a tilted (because of shear) double Lorentzian function + flat background
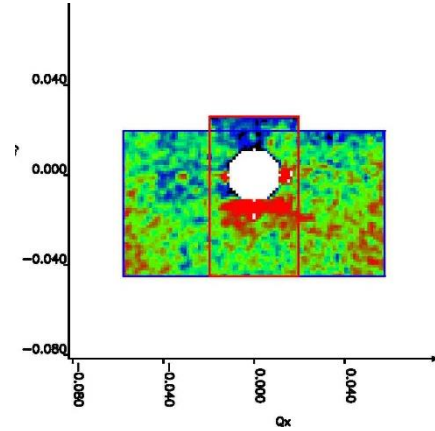
Figure 3. A display of the data – calculated intensity shows a vertical misset of the centre position

3. Fitting process

There are several ways to fit a model to data. A very good introduction to data reduction and error analysis may be found in Bevington [11]. In the PXY software we use the mean-square minimization with steepest descent, which is indeed a very common process. We consider useful to remind the main principles.

The distance between the data and the model is evaluated thanks to a "distance" function. Among several properties such a function should be a positive scalar function. Very often the distance function is a χ^2:

$$\chi^2 = \frac{1}{N-p} \sum_{i=1}^{i=N} \left(\frac{I_i - Y_i\{P\}}{\Delta I_i} \right)^2 \quad (1)$$

where

I_i - intensity in pixel i
N - number of data points
p - number of free parameters
{P} - set of parameters
Y_i - calculated intensity in pixel i
ΔI_i - uncertainty of I_i

If the data probability law is a normal law, χ^2 decreases to 1 as the fit converges. This property is very useful to appreciate the quality of a fit. In particular, it helps to detect systematic errors due to bad correction of the raw data.

The minimization process runs in cycles. Giving increments to the parameters during one cycle, the first and second derivatives of the χ^2 versus the parameters are calculated. This allows to build an approximate set of linear equations. Solving this set of equations provides parameter increments. Assuming that the current position in the parameters space is close to the solution, the χ^2 will be close to the bottom, and the obtained increments will drive to it. Hopefully the χ^2, calculated for the new parameter set, is smaller than the previous one. The process is cycled until the χ^2 does not decrease significantly.

Unfortunately, the model functions of interest make the minimization process highly non-linear. It is therefore important to start from a not too bad set of parameters. For this purpose, it is helpful to select narrow data filters which will be broadened for the final fit. Also it is advisable to let free only a part of the parameters while the most obvious (background, centre position) are kept fixed. Indeed, the more is the number of the free parameters, the highest the risk that the minimization process falls in a "false" minimum from which it is impossible to escape. When this happens (a hint is a χ^2 far from 1), the only solution is to try better with other sets of starting parameters.

4. The problem of bad statistics

When dealing with 2D data, the problem of bad statistics occurs very often. Bevington [11] proposes two ways to improve the statistics: repeat the experiment increasing the measurement time, or smooth out the data. We shall consider the smoothing in a subsequent section: before applying Bevington's advices the SAS raw data correction should be considered.

4.1. SAS raw data correction

Classically SAS raw data correction includes subtracting a reference data file from the sample file and calibration by a specific incoherent scatterer (water, PMMC, vanadium) from which the background has been removed.

For each pixel the corrected scattered intensity is:

$$\left(\frac{d\Sigma}{d\Omega}\right) = F_w \frac{I_s/C_s - I_r/C_r}{I_w/C_w - I_c/C_c} \qquad (2)$$

$$C_s = \frac{(L_{SDs})^2}{A_s d_s M_s T_s} \qquad (3)$$

Where I is the intensity and C a coefficient.

The index mean:
      s - sample
      r - reference
      w - calibration (water, etc.)
      c - background (container, etc.)

and the factors are:

A - beam area

d - sample thickness

M - monitor

T - transmission

L_{SD} - sample to detector distance

F_w - normalization prefactor

I_s, I_r, I_w, I_c and C_s, C_r, C_w, C_c are the pixel intensities and coefficients for sample, reference, calibration and background, respectively.

Of course bad statistics make the fit difficult because of the large associated uncertainties (error bars). It is trivial to observe that the uncertainty over the corrected file is the sum of the uncertainties of all the elements of **Equation 2**. We shall assume that the coefficients uncertainty is negligible, including the transmissions. We shall therefore examine the usefulness of the correction files which are few and therefore much less time consuming than the data files acquisition. At this point we should remember Bacon's remark in is famous book about diffraction [13]: "*the uncertainty of the correction files should not be worse than that of the measured files*". He was referring mostly to the problem of a background measurement: this should be measured during a much longer time than the data in order to get the same level of uncertainty. In a modern SANS (small angle neutron scattering) spectrometer at the end of a neutron guide, the background is very low indeed and experimentalists do not want to lose very much of their precious experimental time just to obtain good statistics. Meanwhile the calibration file usually exhibits small error bars; therefore, it makes sense to forget the background correction just to avoid increasing a lot the final uncertainty!

The calibration file itself is extremely important. For gas detectors the efficiency of each cell exhibits a slow drift versus time and it depends mostly of the preamplifier gain for the anode and cathode which define the cell. This last remark leads to a very useful trick. If the efficiency of a given cell is assumed to be merely the product of the gain of the anode preamplifier and of the gain of the cathode preamplifier, a calibration matrix can be built in the following way: calculate the average intensity of the calibration file, reject all pixels with intensity too far from the average, calculate again the average intensity for the remaining pixels, then calculate the average intensity of each line A_l and each column A_c and normalize them by the overall average intensity, finally build a new calibration matrix whose element A_{lc} will be the product of A_l and A_c. For a square matrix with n^2 elements the uncertainty of element A_{lc} will be smaller than that of the initial matrix by a factor $2/n$. Of course this is not fully accurate but the fit will be more precise! In most cases this is a very efficient way to reduce the uncertainty.

The reference file should not be discarded, as it sometimes contains useful information. For instance, in case of protonated materials, it allows to determine accurately the background. However, for the data treatment it might be more preferable to use only a single fitted background parameter. Assuming the error bars of the reference file are of the same order of magnitude as that of the sample files, replacing it by a single background parameter, would divide the uncertainty by 2. Most often this is a worthwhile transaction.

4.2. Smoothing

The true probability law of data obtained with gas detectors is a Poisson law, which differs quite a lot from a normal law at the smallest counting rates, which is the case for many pixels close to the background; it has a strong influence on the fitting process: in **Equation 1** the data uncertainty ΔI_i is usually approximated by $\sqrt{I_i}$, which is correct for a normal law but introduces a strong disturbance in case of a Poisson law. For instance, the fit may converge towards an acceptable shape of the model but with a too high background parameter. To remedy this feature Bevington [11] advises to smooth the concerned data (it is enough to smooth only the smallest countings).

The least disturbing method is the so-called "parabolic" smoothing where a pixel intensity is replaced by a weighted average over the neighbouring pixels. The weight of the relevant pixel is 1/4, while the weight for the 4 next pixels on the neighbouring lines and columns is 1/8 and the weight for the other 4 pixels on the diagonal is 1/16. This is very efficient to improve the fitting process. A single smoothing pass is enough.

Meanwhile this manipulation has a drawback: it subtly changes the statistics and now the χ^2 decreases to a value lower than 1, which invalidates the convergence criteria and complicates the parameter error bar calculation. Papoular [14] pointed to a solution to this problem, namely replacing not only the intensity but also the associated uncertainty. Let Δ_j be the mean square deviation (uncertainty) of pixel j and w_j the relevant weight, after smoothing the uncertainty of pixel i should be:

$$\Delta I_i = \sqrt{\sum_j \left(w_j . \Delta_j\right)^2} \qquad (4)$$

where the sum runs over the pixels as shown in **Table 1**. This restores the behaviour of the χ^2.

Table 1. *Sum runs over the pixels*

1/16	1/8	1/16
1/8	1/4	1/8
1/16	1/8	1/16

5. Running a 2D data treatment

The experimentalist must be aware that no method will ever improve a bad experiment! The first task will be to read the data and use a representation best suited to the experiment. Do not forget to include a smoothing of small intensity pixels. Then a simple filter or multiple filters will be chosen, narrow enough to select the most significant pixels (in order to further limit the fitting time while getting a first approximation of the parameters). The intensity of the pixels inside the filter is displayed on a I = f(v) diagram, where v is one of the variables x, y, ρ, θ. The model function includes at least a background parameter and one or several functions. It is highly recommended to have a first look at

the model shape produced by the input parameters; it should not be too far from the data. Once it is satisfactory the fitting program can be run. Hopefully it will converge. A χ^2 far from 1 is an unmistakable signature of a false minimum, one should start again the fit with another set of parameters. The calculation of the parameter uncertainty depends on the χ^2 being close to 1. Most often the results are good and it is not necessary to repeat the fit with a large filter only to somewhat improve the parameter error bars.

6. Conclusion

We have reviewed many practical aspects for a successful data treatment: the choice of the representation of the data and the filters, the criteria to include (or not) some corrections and smoothing of the raw data, not forgetting a trick to improve the calibration statistics, how to take care of wild points and, last but not least, how to identify a false minimum though the χ^2 observation.

Acknowledgements

References

[1]   Pépy G, ECNS99 proceedings, Data imaging introductory course, 1999, KFKI-1999-04/E report

[2]   Pépy G http://www-llb.cea.fr/cours/pepy/dl.htm

[3]   Pépy G, *J. Appl. Cryst.* (2007). **40**, s433–s438

[4]   Keller P, Carvalho B, Cotton J P, Lambert M, Moussa M and Pépy G 1985 *J. Physique Lett.* **46** L1065-L1071

[5]   Vicentini F, Noirez L, Pépy G and Mauzac M 1995 *Europhys. Lett.* **32** (8) pp657-662

[6]   Noirez L and Lapp A 1997 *Phys. Rev. Lett.* **78** 1 pp70-73

[7]   Noirez L H. Mendil, L. Noirez,* and P. Baroni,I. Grillo PRL 96, 077801 (2006)

[8]   Kiselev M A, Janich M, Lesieur P, Hoell A, Oberdisse J, Pépy G, Kisselev A M, Gapienko I V, Gutberlet T, Aksenov V I 2002 *J. Appl. Phys.* A **74** S1239-S1241

[9]   Rosta L, Len A, Pépy G, Harmat P, Nano-scale Morphology of Inclusions in Tungsten Wires - a Complex SANS Study, *NEUTRON NEWS* **23:**(1) pp. 13-16. (2012)

[10]   Pépy G, Boesecke P, Kuklin A, Manceau E, Schiedt B, Siwy Z, Toulemonde M Trautmann C *J. Appl. Cryst.* (2007). **40**, s388–s392

[11]   Bevington P R 1969 *Data Reduction and Error Analysis for the Physical Sciences* (New York: McGraw-Hill)

[12]   James F 1994 Geneva http://wwwasdoc.web.cern.ch/wwwasdoc/minuit/minmain.html

[13]   Bacon G 1955 *Neutron diffraction* (Oxford: Clarendon Press)

[14]   Papoular R, LLB (Saclay), private communication

[15]   Soloviev A, Stadnik A, Islamov A and Kuklin A 2007 Dubna http://wwwinfo.jinr.ru/programs/jinrlib/fitter/docs/html/index.html

[16]   Huber P 1981 *Robust statistics* (New York: Wiley)

[17]   Fox J 2002 An R and S-PLUS Companion to Applied Regression (Thousand Oaks: Sage publications)

GINA, neutron reflectometer

László Bottyán, Dániel Géza Merkel

1. Introduction

It was recognized early, that neutrons get totally reflected from a surface at shallow angles of incidence. In many respects, neutron reflection, refraction and interference ('neutron optics') can be assessed by the methods of classical optics. Total reflection of neutrons has been and is being exploited to construct a number of instrument components, such as neutron transport over long distances in neutron guides, in filter systems and in neutron polarizers. In the latter, use is made of the fact that the reflection of neutrons with their spin parallel and antiparallel to the magnetization are different.

Later it was realized that detailed information about the surface and interface structure can be obtained from the plot of the reflected neutron intensity beyond the total reflection regime. Nowadays neutron reflectometry (NR) – similarly to the complementary X-ray reflectometry and ellipsometry techniques – is an established method to provide important – and in cases unique – information on the near-surface (several thousand angstroms) structure in various materials such as polymer surfaces, Langmuir-Blodgett films, organic and bio-membranes and liquid-liquid interfaces, metallic and semiconductor multilayers, both magnetic and nonmagnetic.

The technique involves shining a strongly collimated neutron beam onto a rather flat and smooth surface and measuring the intensity of the reflected radiation as a function of angle or neutron wavelength. Scattering is often described in terms of the momentum transfer vector *q* which quantifies the change of the momentum of the neutron upon being reflected on the target material. Here and during this reflectometry hands-on exercise we will restrict consideration to specular reflectometry, in which the angle of incidence and reflection are equal, consequently the momentum transfer is perpendicular to the sample surface (chosen conventionally as the *z*-direction, see **Figure 1**). A typical neutron reflectogram is a plot of the normalized reflected intensity as function of the scattering vector's surface-perpendicular component, $q_z = (4\pi/\lambda)\cdot\sin(\theta)$, collected by varying either *θ* (monochromatic technique) or *λ* (TOF technique) with *θ* and *λ* being the angle of incidence and the neutron wavelength.

2. Theoretical basics[4]

The neutron incident on the sample surface is described by a plane wave of wave vector *k* with magnitude *k = 2π/λ* and with kinetic energy

$$E = \frac{\hbar^2 k^2}{2m} \tag{1}$$

---

[4] This introduction to the basics closely follows that of A.A. van Well in „Lecture notes on neutron scattering – Introductory course" KFKI Report 1999-04/E

The interaction with matter is described by an effective (or 'optical') potential

$$V(\mathbf{r}) = \frac{2\pi \cdot \hbar^2}{m} \rho(\mathbf{r}) - \boldsymbol{\mu}_n \cdot \mathbf{B}(\mathbf{r}).$$ (2)

Here the first term describes the nuclear, the second describes the magnetic interaction between the neutrons and the scatterer, m is the mass, and μ_n is the magnetic moment of the neutron (latter in SI units), and the scattering length density is defined as

$$\rho(\mathbf{r}) = \left\langle \sum_j N_j b_j \right\rangle,$$ (3)

where N_j and b_j are the number density and coherent scattering length of species j. The <…> sign denotes the average at $\mathbf{r}$. The neutron absorption is taken into account by the imaginary part of b. Except for very thick absorbers or strongly absorbing elements, such as Gd and Cd the neutron absorption may be neglected.

2.1. Reflection on a single interface

The reflection is described by the Schrödinger-equation

$$-\left(\frac{\hbar^2}{2m}\right)\nabla^2\Psi(\mathbf{r}) + V(\mathbf{r})\Psi(\mathbf{r}) = E(\mathbf{k})\Psi(\mathbf{r})$$ (4)

Assuming isotropy in the film's (x-y) plane, the potential $V(r)$ only depends on the out-of-film-plane z-component and the potential is absent in the medium of incidence ($V(z) = 0$ for $z < 0$). Then **Equation 4** reduces to the one-dimensional

$$\frac{d^2\psi(z)}{dz^2} + \left(q_0^2 - G(z)\right)\psi(z) = 0$$ (5)

formula with $\psi(z)$ being the plane-perpendicular component of the neutron wave function and $q_0 = k_0 \sin\theta_0$ is that of its wave vector in the medium of incidence ($z < 0$). The wave vector transfer during reflection is $Q = 2q_0$ and the optical potential in the usual units of wave vector squared is

$$G(z) = \frac{2m}{\hbar^2} V(z)$$ (6)

The perpendicular component of the wave vector varies with depth as

$$q(z) = \sqrt{q_0^2 - G(z)}$$ (7)

The treatment of the magnetic scattering is more complicated especially for arbitrary direction of the magnetization. Here we only consider the collinear case, when the neutron

spin is either parallel or antiparallel to the magnetic induction B. The total (nuclear + magnetic) optical potential can be written as

$$G(z) = G_n(z) + G_m(z) = \pm 4\pi \left\langle \sum_j N_j (b_j \pm p_j) \right\rangle,$$ (8)

where the 'magnetic scattering length' (p_j) is proportional to μ_j, the magnetic moment of species j in units of μ_B, the Bohr magneton and the factor C is defined by $p_j = C\mu_j = m\mu_n \mu_B \mu_0 / 2\pi\hbar^2 = 2.699\text{fm}/\mu_B$. The $\pm$ sign in **Equation 8** refers to the case of spin parallel (+) and antiparallel (-) to the magnetic induction. In the more complicated general case of arbitrary relative orientation of the spin and the magnetic induction spin-flip may occur during reflection resulting in up to four different reflectivity curves for the ++, +-, -+ and -- channels. Analogously to the case of light, a refractive index n can be defined for neutrons by

$$n(z) = \frac{k(z)}{k_0} = \sqrt{1 - \frac{V(z)}{E_0}} = \sqrt{1 - \frac{G(z)}{k_0^2}}$$ (9)

For the non-magnetic case this yields

$$n(z) = \sqrt{1 - \frac{\lambda^2 \rho(z)}{\pi}} \approx 1 - \frac{\lambda^2 \rho(z)}{2\pi}.$$ (10)

An interface between two media with $G_0 < G_1$ (see **Figure 1**) acts as a potential barrier for the neutron with a height of $\Delta V = \hbar^2 \Delta G / 2m$ with $\Delta G = G_1 - G_0$. If the kinetic energy of perpendicular incidence is smaller than this barrier, a total reflection occurs, i.e. $R(q_0) = 1$ for $q_0 < q_c = \sqrt{\Delta G}$.
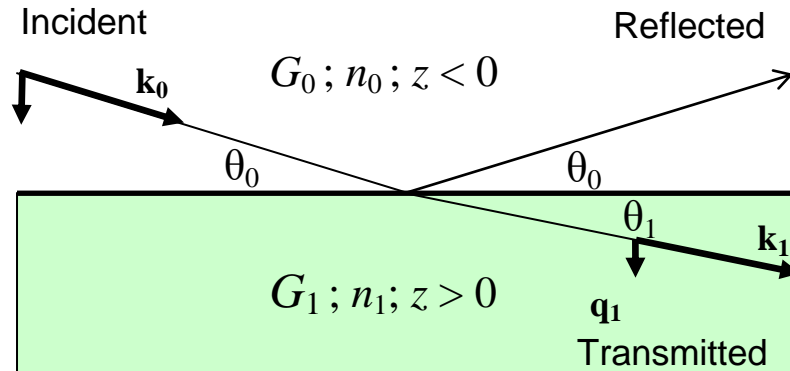

Figure 1. The specular reflection geometry

In this regime q_1 is imaginary, corresponding to an exponentially damped evanescent wave. For $q_0 > q_c$ the reflectivity and transmissivity decay according to the Fresnel formulas

$$R_F(q_0) = \left| \frac{q_0 - q_1}{q_0 + q_1} \right|^2 \qquad T_F(q_0) = \left| \frac{2q_0}{q_0 + q_1} \right|^2 . \tag{11}$$

Refraction at the interface is governed by Snell's law: $n_0 \cos\theta_0 = n_1 \cos\theta_1$. At the critical angle $n_1/n_0 = \cos\theta_c$ and $\theta_c = \arccos(n_1/n_0) = q_c/k_0 = \sqrt{\Delta G}/k_0 = \lambda\sqrt{\Delta G}/2\pi$. For thermal and cold neutrons n is below 1 for most materials. It means that the transmitted beam is refracted towards the surface which is opposite to the daily experience with light refracted at a glass or liquid surface. Since ($1 - n \sim 10^{-6}$ to 10^{-5}), the critical angle is typically of the order of 10 mrad, a fraction of a degree.

2.2. Reflection from layered systems

Reflectivity from a layered system is a result of interference of the incoming and the reflected beams. Reflectivity and transmissivity can be deduced recursively from the continuity relations of the wave and those of its derivatives at each interface. Two simple cases will be considered here. In **Figure 2** neutron reflectivity of Ni layers of 15 and 30 nm on float glass substrate are displayed.
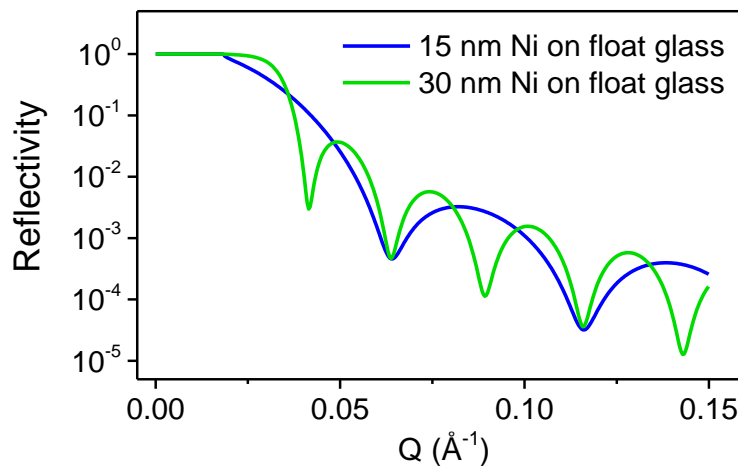

Figure 2. Neutron reflectivity of a 15 and a 30 nm Ni layer on float glass.
The („Kiessig") oscillations corresponds to the respective film thickness

In **Figure 3** the reflectivity of a float glass/[Ti(4nm)/Ni(7nm)]$_5$ periodic multilayer is shown (in green) along with that of the bilayer float glass/Ti(4nm)/Ni(7nm) (in blue). The modulation of the multilayer reflectivity curve according to the bilayer contrast and the reciprocal relation (above $q \approx 2q_c$) between the small and large q-space periods and the total layer thickness and bilayer period length (as indicated in the figure) are salient.
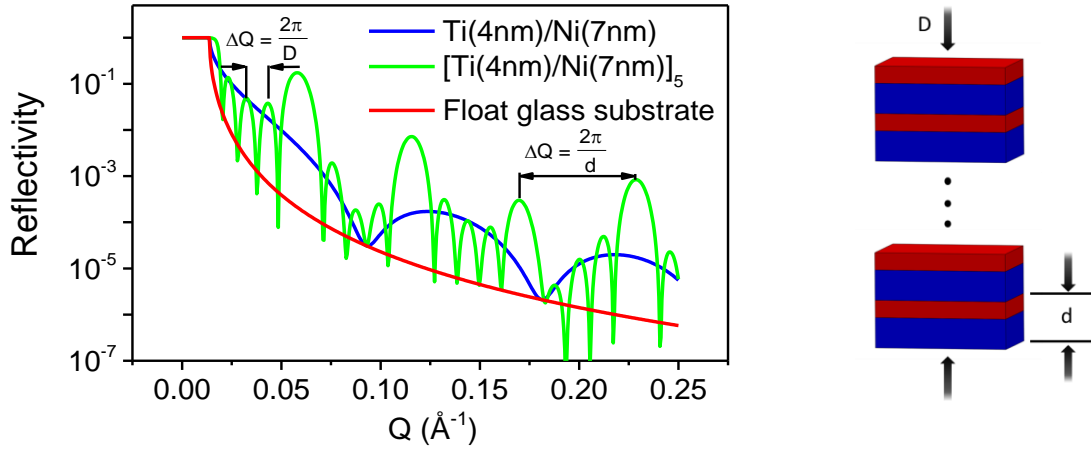
Figure 3. Neutron reflectivity of the [Ti(4nm)/Ni(7nm)]$_5$ multilayer (green) and of the respective Ti/Ni bilayer (blue) along with that of the float glass substrate Red). The bilayer thickness and the total thickness – demonstrated on the right – are in reciprocal relation to the Bragg peak distance and the Kiessig oscillation period, respectively.

2.3. Interface roughness

So far we assumed perfectly smooth surfaces. Real interfaces always exhibit roughness at the nanoscale. The height profile of an interface can be described by a *z(x,y)* function (**Figure 4a**), which can statistically be characterized by the mean squared deviation from an ideally smooth interface, the lateral correlation length and Hurst parameter. Since specular scattering is insensitive to the in-plane scattering objects, it is dependent only on the lateral average of the scattering lengths along the rugged interface, or, in other words on the
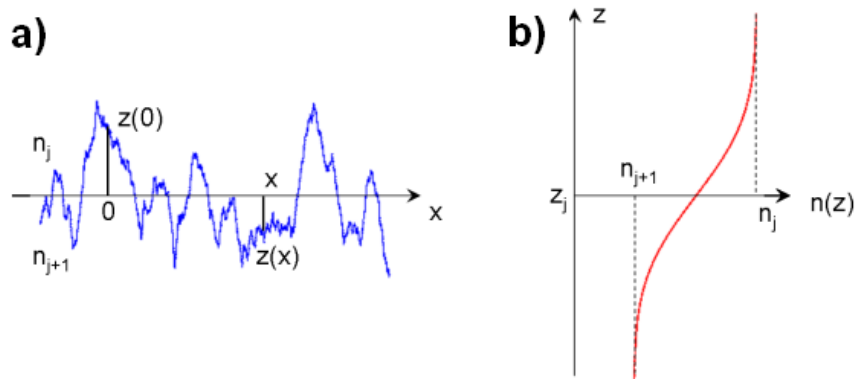

Figure 4. Interface roughness at the nanoscale characterized by the z(x,y) height correlation function. (a) and the corresponding z-dependence of the refractive index (b).

z-dependence of the index of refraction (c.f. **Figure 4b**). Assuming a random distribution of the height coordinate, the index of refraction profile is an error function which finally modifies the flat interface reflectivity as:

$$R_{rough} = R_{flat} \cdot \exp\left(-4\sigma_j^2 q_j q_{j+1}\right), \qquad (12)$$

where σ_j is the root mean square (rms) deviation from the nominal position of a flat interface. ("rms roughness").

3. Experimental techniques

Reflected intensity has to be recorded as a function of $q = (2\pi/\lambda)\sin\theta$. Using a monochromatic beam, it can be performed by a θ-2θ scan. Using the time-of-flight (TOF) method neutrons in a broad λ–range can be detected almost simultaneously, while the incident angle and the entire experimental geometry are kept constant. Both methods have their advantages. The TOF method well suits to pulsed neutron sources and facilitates dynamic studies. GINA at BNC is a monochromatic reflectometer.

Nowadays extra options, such as polarizers, analysers and spin flippers as well as position sensitive detectors are used at almost all present day neutron reflectometers to allow measuring the reflectivity of polarized neutrons, to analyse spin-flip processes and off-specular scattering in a large variety of sample environments.

3.1. The GINA reflectometer

The GINA reflectometer is a dance-floor type angle-dispersive vertical sample reflecto-meter with various options for non-magnetic and magnetic sample environment. **Figure 5** displays the schematic diagram of the instrument, located on the BNC research reactor's horizontal cold neutron channel 10 guide 3 of size 4"/1" (height/width) (see chapter "Introduction to neutron beam experiments") The 5-element focusing HOPG (highly oriented pyrolytic graphite) monochromator unit (behind the biological shielding) provides neutrons with base harmonics of $\lambda = 4.67$ Å and about 40% of higher harmonics intensity.
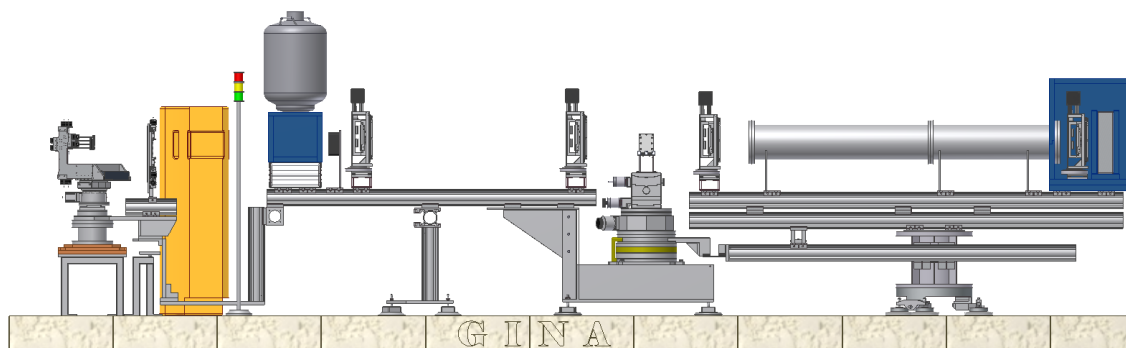

Figure 5. Schematic view of the non-polarized beam setup of the GINA reflectometer

The latter are removed by the Be-filter behind a rough collimator. For lower absorption the Be-block is cryo-cooled to liquid N_2 temperature. Normalization of the intensity is performed by the counts measured by the intensity monitor (a low-efficiency ^{3}He gas detector). The precision slit system provides tight collimation of the beam to the sample surface with an accuracy of 50µm/blade. The incident angle (θ) is set by the encoded θ-goniometer and the detector angle (2θ) by the motorized wheel under the detector arm (also encoded). The delay-line type two-dimensional gas detector (with ^{3}He being the active agent) is suitable for studies of off-specular scattering, but it is also handy in fast adjustment of the setup for specular scattering. The entire instrument is computer controlled. The actual motor names and macro names to operate the control program along with the suggested scan sequence for the experiment of the hands-on practice is available in the experimental hutch.

3.2. Hands-on exercise using the GINA reflectometer

The plan is to extract reliable layer thickness and rms roughness values for a float glass/[Ti/Ni]$_5$ periodic multilayer sample.

The sample has been prepared with a Ni target with 8w% Mo, so that the multilayer is nonmagnetic to far below room temperature. We will use monochromatic non-polarized neutrons. Study the instrument components in their physical reality and discuss their function.

Tasks of the hands-on practice (make sequential notes of all what you do)

- Using the slit positions (see rulers underneath) calculate and set slit sizes to resolve Kiessig oscillations of the nominal layer structure

- (Make sure the beam shutter is closed.) Mount the sample

- Using the GinaSoft instrument control program (short guide available):

- Open shutter

- Align the reflectometer to zero θ and 2θ angles – check direct beam

- Align the sample in the beam by scanning motor 'ytrans' at nominal θ = 0 and set 'ytrans' to half beam

- by θ-scans (from -0.6° to 0°) at 2θ ≈ 0.6º and 'ytrans' at half beam

- Estimate optimum step width and time per step for θ-2θ scan

- Start θ-2θ scan for the float glass/[Ti/Ni]$_5$ multilayer.

- During the automatic data collection period use the program FitSuite to evaluate data collected by another experimental group

- When the θ-2θ scan is finished, save the reflectogram.

4. Interpretation of the results

The purpose of a reflectometric experiment is to gain as much information on the G(z) from the measured R(q) as possible. This is usually performed by fitting models to the data. By modelling G(z) with adjustable parameters, the shape of G(z) is treated by some weighted least squares algorithm to provide parameter values which give the smallest integral deviation from the experimental data, taking the experimental conditions, the statistical accuracy of the data and the finite resolution into account. The usual method is an approximation of the scattering length density (SLD) profile by that of a finite set of layers (of constant G or SLD and allowing for an rms roughness between them) and numerically calculating R(q) by the optical matrix method. Although unique solutions cannot be assured, the derived parameters often reproduce the measured reflectivity to high accuracy. For difficult cases innovative methods are available to scan the parameter space.

In the actual case the data collected during the hands-on exercise will be evaluated by the Neutron_Reflection module of the general purpose simulation and fit program FitSuite

(www.fs.kfki.hu). The Linux or Windows program can be downloaded from the given URL and setups are provided to install it on your own computer. There is a Windows copy available on the lab computer. The program has an extended help and self-explanatory video demos. However, an independent quick reference guide and step-by-step instructions for the actual data evaluation is also available in the experimental hutch.

4.1. Evaluation tasks

Estimate the bilayer thickness and total thickness of the multilayer from the plot of the reflectivity curve (without computer fit).

Using FitSuite: evaluate data collected by another experimental group. Set up the fit problem, add incoherent part, add substrate and layers, add data to the model. Then initialize simulation parameters corresponding to the experimental setup (wavelength, wavelength distribution, beam divergence) according to the actual experiment and initialize values for the layer thicknesses, for the (real and imaginary) scattering length densities and interface roughness and allow the program to fit the data. Discuss and refine the model until satisfied.

References

J. Daillant A. Gibaud (eds.): X-ray and Neutron Reflectivity – Principles and Applications, Springer, Berlin, Heidelberg, 2009 ISBN-13: 978-3540885870

https://www.ncnr.nist.gov/instruments/index.html (reflectometers)

https://www.e-neutrons.org

FitSuite manual at www.fs.kfki.hu

Measuring collective modes with a Three-axis spectrometer

Alex Szakál, Gérard Pépy

1. Introduction

A neutron Three-axis Spectrometer (TAS) is an extraordinary powerful tool, however, it is very difficult to drive… Many parameters are free and may wreck your TAS run. One may group these parameters in two classes. The first class includes parameters which intervene in the scattering cross section; they vary according to the object under study, phonon or magnon, in a defined sample. We shall examine how to manage them in the next chapter. The second class parameters are linked to the used TAS spectrometer, but in some way they also depend of the choices made for the first class of parameters. We shall consider them in a following chapter. Throughout this paper bold script will design vectors or matrix.

Three-axis Spectrometers (TAS) are suited for investigation of dynamical properties of samples typically with meV energy resolution. These machines are effectively operated at continuous neutron sources. Taking into consideration the energy of the neutrons we can sort them in three classes. There are cold three-axis instruments which use neutrons in the energy range 1-10 meV. These instruments are installed on a supermirror guide-tube which looks directly into a cold source. This class of three-axis instruments has the best energy, $\mathbf{Q}$ (momentum transfer) resolution and signal to noise ratio among the three-axis instruments, but they have the disadvantage that the small neutron energy limits the possibility of measuring high energy excitations and high $\mathbf{Q}$ values. Another class of TAS machines looks directly at the reactor moderator, using thermal neutrons in the energy range 10-100 meV. TAST at the Budapest Research Reactor belongs to this category. A last and rare class looks to a hot source, with neutrons energy larger than 100meV. These instruments have lower resolution and signal to noise ratio than the cold TAS but enable to measure higher energy excitations.

Contrary to Time-of-Flight (TOF) techniques, TAS use the wave property of neutrons (selective reflection on monochromator and analyser crystals) for the measurement of the dynamical properties of samples. The apparatus is called three-axis because there are three main axes of the instrument. The first is the monochromator axis determining the wavelength of the incoming neutrons, the second is the scattering angle which defines the direction of the analysed neutrons, the third is the analyser axis which selects a narrow energy range of the scattered neutrons and reflects them to the detector.

The outline of the TAST spectrometer installed on a radial beam tube is shown in **Figure 1.** The neutrons escape from the reactor through the guide-tube, and hit the monochromator of the instrument. Depending on the angle between the reflecting crystal planes of the monochromator, and the incoming white neutron beam, the monochromator selects neutrons with wavelength satisfying Bragg's law. In order to narrow the distribution of neutrons in the $(\mathbf{Q}, \omega)$ space, i.e. affect the resolution of the experiment, Soller collimators are used before and after the monochromator. With the proper use of these collimators one can narrow the resolution function to the expense of intensity, which is the usual problem for every scattering experiment. The wavelength spread of the neutrons monochromated by this method is typically in the order of 1%. These neutrons go through

a low efficiency neutron detector called monitor and reach the sample. The first part of the instrument, which has been defined up to this point is often called "the primary spectrometer". Neutrons interact with the sample and part of the beam is scattered. The scattered neutrons can be divided into two classes. The major part of them does not change their energy (elastic scattering) but some of the neutrons excite (or absorb) energy and change their energy.
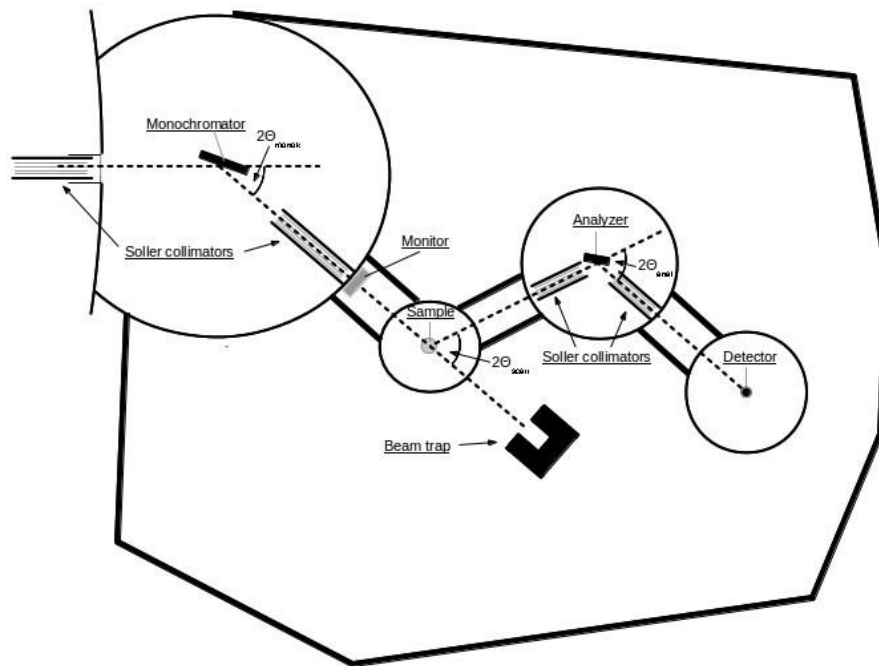

Figure 1. Schematic view of a thermal three-axis spectrometer installed at the end of a horizontal beam-tube

The secondary spectrometer analyses the direction and energy of the scattered neutrons. This part of the spectrometer uses the same principle as the primary spectrometer – scattering on a single crystal – to select one energy from the scattered beam. The analyser drum can be rotated around the sample and in this way both the energy and direction of neutrons leaving the sample can be analysed. Soller collimators are used before and after the analyser to maintain the resolution, but at the same time they also reduce the background coming from other sources than the sample, which is a crucial point when dynamic phenomena with very low scattering cross section is studied.

2. The goal

The most common reason to measure collective modes is to draw a picture of the dispersion curves as on **Figure 2.** N atoms in the elementary cell generate 3N phonon dispersion curves. Because of the crystal periodicity, to understand its properties, it is enough to consider a small volume in the reciprocal (Fourier) space called the Brillouin zone (BZ); in some way it is a Fourier counterpart of the elementary cell. The three dispersion curves which have 0 energy at the Brillouin zone origin are called acoustic

branches, because their slopes are the sound velocities. If any, the other dispersion curves are called optic branches, because they appear in optic experiments like Raman scattering. It is common to distinguish longitudinal and transverse branches; strictly speaking the polarization is such only close to the BZ centre. Concerning spin waves, N magnetic ions in the elementary magnetic cell generate N magnon branches. Antiferromagnets have an even number of magnetic ions, they often show only N/2 degenerate branches. But anisotropy may lift the degeneracy near the BZ centre. Usually, to get an understanding of the dynamic behaviour of the sample, it is enough to measure the dispersion curves along some high symmetry crystal axis, the [0 0 1], [1 1 0] and [1 1 1] directions.

Of course this understanding is greatly enhanced by building an interatomic force model (dynamic matrix) and fitting the calculated phonon modes to the data; for magnons the model is built from magnetic interactions, most often a Heisenberg and a dipolar Hamiltonians. In some cases, only a part of the dispersion curves is interesting for instance to study the electron-phonon interaction in superconductors or the temperature vanishing frequency of a soft mode. Sometimes not only the dispersion curve frequency but also its anharmonic broadening is a valuable information, for instance to characterize a phase transition.
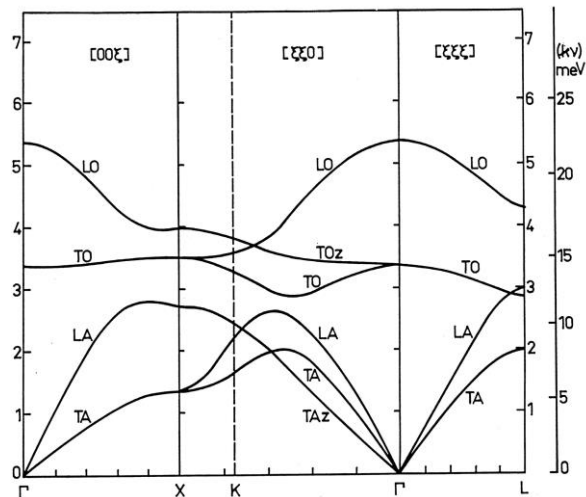

Figure 2. Phonons in KBr (G. Krexner courtesy)

3. Cross section

In this paper we shall limit ourselves to the classic vibration collective modes, which take place in single crystals. We shall not consider other modes (e.g. librons), neither TAS application to other methodologies like diffuse scattering. The observed intensity, better called neutron cross section, is proportional to the scattering function [1]

$$\frac{d^2\sigma}{dEd\Omega} = \frac{k_f}{k_i} S(\mathbf{q}, \hbar\omega)$$

where:

k_i - incoming neutron wave-vector

k_f - outcoming neutron wave-vector

$\mathbf{q}$ - collective mode wave vector

$\hbar\omega$ - energy transfer to the interacting neutron

For phonons:

$$S(\mathbf{q},\hbar\omega) = \frac{\hbar}{4\pi N}\left|\sum_k b_k \frac{\mathbf{Q.e_{kj}(q)}}{\omega_j(\mathbf{q})\sqrt{m_k}}e^{-i\mathbf{Qr_k}}e^{-w_k}\right|^2 n_j(\mathbf{q})\ \delta\!\left(E_f - E_i \mp \hbar\omega_j(\mathbf{q})\right)\delta(\mathbf{Q}-\boldsymbol{\tau}_{hkl}\mp\mathbf{q})$$

For magnons (collinear structures):

$$S(\mathbf{q},\hbar\omega) = \frac{\hbar}{4\pi N}\left(1-\left(\hat{\mathbf{Q}}.\hat{\mathbf{M}}\right)^2\right)\left|\sum_k f_k(\mathbf{Q})\mathbf{e_{kj}(q)}e^{-i\mathbf{Qr_k}}e^{-w_k}\right|^2 n_j(\mathbf{q})\ \delta\!\left(E_f - E_i \mp \hbar\omega_j(\mathbf{q})\right)\delta(\mathbf{Q}-\boldsymbol{\tau}_{hkl}\mp\mathbf{q})$$

where:

N - number of atoms (or spins) in the elementary cell

b_k - coherent scattering length of atom k, m_k is its mass, $\mathbf{r_k}$ is its position in the elementary cell

$\mathbf{Q}$ - scattering vector

$\boldsymbol{\tau}_{hkl}$ - any vector of the reciprocal lattice, with hkl Miller indexes

$f_k(\mathbf{Q})$ - magnetic form factor of atom k (useful only for magnetic scattering)

$\exp(-w_k)$ - Debye-Waller factor, for atom k

$\hat{\mathbf{Q}}$ - unit vector along the scattering vector $\mathbf{Q}$

$\hat{\mathbf{M}}$ - unit vector along $\mathbf{M}$, the magnetisation

E_i - incoming neutron energy

E_f - outcoming neutron energy

$\mathbf{e_{kj}(q)}$ - polarisation vector or amplitude of the phonon wave

The index k runs over the n atoms in the elementary unit cell (on the magnetic ions in case of magnons). The index j runs over the collective modes.

The expression between the bars is called the dynamic structure factor. Next is the population factor, $n_j(\mathbf{q})$. Finally the two Dirac functions express the conservation of energy and momentum; the higher sign in $\mp$ holds for annihilation (neutron energy gain) and the lower for creation of a quasi particle (neutron energy loss).

3.1. Reciprocal space

Running a collective mode measurement implies thinking in the reciprocal space. It is useful to consider the vectors in real and reciprocal space in **Figure 3.**
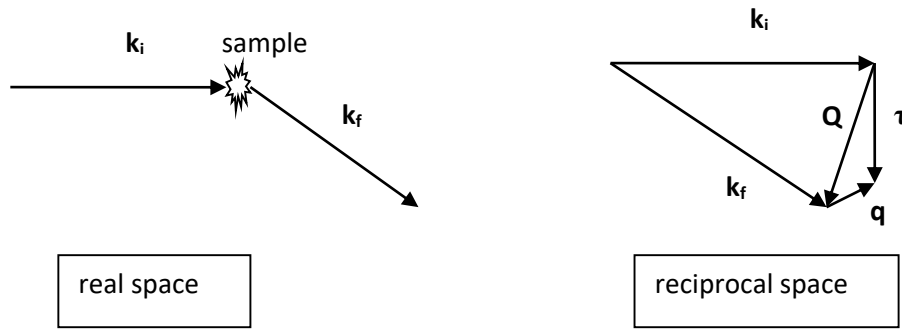
Figure 3. *Direct and reciprocal (Fourier) space. On the right of the picture, the relations between neutron incoming, k_i, and outgoing, k_f, wave vectors, the scattering vector Q, a reciprocal lattice vector τ*

Before running a TAS experiment the first task consists in determining the elementary unit cell and drawing the Brillouin zones in the reciprocal space. Unlike diffraction measurements where considering multiple cells is often preferred to unit cell for simplicity sake, while Brillouin zone with 0 scattering are discarded, in the case of dynamic studies it is very important to determine the shape of a unit elementary cell and of the Brillouin zone. One should also note that phonons can be observed in Brillouin zones with 0 structure factors, notably optic branches. To illustrate these remarks, let us consider a cubic or orthorombic face centred lattice. Most often, in order to have access to the three most important crystallographic directions ([0 0 1], [1 1 0], [1 1 1]), the sample will be oriented with the [0 0 1] and [1 1 0] axis in the horizontal scattering plane. Thence the reciprocal space will be paved by Brillouin zones as shown on **Figure 4.**
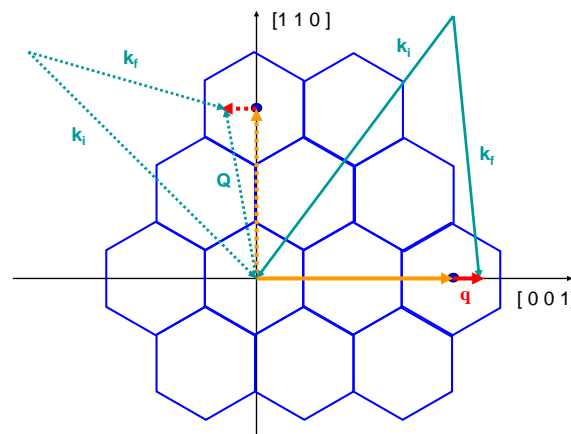

Figure 4. *Scheme of the inelastic scattering in the horizontal reciprocal plane. Brillouin zone contours are shown for a face centred orthorhombic Bravais lattice. Two configurations are represented. In full lines a configuration is designed to observe a phonon with wave vector (0. 0. 0.5) in the [0 0 4] Brillouin zone. This configuration is suited for phonons with longitudinal polarisation. In dashed lines a second configuration is designed to observe a phonon with wave vector (0. 0. -0.5) in the [2 2 0] Brillouin zone. This configuration is suited for phonons with transverse polarisation*

3.2. Dynamic structure factor

While phonons and magnons dynamic structure factors have in common the phase shift and Debye–Waller factors, their structure is very different:

3.2.1. Extension in reciprocal space

Inside the dynamic structure factor of phonons we find a scalar product, $\mathbf{Q}.\mathbf{e_{kj}}(\mathbf{q})$, between the scattering vector and the polarisation. This means that the intensity will increase roughly as the square of the scattering vector; therefore phonons are always searched for at the largest available scattering angles.

For magnons, the first factor is the magnetic form factor. Spin waves imply the atomic magnetic moments, sum of the contribution of non-compensated electronic spins, which exhibit a large size compared to the neutron; this translates by a limited extension in the reciprocal space: the magnetic form factor falls rapidly when the scattering vector increases. Magnons will be looked for at small scattering angles

3.2.2. Polarisation effect

Polarisation effects are governed by the polarisation vector $\mathbf{e_{kj}}(\mathbf{q})$.

- let us assume that the sample structure has a high symmetry and that we are looking at the dispersion of phonons along a high symmetry direction. In this case, close to the Brillouin zone centre, the polarisation of acoustic phonon branches is either fully transverse or fully longitudinal (versus the wave vector). As the scalar product $\mathbf{Q}.\mathbf{e_{kj}}(\mathbf{q})$ involves the scattering vector, for longitudinal phonons the scattering will be maximised when the wave vector will be parallel to the scattering vector ($\mathbf{e}$, $\mathbf{q}$ and $\mathbf{Q}$ are parallel, full lines in **Figure 4**). On the contrary, for transverse modes, the scattering will be maximised when the wave vector will be orthogonal to the scattering vector ($\mathbf{e}$ and $\mathbf{Q}$ are parallel, orthogonal to $\mathbf{q}$, dashed lines in **Figure 4**).

- for magnons the polarisation effect comes from the fact that the neutron spin interacts with the part of the magnetization orthogonal to the scattering vector. Let us consider the simple case of collinear ferromagnetic structures; as spin waves are fluctuations of the transverse components of the magnetisation, the scattering will be maximal when the magnetisation is orthogonal to the scattering vector. If the magnetisation is parallel to the scattering vector, the intensity collapses; indeed for ferro or ferrimagnetic structures applying a strong horizontal magnetic field along $\mathbf{Q}$ is a way to check that an assumed magnon peak is really magnetic.

3.2.3. Phase-factor

Combined to the polarisation vector $\mathbf{e_{kj}}(\mathbf{q})$, the phase factor $e^{-i\mathbf{Q}\mathbf{r_k}}$ has a deep influence on the cross-section, thanks to its Brillouin zone dependence. The intensity scattered by a given collective mode changes tremendously from one Brillouin zone to another. However, to foretell this feature, the only way is to have a Hamiltonian model of the force field and to diagonalize it (the dynamic matrix) in order to obtain the polarization vectors $\mathbf{e_{kj}}(\mathbf{q})$. This is a very difficult task rarely performed, especially for phonons, while some software like UNISOFT [3] may provide help. Moreover scientists are usually happy

obtaining the dispersion curves while measuring the intensity of some collective modes in various Brillouin zones would allow to test the assumed force field in a much more sensitive manner; such experiments are excessively rare. On **Figure 5** one may find a map of the intensity of a collective mode calculated with UNISOFT.
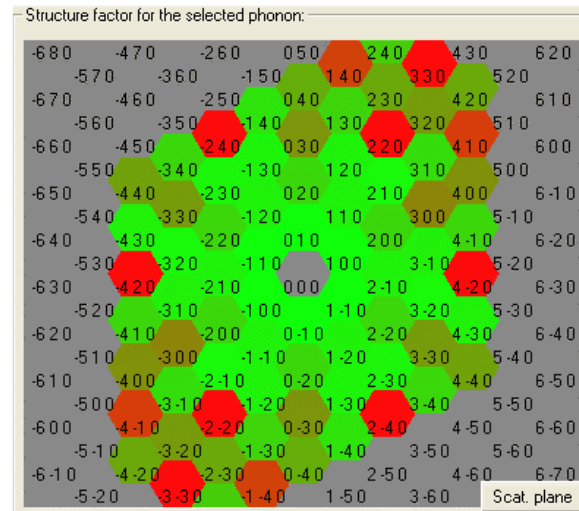

Figure 5. *Variation of the dynamical structure factor for a low lying mode in the hexagonal plane in quartz. This flat branch with frequencies below 1 THz which is known as the soft mode responsible for the well-known α-β phase transition. The UNISOFT program package is used to calculate not only the phonon frequencies but also the expected scattered intensities in different Brillouin zones. This figure shows the variation of the visibility of this particular phonon across some part of the reciprocal space [4]*

3.2.4. Population factor

The detailed balance theorem relates the creation scattering function on the left (neutron energy loss) to the annihilation scattering function on the right (neutron energy gain):

$$S(\mathbf{q}, \hbar\omega_j(\mathbf{q})) = e^{\frac{\hbar\omega_j(\mathbf{q})}{k_B T}} S(\mathbf{q}, -\hbar\omega_j(\mathbf{q}))$$

where k_B is the Boltzmann constant and T the temperature.

Thence, considering the boson nature of the phonon and magnon quasi-particles, the population factor will be different whether a quasi-particle creation takes place,

$$n_j(\mathbf{q}) = \frac{1}{e^{\frac{\hbar\omega_j(\mathbf{q})}{k_B T}} - 1} + 1$$

or a quasi particle annihilation takes place :

$$n_j(\mathbf{q}) = \frac{1}{e^{\frac{\hbar\omega_j(\mathbf{q})}{k_B T}} - 1}$$

The creation process always benefits of a higher population factor, which may be very significant for modes with energy large compared to the temperature of the experiment. Generally the creation mode will be preferred, furthermore when working at temperature much lower than the energy transfer. However the energy of the created quasi particle is obviously limited by the incoming neutron energy. This is not the case in the annihilation mode. Meanwhile another limit occurs: in all cases the momentum triangle must close: $\mathbf{k}_f = \mathbf{k}_i + \mathbf{Q}$. As the population factor is higher for creation this will be the most commonly used mode, which means that generally k_f will be smaller than k_i.

4. Spectrometer optimization

4.1. Resolution function

The TAS resolution function is probably the most important feature of this apparatus. The resolution function concept means that, for a given TAS geometry, the explored volume is not an infinitely small dot, but rather an extended volume called the resolution ellipsoid. Properly speaking the resolution function is a neutron scattering probability extending over the whole workspace (reciprocal space + energy transfer axis); the resolution ellipsoid is the volume where the resolution function is bigger than 0.5. The observed intensity is the convolution product of the resolution function (characteristic of the spectrometer) and the scattering function (characteristic of the sample). The importance of the resolution function for finding the best TAS configuration and performing a correct data treatment was realized early [2]. Meanwhile the description of the resolution function calculation is too long to be included in this paper. Let us simply mention some of the properties of the resolution ellipsoid. As the vertical component of the neutron reflection on the monochromator and analyser is classic (i.e. not selective), the vertical divergences do not play a role in the shape of the resolution ellipsoid; merely increasing the intensity for larger apertures. However, because of the asymmetry of the neutron selective reflection over the monochromator and analyser there is a strong correlation between the wavelength and angular dispersion of the beam. This produces a quite anisotropic "resolution ellipsoid": it is quite elongated in a direction between $\mathbf{k}_i$ and $\mathbf{k}_f$. Moreover, its long axis is never parallel to the horizontal plane of the reciprocal space but exhibits a significant slope versus the energy transfer axis. This has a significant effect on the way TAS should be run.

4.2. Resolution function versus dispersion curve

In any Brillouin zone, along a determined crystallographic direction, one can observe a mode with $+\mathbf{q}$, or $-\mathbf{q}$ wave-vector, by annihilation of an existing mode (positive energy transfer to the neutron) or mode creation (negative energy transfer). The exploration can be made at constant energy transfer along the crystallographic direction, but most often at constant momentum transfer (constant Q), because that allows for an easier comparison of mode behaviour versus temperature. Moreover if a mode frequency broadening is

taking place, it is better to study it at a constant Q. Let us consider a simplified case: an acoustic dispersion curve in a frame consisting of a high symmetry crystalline axis and the energy transfer axis as on **Figure 6.**

The four possible configurations are clearly not equivalent. A major item is the shape of the resolution ellipsoid as shown on **Figure 6.** According to the way this ellipsoid matches the slope of the dispersion curve one will get a sharp intensity peak or a broad one. This effect is obviously reversed when wave vector and energy transfer are exchanged (the resolution ellipsoid shape changes slowly versus **Q**). While the population factor will not affect small energy modes at high temperature, it may strongly deteriorate the intensity observed when temperature is low. In such a case only one configuration is good.
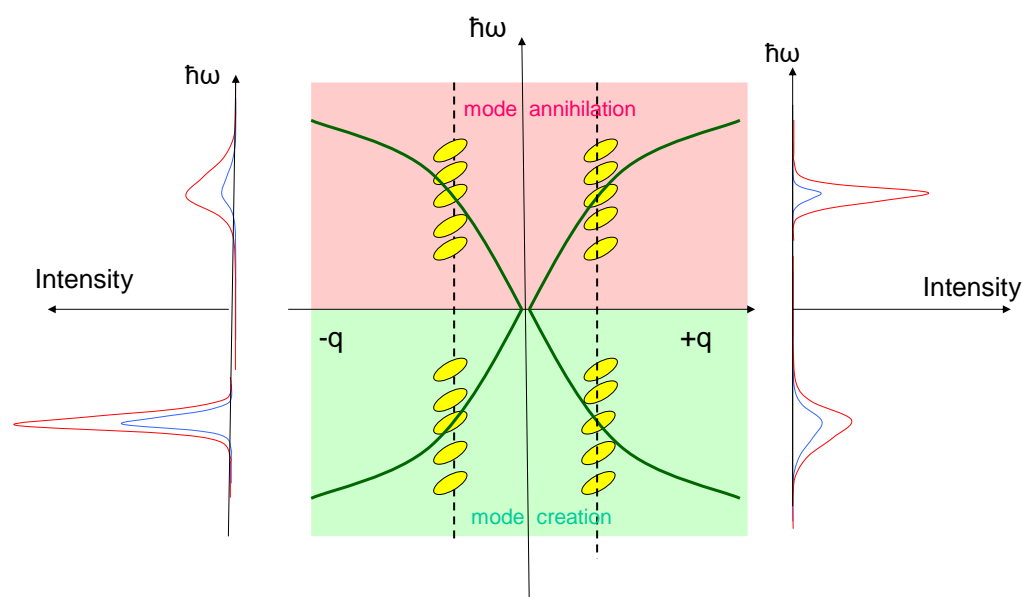

Figure 6. Inelastic scattering scheme in the generalised reciprocal + energy transfer space. An acoustic dispersion curve is shown on a diagram with a crystallographic axis as abscissa, and the energy transfer as ordinate. A positive energy transfer (for the neutron) corresponds to the annihilation of a collective mode. The exploration is assumed to be "constant Q" type. Each step corresponds to a small ellipsoid symbolising the spectrometer resolution function. Two exploration tracks (for +/-q) are marked by dashed lines. On each side of the picture is shown a tentative model of the expected intensity observed; blue lines hold for low temperatures, red lines for higher temperatures

Of course we shall note that the best choice is very much linked to the dispersion curve slope. When this later inverts, which is often the case close to the Brillouin zone border, the configuration will be changed to match the resolution ellipsoid to the dispersion curve in order to cross it with as few steps as possible.

4.3. Constant Q or constant E for a TAS run

While the constant Q mode is usually preferred as was said above, it may be advantageous sometime to move to constant E scans for instance to measure acoustic branches with very steep slopes (also when very strong dispersion). In this case it is quite difficult to part the neutrons scattered by the +q and –q mode. The constant Q mode will show only one of

the collective mode with a strong pollution by the other one. A constant E experiment will display both +q and –q mode and the data treatment will more easily model them together. Rarely another type of run is interesting where the sample is kept at constant angular position; this is the case for instance when very heavy and cumbersome equipment is used for the sample environment like very big cryostats or cryogenic Helmholtz coils.

4.4. Resolution function and focused/defocused spectrometer configuration

The resolution ellipsoid has some narrow extension only for the so-called focused (or W) TAS configuration, where the scattering angle senses alternate. Simulation shows that this provides the narrowest and tallest neutron peaks; it should be generally preferred. Meanwhile this is sometimes impossible. A frequent case takes place when a TAS has been built on a neutron guide with further use as on **Figure 7.** Assume the experiment requests a large incoming neutron energy. The monochromator take-off angle will be small, which will carry the sample close to the wall shielding the guide and the analyser even closer, if we keep the W configuration. If the experiments concerns spin waves observed at rather small scattering vector, this may fit. Meanwhile if the experiment concerns phonons, it is essential to work at the largest possible scattering vector (and therefore scattering angle) in order to maximise intensity. We have seen that the intensity changes as the square of the scattering vector; this is indeed an important feature. It is then compulsory to consider other configurations where the scattering angle will be inverted and possibly the analyser take-off angle as well, as on **Figure 8.** Only a full simulation of the experiment will show whether it is better to leave the focused configuration or to limit the scattering vector.
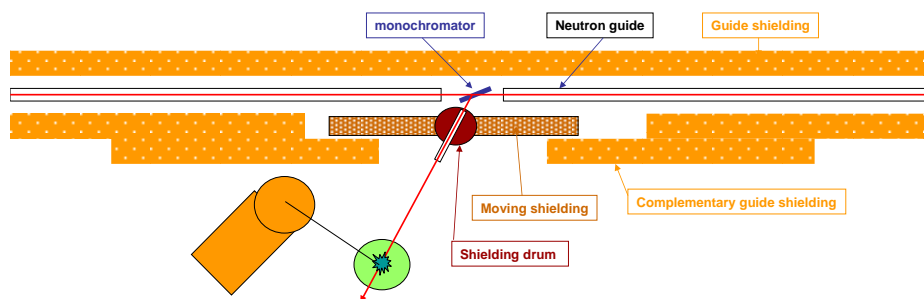

Figure 7. Scheme of a TAS spectrometer built sideways to a neutron guide. The neutron beam comes from the right. For common incoming neutron energies the sample and the analyser will be close to the guide shielding wall
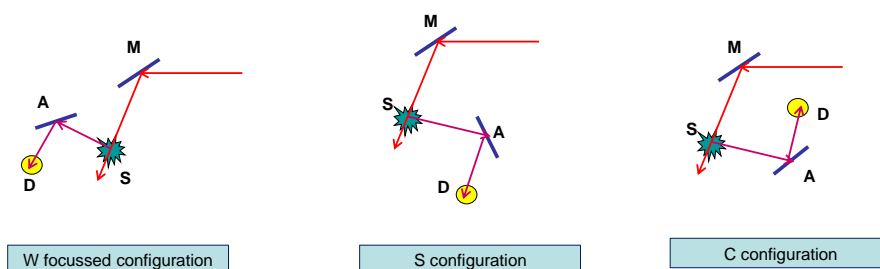

Figure 8. Various TAS configurations

The reader will note that we dropped the configuration where the sample scattering angle keeps the same sense and the analyser take-off is reversed. This usually worsens the collision geometry. Also going to annihilation mode would be wrong: assuming k_i and k_f be exchanged, the analyser-detector system would be straightened and sweep more room.

4.5. Harmonics filtering

Inelastic neutron scattering does not exhibit severe selection rules as light. Generally, it is advantageous but may become a drawback as there are many sources for scattering. One must be particularly careful about harmonics, which are a real nuisance. One must pay attention to the fact that the monochromator and analyser are ready to reflect not only the foreseen neutron wavelengths, but their harmonics as well following the formula, where l and m are integers:

$$l \cdot k_i = m \cdot k_f$$

The scattering angle is kept the same, and if there is some reason for scattering corresponding to multiple of $\mathbf{k_i}$ and $\mathbf{k_f}$ a pollution may appear, always difficult to track. A trivial case is the scattering by incoherent scattering when for instance k_f is half of k_i. In this case the second harmonic of k_f will be equal to k_i and a zero energy transfer incoherent scattering may take place anywhere in the reciprocal space, thus increasing the background. The most annoying case is a configuration including harmonic(s), which leads to a scattering by some (higher energy) mode in a farther Brillouin zone.

For thermal neutrons the simplest way to avoid harmonics of k_i is to take advantage of the Maxwellian shape of the incoming neutron flux, choosing a high value of k_i, where the flux is still large but decreasing fast for higher k_i.

Two filters exist to avoid (some) harmonics, the pyrolitic graphite (PG) and the beryllium. The pyrolitic graphite filter is a group of PG blades about 2 to 3 cm thick, usually with a broader mosaicity than the ones used for monochromator (typically 2° or 3°), carefully oriented perpendicular to the neutron beam. Thanks to Bragg peaks outside the hexagonal axis neutrons with wave-vector twice 23.6 nm^{-1} will be strongly scattered out. For a typical filter 3 cm thick the attenuation reaches a factor 2000 for the second harmonic of 23.6nm^{-1} wave-vector (2.662 Å, about 13 meV).

Metallic beryllium is a crystalline material with cubic structure and a very small unit cell. Therefore, no neutron with a wavelength bigger than 4 Å can be scattered. This limit is called the Bragg cut-off and it is one of the smallest. Therefore, if one puts a beryllium polycrystal block on the path of a neutron beam, most neutrons with wave-length shorter than 4 Å will be scattered out. Here again the attenuation factor is about 2000 over a 10 cm path. As beryllium is highly transparent the main beam absorption is negligible. Meanwhile, for a long block, the phonon scattering is important, about 30% of the "good" neutrons are lost. To avoid this problem, the beryllium block is usually located in a cryostat at liquid nitrogen temperature, which kills phonon scattering. One should note that encasing the beryllium block is also important for safety reason: beryllium oxide is one of the most powerful poison on earth (however nobody will inhale a solid metallic block contrary to thin powder). The advantage of beryllium filter is its lack of selectivity: all smallest wavelength neutrons are removed.

The last method consists in avoiding the reflection of (at least some) harmonics altogether. Current materials as germanium and silicon with "diamond" cubic structure exhibit zero scattering for all even Bragg peaks. Therefore, a monochromator using for instance the (1 1 1) or (3 1 1) reflections will be free of second and fourth harmonic (but not of third harmonic). The drawbacks of these monochromators (or analysers) is their poor reflectivity compared to pyrolitic graphite (about half) and the significant absorption of germanium which may be a nuisance if installed on a neutron guide with downwards instruments?

This chapter about harmonics is certainly long and tedious, but experimenters should be very careful about the hidden dangers of harmonics and prevent their effects.

4.6. Constant k_i versus constant k_f

From the above discussion one understands that strong constraints come from the filtering. They will influence the choice of constant k_i or constant k_f. Meanwhile if some freedom is kept, one will usually prefer the constant k_f mode. This has several advantages for the intensity corrections:

- as the monitor efficiency is usually inversely proportional to k_i it will automatically compensate for the k_f/k_i in the cross-section

- with the usual constant monitor acquisition one will also take into account the incoming flux variation versus k_i whatever its origin, either the Maxwellian flux or the monochromator efficiency

- last but not least a constant k_f will avoid difficult corrections for the analyser efficiency

5. Practical work

1) Glue the Al single crystal to the holder to have the (hkl) plane horizontal.

2) Rotate the sample on the goniometer table to be able to tilt separately the [h h 0] and [0 0 l] reciprocal vectors separately

3) Draw the scheme of the scattering plane. Identify the points in reciprocal space where longitudinal and transversal phonons can be measured.

4) Measure the longitudinal acoustic mode. Do scans on both sides of the selected Brillouin zone with neutron energy gain and energy loss. Calculate the velocity of sound.

6. Conclusion

We have reviewed and tried to organize a hierarchy of the TAS features.

Complementary reading is obviously useful. The interested newcomer may find some other points of view in various presentations [5, 6].

Acknowledgements

References

[1]   Squires G L 1978 *Introduction to the theory of Thermal Neutron Scattering* (Cambridge University Press
      Lovesey S W 1984 *Theory of Neutron Scattering from Condensed Matter* (Oxford University Press)

[2]   Cooper M J, Nathans R (1967) *Acta Cryst..* **23**, 357
      Dorner B (1972) *Acta Cryst..* **A28**, 319
      Chesser N J, Axe J D (1973) *Acta Cryst.* **A29**, 160
      Dorner B (1984) *Acta Cryst..* **A40**, 722-723

[3]   Eckold G, Stein-Arsic M and Weber H J 1987 *Appl. Cryst.* **20**, 134
      Eckold G, JÜL-2639, Jülich 1992, ISSN 0366-0885

[4]   Eckold G, ECNS 2003, Introductory course

[5]   Pynn http://www.ncnr.nist.gov/summerschool/ss09/pdf/Lecture_1_Theory.pdf
      http://www.ncnr.nist.gov/summerschool/ss09/pdf/Lecture_6_Inelastic.pdf

[6]   Brockhouse
      http://www.nobelprize.org/nobel_prizes/physics/laureates/1994/brockhouse-lecture.pdf

[7]   Hennion B 2009 *J. Phys. IV France* (Les Ulis, EDP Sciences)